LSSA Project
Task Report

5101-53

DOE/JPL-1012-77/6
Distribution Category UC-63

Compatibility Studies of Various Refractory Materials in Contact with Molten Silicon

Prepared for
Department of Energy
by
Jet Propulsion Laboratory
California Institute of Technology
Pasadena, California

(JPL PUBLICATION 78-18)

LSSA Project
Task Report

5101-53

DOE/JPL-1012-77/6
Distribution Category UC-63

Compatibility Studies of Various Refractory Materials in Contact with Molten Silicon

T. O'Donnell
M. Leipold
M. Hagan

March 1, 1978

Prepared for
Department of Energy
by
Jet Propulsion Laboratory
California Institute of Technology
Pasadena, California 91103
(JPL PUBLICATION 78-18)

ACKNOWLEDGMENT

The authors are indebted to D. Dixon for his support in sample preparation, testing and evaluation.

ABSTRACT

The production of low cost, efficient solar cells for terrestrial electric power generation involves the manipulation of molten silicon with a present need for noncontaminating high-temperature refractories to be used as containment vessels, ribbon-production dies and dip-coated substrates. Studies were conducted on the wetting behavior and chemical/physical interactions between molten silicon and various refractory materials.

CONTENTS

Figures

Tables

SECTION I

INTRODUCTION

A. BACKGROUND

The JPL Low-Cost Silicon Solar Array (LSSA) Project was established with the goal of decreasing the cost of solar arrays by improving the technology and by increasing production volume. Silicon solar cells have widely been used for generation of electrical power in space and have found some limited uses on Earth. It has been proposed in recent years to use silicon solar cells for the routine generation of electrical energy for commercial use; and the present energy crisis has placed renewed emphasis on this proposal.

The major shortcomings in the use of silicon solar cells for terrestrial power generation are the expensive processing in terms of equipment cost, the large energy consumption during growth, and the lengthy and sometimes wasteful processing needed to prepare solar-arrays (Reference 1-1). Considerable attention is therefore being given to the problem of developing better methods of processing the cells. The present method of wafer-slicing and polishing of Czochralski boules into cells is very inefficient in terms of percentage of a single boule which can actually be produced. Several potentially economic processes are under consideration. One such technique that shows great promise is silicon ribbon growth, which includes such processes as edge-defined, film-fed growth (EFG) (Reference 1-2), web dendritic growth (Reference 1-3), inverted ribbon growth (IRG) and laser zone growth in a ribbon-to-ribbon (RTR) process. Other silicon technologies being investigated include the dip coating process on low-cost substrates and ingot growth by the heat exchanger method.

Most of the programs being supported under the Silicon Material Task and the Large Area Silicon Sheet Task of the LSSA Project involve the manipulation of molten silicon. In several cases (e.g., edge-defined film-fed growth and inverted ribbon growth) such high-temperature materials for use as shaping dies appear to be the limiting factor in the development of the technique. In spite of the importance of this, only minor efforts have been made to evaluate existing materials and to develop materials for this purpose and for use in vessels to contain and transport silicon. Generally, results which have been reported are inconclusive, primarily because of the failure of the investigator to properly characterize and document the history of the materials being evaluated.

There is a pressing need for materials evaluation and development programs by which various high-temperature materials may be processed and evaluated for their use as components in direct contact with molten silicon. Molten silicon is quite corrosive even to the point of being labeled a "universal solvent." A major problem with molten silicon contact material is dissolution, which results in both detrimental level impurity contamination of the silicon and changes in geometry of the refractory. There are indications that recently grown EFG silicon ribbon approximately 7.6 centimeters wide at 7.6 centimeters per minute is limited in efficiency by unintentionally induced chemical impurities

with resistance-furnace-produced EFG material (Reference 1-4). Depending on the specific application, there are many other requirements for molten Si contact materials besides very low reactivity. For example, die applications require substantial wetting by molten silicon to draw ribbons by capillary rise through a partially immersed die (Figure 1-1).

The existence of such generally opposing requirements of good wetting and low reactivity poses obvious problems. Potential problems, however, are not limited to wetting and reactivity. For dip-coated substrates, matching coefficients of expansion with silicon becomes important in order to avoid cracking the silicon layer, and crucibles used in the heat exchanger method must exhibit a lack of bonding at the ingot wall surface to prevent cracking of the silicon ingot during solidification. Silicon will expand approximately 9% by volume when it solidifies. Some general applications and requirements for these refractory materials are shown in Figure 1-2.

In view of the importance of high-temperature materials to the success of Low-Cost Silicon Solar Array (LSSA) Project, JPL initiated an in-house study of the compatibility and wetting of silicon on selected refractory materials. This report is intended to bring together all the materials-related problems as they pertain to the production of quality silicon for solar cell applications. It is hoped that this will lead to more detailed consideration of the specific material developments needed to produce cost effective cells useful for terrestrial applications.

B. WETTING BEHAVIOR

One of the oldest, most useful and convenient means of measuring wettability and obtaining information about interfacial reaction is the sessile drop experiment. Even recently, many have used this experiment in evaluating liquid-solid-vapor material systems (References 1-5 through 1-9). Quinke (Reference 1-10) made the earliest use of the sessile drop method to determine surface tension.

The wetting of a solid refractory can be quantified in terms of a wetting or contact angle θ, which is the angle formed by the tangent to the liquid surface at a point of contact with the solid (Figure 1-3). Complete wetting occurs when $\theta = 0$, partial wetting when $0 < \theta \leq 90^\circ$ and nonwetting when at $\theta > 90^\circ$. Industry experience in ribbon growth techniques has indicated that a contact angle of less than 80° was required for stable growth in capillary action shaping techniques.

The contact angle of a drop of liquid silicon resting on a flat substrate is determined primarily by the equilibrium between the surface tension of the solid σ_{SV}, the surface tension of the liquid σ_{LV}, and the solid-liquid interfacial surface tension, σ_{LS}. This angle is determined by the relative magnitude of these three interfacial tensions.

$$\sigma_{SV} = \sigma_{LS} + \sigma_{LV} \cos\theta \qquad (1)$$

Equation (1) always applies as long as σ_{SV}, σ_{LS}, σ_{LV} refer to the conditions at the time of measurement -- but not necessarily to the pure

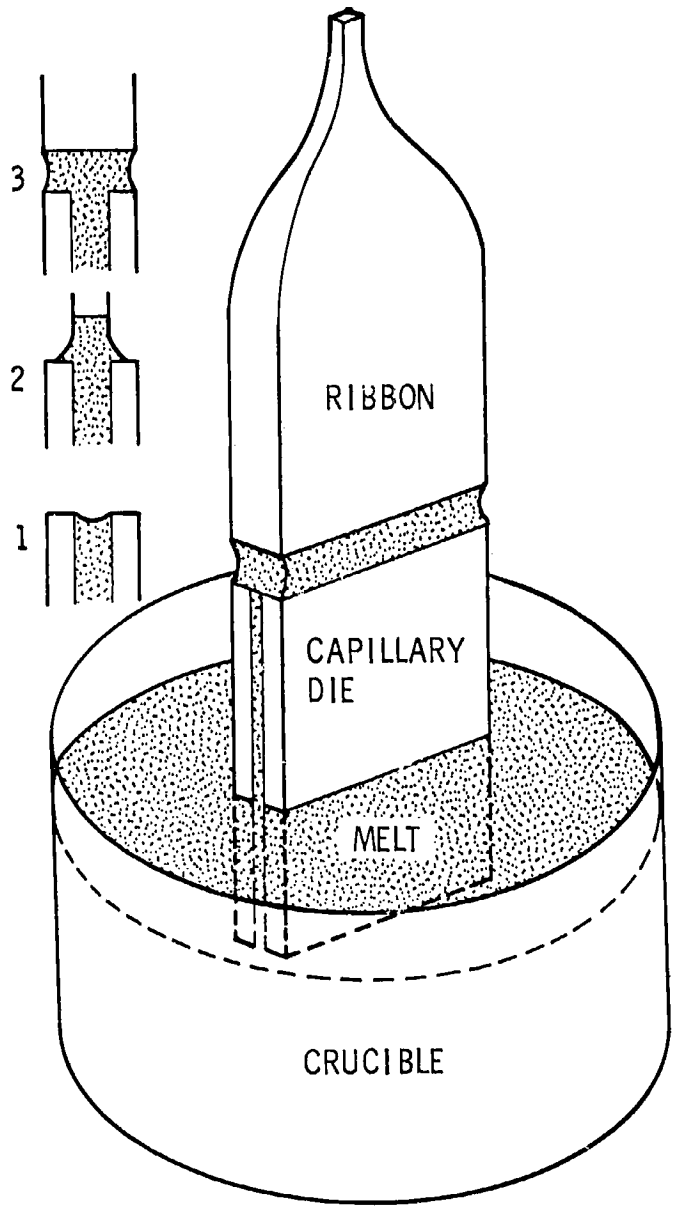

Figure 1-1. Schematic View of Edge-Defined Film-Fed Growth (EFG)

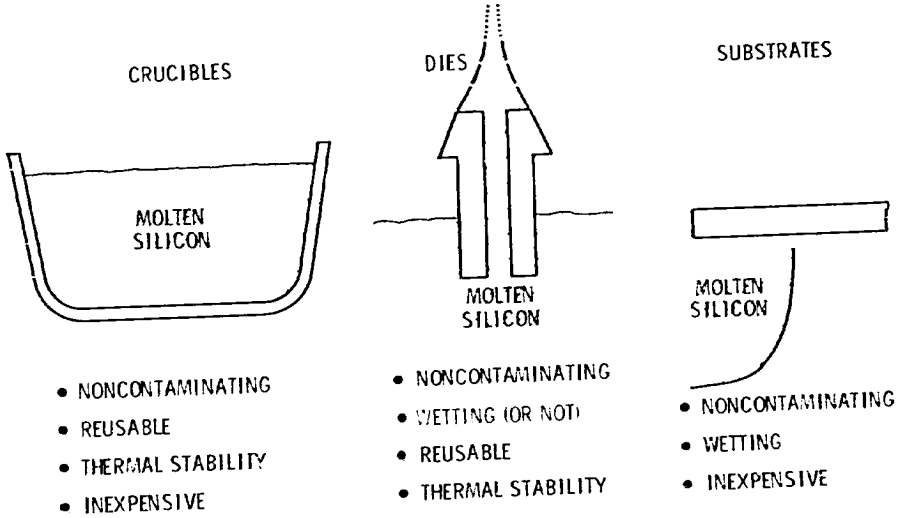

Figure 1-2. Refractory Material Applications and Requirements

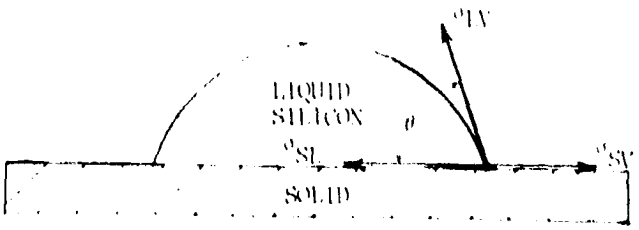

Figure 1-3. Schematic of Contact Angle of Liquid Drop on Solid Surface

materials that were started with. A complete analysis of wetting behavior is in general more complex than indicated by Equation (1) because the solid, liquid and interface energies are different in the mutually saturated condition than for the initially pure phases. In general, the solid, liquid and interface energies may each be affected by changing composition, and cases of both "delayed" wetting and of initial spreading followed by "dewetting" are known to occur (Reference 1-11).

Aksay et al. (Reference 1-12), who extended wetting analysis to nonequilibrium conditions, treated the thermodynamics of wetting in a solid-liquid-vapor system by considering the conditions that minimize the total free energy of the system. They showed that an interfacial reaction resulted in the lowering of the solid-liquid interfacial tension by a contribution of the free energy of the reaction which could result in the spreading of a liquid drop on a solid substrate.

Kingery (Reference 1-11) reminds us that in evaluating wetting behavior in various systems the pertinent factor of interest is $\sigma_{LV} \cos\theta$. He states that neither the surface tension nor the contact angle alone is sufficient for a comparison between different materials or conditions. It must be noted, however, that contact angle measurements conducted on material systems, wherein the only variable is the substrate material, remain a viable method for relative comparison in degrees of wetting. Sessile drop experiments that were conducted during this study all were exposed to the same environmental conditions (except for substrate).

The amount of capillary rise of liquid silicon in a vertical die slot is an important factor in choosing a viable die material for EFG-type ribbon growth. The maximum height H that can be filled between two vertically smooth, perfectly flat plates having a separation D is given by:

$$H = \frac{2\ \sigma_{LV} \cos\theta}{\rho g D} \qquad (2)$$

when this height is reached, the pressure due to surface tension is equal to the hydrostatic pressure (Figure 1-4). The driving force causing the liquid to flow up into the die is therefore directly proportional to the surface tension times the cosine of the contact angle. Difficulties arise in the use of Equation (2) with silicon

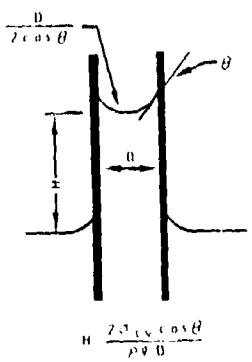

Figure 1-4. Rise of Liquid in Capillary Die

since the solvent action of molten silicon causes impurity element contamination which may appreciably change its surface tension.

Assuming that a given die configuration is capable of producing and maintaining a capillary column of silicon 1 cm x 0.001 cm to a height of at least 2.5 cm and a σ_{LV} for silicon of 720 dyne/cm (Reference 1-13), we can calculate a required contact angle θ:

$$\theta \leq \cos^{-1} \frac{H\rho gD}{2\ \sigma_{LV}} \qquad (3)$$

$$\theta \leq 87.73^{\circ}$$

It is interesting and important to note that even a 50% decrease in the silicon surface tension (σ_{LV}) will lower the minimum required contact angle to only approximately 85.5°. It appears that any material exhibiting even slight wetting characteristics has potential use in capillary die applications. However, in allowing for imperfect die surface conditions (i.e., roughness), a minimum required contact angle of approximately 80° has been used as a criterion.

C. EFFECT OF IMPURITIES IN SILICON

The unintentional contamination of molten silicon with detrimental levels of impurity elements is believed to be a major limiting factor in attempts to reach the theoretical photoelectrical conversion efficiency for silicon (approximately 22%). Mobil-Tyco has concluded, after many experiments, that chemical impurities play a significant role in degradation of conversion efficiency in EFG ribbon material. In view of this factor, programs to investigate the effects of various processes, metal contaminants, and contaminate-process interactions on the performance of terrestrial solar cells are in progress (Reference 1-14).

Solar cell performance is strongly influenced by the nature and concentration of centers such as chemical contaminants or lattice defects which act as sites for carrier recombination. Westinghouse studies have related cell performance to total measured impurity content, although in fact the impurities may be present in a variety of forms such as precipitates or complexes of differing electrical character. The single electrical effect of several different elements is shown in Figure 1-5. It is sobering to keep in mind that approximately 5×10^{16} atoms/cc is equal to 1 ppm and that only 1 ppb of titanium in silicon is capable of reducing cell efficiency to 60% of a baseline (uncontaminated) cell. The baseline cell is a P-type silicon having an acceptor concentration in the 2.5×10^{15} to 7.0×10^{15} atoms/cc range (Reference 1-14).

Recently, Spectrolab, Inc., Sylmar, California (Reference 1-15), fabricated 39 separate lots of silicon samples into solar cells using conventional aerospace technology. The effect of known impurity concentrations on short-circuit current and efficiency was investigated. It appeared that the presence of copper acted to neutralize the harmful effects of other contaminants. Preliminary data suggests that copper may be acting as a "gettering" agent or impurity sink during diffusion processing, whereby effects of detrimental impurities (e.g., titanium) are offset. Possible synergistic effects of various "impurity" elements in silicon are an area of great interest.

H. E. Bates and M. H. Leipold (Reference 1-16) have had some preliminary experience with die materials for EFG growth of silicon. In examining the elemental materials with sufficiently high melting points (shown in Table 1-1), they found that all of the refractory and transition metals reacted with silicon to form a variety of silicides. In all these systems, the highest silicide (i.e., the one containing the most silicon) formed a eutectic with silicon. Thus, these materials appear to be excluded from consideration since they would react with and dissolve in silicon, destroying its electrical properties. However, it should be emphasized that in all cases the testing done represented available materials and fabrication technique with no attempt at optimizing chemistry, microstructure, or density. Tests with these preliminary materials indicated SiC to be the most stable carbide, Si_3N_4 the most stable nitride and BeO the most stable oxide beside SiO_2.

Table 1-2, compiled by RCA Laboratories (Reference 1-17), contains compatibility data on the reactions of possible die and crucible materials with liquid silicon. The solvent nature of molten silicon has been clearly observed.

RCA Laboratories has also had direct experience evaluating different refractory materials used in contact with molten silicon (Reference 1-18). In evaluating material for possible use in RCA's inverted ribbon growth process, a basic sessile drop test was conducted. Subsequent sections of these sessile drops were analyzed for chemical reactions and electrical degradation. 4-point probe resistance measurements were made but the values are very approximate. Table 1-3 illustrates the data obtained from these tests. These tests indicate the potential of CVD Si_3N_4 and SiO_xN_y material and otherwise show the poor performance of a variety of compounds.

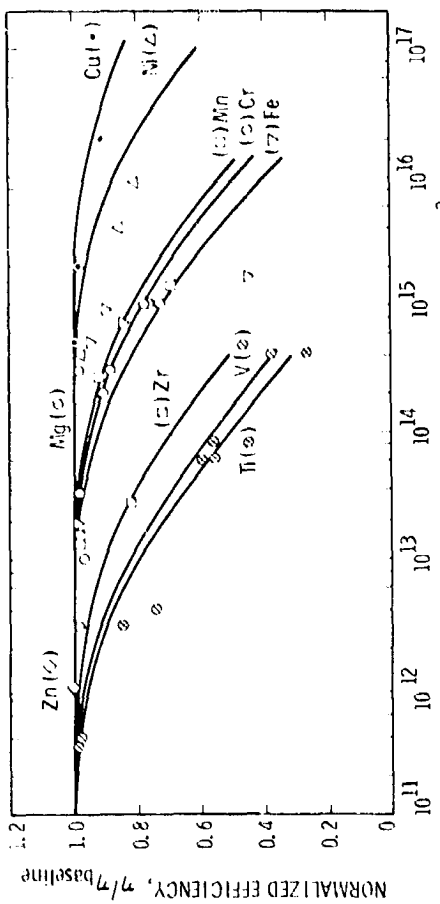

Figure 1-5. Normalized Solar Cell Efficiency as a Function of Substrate Metal Impurity Concentration: Experimental Data and Model-Derived Curves

Table 1-1. Materials Tested for Stability with Molten Silicon

SiC	Hot-pressed, polycrystalline	Haselden Corp.
HfC	Hot-pressed, polycrystalline	Haselden Corp.
WC	Hot-pressed, polycrystalline	Haselden Corp.
AlN	Hot-pressed, polycrystalline	Haselden Corp.
TiN	Hot-pressed, polycrystalline	Haselden Corp.
WB_2	Hot-pressed, polycrystalline	Haselden Corp.
$MoSi_2$	Hot-pressed, polycrystalline	Kanthal Corp.
Si_3N_4	Hot-pressed, polycrystalline	Cerac/Pure Inc.
BeO	Pressed and sintered	Brush-Wellman Corp.
ThO_2	Pressed and sintered	Haselden Corp.
ZrO_2	Pressed and sintered	Haselden Corp.
Y_2O_3	Pressed and sintered	Haselden Corp.
$ThSiO_4$	Powder	Cerac/Pure Inc.
$ZrSiO_4$	Powder	Cerac/Pure Inc.

Only a limited number of materials have been used with any success as dies or containers. Silica is universally used as the crucible material for (Czochralski) growth of semiconductor grade silicon. The concentration of unintentionally added impurities found in typical Czochralski silicon crystals is shown in Table 1-4. Silica is compatible with silicon, the solubility of oxygen in silicon being 2.7×10^{18} and the liquid solubility, 2.2×10^{18} atoms/cm^3. Patel and Batterman (Reference 1-19) have shown that high-temperature aging (1,200°C) of crucible-grown silicon can cause clustering and precipitation of the oxygen incorporated during crystal growth. These defect structures act as recombination sites (Reference 1-20), causing electrical degradation.

For general information, Tables 1-5 and 1-6 have been included to show qualitative behavior of various metal impurities in silicon and a compiled list of effective segregation coefficients, respectively.

Much more work is needed to fully characterize the effect of impurities in silicon. The relation between impurities, generated silicon structure and resulting electrical efficiency is in need of critical evaluation.

Table 1-2. Reaction of Possible Die and Crucible Materials With Liquid Silicon

Material	Preparation	Temp. Tested, °C	Contact Angle, °	Reaction at Interface
C	Molded[a]	~1430	35	SiC formation[b]
	Vitreous carbon[a]	~1430	43[c]	Formation of small SiC crystallites[b,c,d];
	Pyrolytic graphite	~1430		Rapid infiltration and disappearance of silicon
SiC	Self-bonded[a] and hot-pressed[a]	1430	40[b]	Dissolution to some extent; penetration along grain boundary[b,d]
SiC + 10% SiO_2	Hot-pressed[a]	1430		Dissolution became less than SiC itself; penetration into bulk[e]
SiO_2	Fused silica[a]	1430	~87	Erosion due to formation of volatile SiO
SiO_2 + 3% C	Hot-pressed[a]	1430	~55[f]	Erosion and SiC formation[c]
SiO_2 + 3% Si_3N_4	Hot-pressed[a]	1430		Erosion and penetration into bulk[c]
Si_3N_4	Hot-pressed[a]	1430	~80[g]	Appearance of reaction layer[d]

Table 1-2. Reaction of Possible Die and Crucible Materials With Liquid Silicon (Continuation 1)

Material	Preparation	Temp. Tested, °C	Contact Angle, °	Reaction at Interface
Si_3N_4	Reaction sintered	1430	~35[g]	Recrystallization and β-Si_3N_4 crystallite formation at interface; penetration into bulk
Si_3N_4 + 10% SiO_2 + 10% C	Hot-pressed	1450		Completely infiltrated with Si[h]
BN	Hot-pressed[a]	1430	105	Formation of β-Si_3N_4; dissolution of grains[d]
	Pyrolytic	1430	110[i]	β-Si_3N_4 formation[i]
AlN	Hot-pressed	1450		Penetration into bulk; Al-Si eutectic formed along grain boundary[k]
BeO	Pressed and sintered[a] at 1850°C	1600	76[j,k]	Slight corrosion; no new phase; slight penetration along grain boundary[c]
Al_2O_3	Pressed and sintered at 1850°C	1600	100[j,k]	Interfacial film on surface[l]

Table 1-2. Reaction of Possible Die and Crucible Materials With Liquid Silicon (Continuation 2)

Material	Preparation	Temp. Tested, °C	Contact Angle, °	Reaction at Interface
MgO	Pressed and sintered at 1850°C	1600	95[j,k]	Definite interfacial layer (Mg_2SiO_4)[a]
ThO_2	Pressed and sintered at 1850°C	1600		Corrosion at surface[l]
	Hot-pressed and sintered	1450		Erosion and penetration; eutectic between Si and new phase ($ThSiO_4$)[a]
ZrO_2	Pressed and sintered at 1850°C	1600	96[j,k]	Interfacial layer of new phase ($ZrSiO_4$)[a]
ZrO_2 (CaO stabilized)	Hot-pressed and sintered	1450		Penetration into bulk; $ZrSiO_4$ formed[b]
ZrO_2 (Y_2O_3 stabilized)	Hot-pressed and sintered	1450		Penetration into bulk; $ZrSiO_4$ formation[a]
TiO_2	Pressed and sintered at 1600°C	1600	107[j,k]	Slight reaction with decrease in porosity near surface; no new phase[l]
Y_2O_3	Hot-pressed and sintered	1450		Erosion and penetration; two new phases formed[b]

Table 1-2. Reaction of Possible Die and Crucible Materials With Liquid Silicon (Continuation 3)

Material	Preparation	Temp. Tested, °C	Contact Angle, °	Reaction at Interface
$ZrSiO_4$	Powder	1430		About 1% Zr found in the last-to-freeze Si[f]
$ThSiO_4$	Powder	1430		About 1% Zr found in the last-to-freeze Si[f]
TiB_2	Hot-pressed[a]	~1430		Not durable in liquid Si[d]
ZrB_2	Hot-pressed[a]	~1430		Not durable in liquid Si[d]
B_4C	Hot-pressed[a]	~1450		Durable in liquid Si[d]

[a]Tested or being used as die in EFG, Stepanov, or inverted Stepanov.

[b]Whalen, T. J., Anderson, A. T., J. Am. Ceram. Soc., 58, 396, 1975.

[c]Bates, H. E., et al., "Thick Film Silicon Growth Techniques," Seventh Quarterly Progress Report, NAS 7-100/JPL-953365, Nov. 1975.

[d]Schwuttke, G. H., Ciszek, T. F., and Kran, A., "Silicon Ribbon Growth by a Capillary Action Shaping Technique," Quart. Progress Report No. 2, JPL-954144, Dec. 15, 1975.

[e]Bates, H. E., Cocks, F. H., and Mlavsky, A. I., "Thick Film Silicon Growth Techniques," First Quarterly Progress Report, NAS 7-100/JPL-953365, May 1972.

Table 1-2. Reaction of Possible Die and Crucible Materials With Liquid Silicon (Continuation 4)

[f]Bates, H. E., et al., "Thick Film Silicon Growth Techniques," Eighth Quarterly Progress Report, NAS 7-100/JPL-953365, Feb. 1974.

[g]Duffy, M. T., and Kim, K. M., unpublished results.

[h]Bates, H. E., et al., "Thick Film Silicon Growth Techniques," Sixth Quarterly Progress Report, NAS 7-100/JPL-953365, Aug. 1973.

[i]Kim, K. M., et al., "Silicon Ribbon Growth by the Inverted Stepanov Technique," Quarterly Progress Report No. 1, ERDA/JPL-954465-76/1, June 1976.

[j]The contact angle was measured at 1450°C.

[k]Humenick, M., Jr., and Kingery, W. D., J. Am. Ceram. Soc., 37, 18, 1954.

[l]Economos, G., and Kingery, W. D., J. Am. Ceram. Soc., 36, 403, 1953.

Table 1-3. Data From Sessile Drop Tests (RCA)

Material	Si Resistivity, ohm-cm	Comments
TiC (HP)	-	Porous, Si absorbed, reacted interfacial layer
ZrC (HP)	-	Porous, Si absorbed
HfC (HP)	-	Porous, Si absorbed
TaC (HP)	-	Reacted with Si completely
TiN (HP)	-	Deep penetration of Si in TiN and formation of another phase in Si
ZrN (HP)	Too low to measure	Deep penetration of Si with formation of reaction zone in ZrN
AlN (HP)	Too low to measure	Deep penetration of Si with possible formation of another phase along the boundary region of Si
AlN + 5% SiC (HP)	Too low to measure	Particulate erosion with precipitation in Si of a crystalline phase, possibly SiC
Si_3N_4 (reaction sintered)	0.2	Particulate erosion with formation of blocky crystals in Si
TiO_2 (conventionally sintered)	Too low to measure	Extensive reaction

Table 1-3. Data From Sessile Drop Tests (RCA) (Continuation 1)

Material	Si Resistivity, ohm-cm	Comments
ZrO_2 (conventionally sintered)	0.2	Penetration of Si with probable formation of another phase in ZrO_2
HfO_2 (single crystal)	Too low to measure	Formation of another phase in Si along boundary with HfO_2
ThO_2 (HP)	Too low to measure	Slight penetration of Si and formation of eutectic phase in Si
LaB_6 (HP)	Too low to measure	No apparent reaction
$MoSi_2$ (HP)	-	Si absorbed
Vitreous carbon	0.8	Interfacial phase formed
CVD Si_3N_4 on vitreous carbon	8.4	CVD layer cracked, Si penetration at cracks
CVD SiC	Too low to measure	Interfacial reaction with formation of another phase, probably SiC
CVD Si_3N_4/ RS Si_3N_4	18-34	After 4 hours at 1440°C
CVD SiO_xN_y/ RS Si_3N_4	2.8-8	After 4 hours at 1440°C

Table 1-3. Data From Sessile Drop Tests (RCA) (Continuation 2)

Material	Si Resistivity, ohm-cm	Comments
CVD SiO_xN_y/ RS Si_3N_4	0.2-0.8	After 22 hours at 1440°C

The silicon used in these tests was "Hyper-Pure" material (from Dow Corning Corporation) with a $\rho > 1000\,\Omega$-cm. The duration of the sessile drop tests was 30 min. in all cases except for the last three samples shown in the table. The resistivities shown here are approximate values.

HP = hot-pressed.

RS = reaction-sintered.

CVD = chemical vapor deposited

Table 1-4. Concentrations of Unintentionally Added Impurities in Typical Czochralski Silicon Crystals (Reference 1-14)

Impurity	Concentration, atoms/cm3	(ppba)
Sb	1.3 x 1011	(0.0026)
As	7 x 1012	(0.14)
Cr	2 x 1012	(0.04)
Cu	5 x 1012	(0.1)
Au	1 x 109	(0.00002)
Fe	5 x 1013	(1)
Ni	5 x 1012	(0.1)
Ti	8 x 1013	(1.6)
Zr	3 x 1013	(0.6)

Table 1-5. Qualitative Behavior of Metal Impurities in Silicon (Reference 1-14)

Impurity Elements	Diffusion Rate	Solid Solubility at Melting Temperature	Precipitation Rate	Gettering Rate	Degradation of Cell Efficiency
Cu, Ni	Fast	High	Fast	Fast	Low
Cr, Mn, Fe	Medium	Low	Slow	Slow	High
Al	Slow	High	Negligible	Very slow	Medium
Ti, V	Medium-slow	Low	Slow	Slow	High

Table 1-6. Segregation Coefficients

Element	Segregation Coefficients	
	Westinghouse (Reference 1-14)	F. A. Trumbore (Reference 1-21)
Al[a]	$3 \times 10^{-2}/2.8 \times 10^{-3}$	2×10^{-3}
As	-	0.3
Au	-	2.5×10^{-5}
B	-	0.8
Bi	-	7×10^{-4}
C	0.05	-
Co	-	8×10^{-6}
Cr	1.1×10^{-5}	-
Cu	6.9×10^{-4}	4×10^{-4}
Fe	6.4×10^{-6}	8×10^{-6}
Ga	-	8×10^{-3}
In	-	4×10^{-4}
Li	-	1×10^{-2}
Mg	3.2×10^{-6}	-
Mn	1.3×10^{-5}	-
Mo	10^{-16}	-
Ni	3.2×10^{-5}	-
P	-	0.35
Sb	-	2.3×10^{-2}
Ta	10^{-7}	-
Ti	3.6×10^{-6}	-
V	4×10^{-6}	-

Table 1-6. Segregation Coefficients (Continuation 1)

Element	Segregation Coefficients	
	Westinghouse (Reference 1-14)	F. A. Trumbore (Reference 1-21)
Zr	$<1.5 \times 10^{-7}$	-
Zn	$\sim 10^{-5}$	$\sim 1 \times 10^{-5}$

[a]Value of 2.8×10^{-3} is based on resistivity while value of 3×10^{-2} is based on SSMS.

SECTION II

EXPERIMENTAL PROCEDURE AND TEST SETUP

The basic experiment conducted involved measuring the wetting or contact angle of drops of molten silicon on various solid refractory substrates at a temperature just above the melting point of silicon. Post-test analyses involved the measurement of the amount, mode and manner of interface reactions as well as documentation of phase and chemical changes that occurred in the silicon or substrate during the test.

An N-type, single-crystal, Czochralski grown silicon with a 1-0-0 orientation was supplied by Wacker Chemical Corp. This material had a resistivity rating of 62-86 ohm-cm. Silicon test samples were obtained by diamond core drilling 6.35-mm-diameter coupons from the 6.35-mm-thick, 50.8-mm-diameter silicon disc blanks. These samples were chemically cleaned in concentrated HF, weighed and stored in a desiccator.

Refractory substrates tested varied in overall size and thickness but were all mechanically ground to provide flat, parallel surfaces and polished to a 15μ finish, unless otherwise indicated in data tables. Each substrate test surface condition was documented at 40X magnification. The refractory test samples were vacuum-furnace-baked at 2400 $\pm$ 10^{o}C for approximately 2 hours, then weighed and stored in a desiccator.

In the laboratory tests all silicon and refractory substrates were heated to 1430 $\pm$ 10^{o}C in a modified crystal growing furnace (Figure 2-1) with a flowing helium atmosphere and allowed to stabilize for 10-15 minutes. Then photographs were taken at 1-min intervals for time periods varying from 20 to 35 min. Helium in silicon has a calculated diffusion constant D_0 of 0.026 cm^2/sec and a solubility S (atm^{-1} cm^{-3}) of 6.5 x 10^{14} exp (-11000/RT) but is electrically inactive in silicon (Reference 2-1).

A motor-driven 35mm single-lens reflex camera with bellows extension and a 135mm, f/2.8 lens with a neutral density filter (ND.6) (Figure 2-2) permitted 3/4 - 1X magnification photographs to be taken at selected time intervals through the use of an intervalometer. Subsequently, visual measurement of wetting angles were made directly from enlarged prints of selected frames, using a protractor (Figure 2-3). Kodak black and white films Tri X, Plus X, and HC-110 were all used successfully. HC-110 gave the best contrast results.

Post-test analyses required sections to be taken through the solidified sessile drop/substrate (Figure 2-4) and mounted for materialographic studies. The results of those studies are discussed within this report for each class of material.

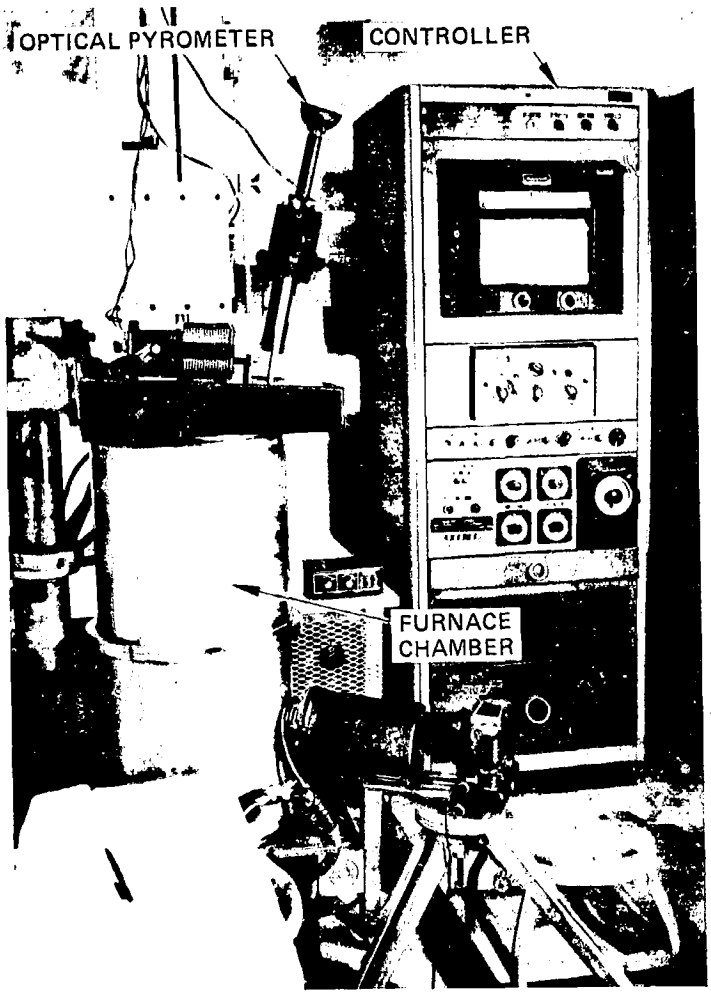

Figure 2-1. Modified Crystal-Growing Furnace and Test Setup Showing Control Panels, Optical Pyrometer, Furnace, 35-mm Camera and Intervalometer

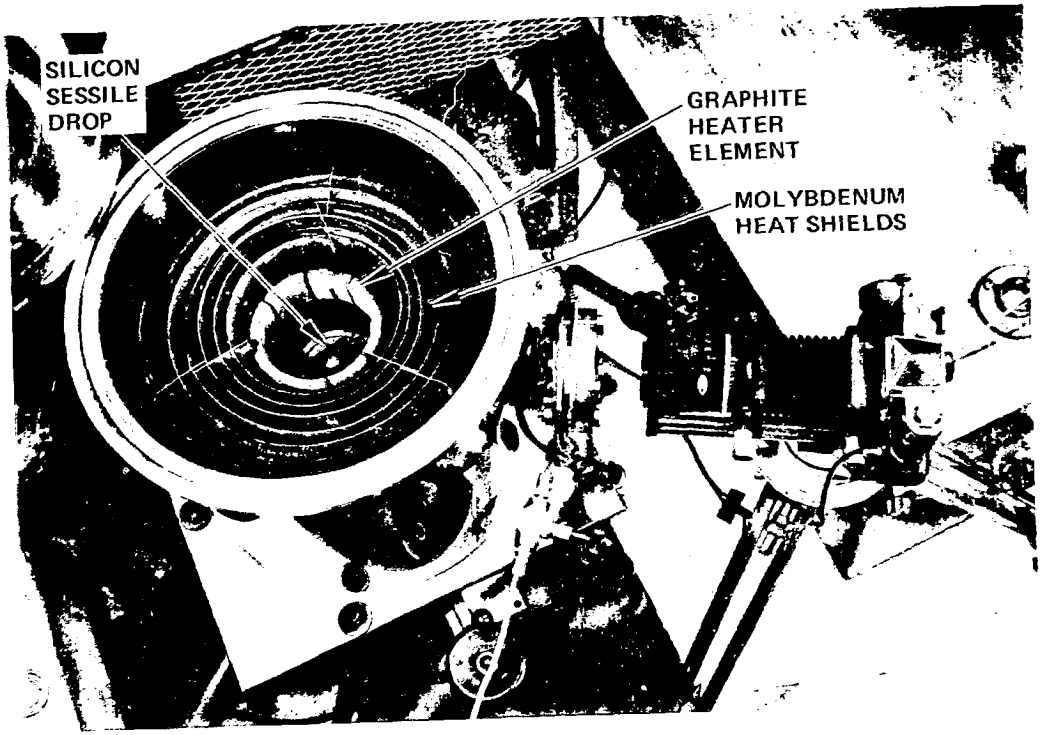

Figure 2-2. Top View, Looking Into Bottom Furnace Chamber, Which Shows Sessile Drop Sample Surrounded by a Graphite Heater Element and Molybdenum Heat Shields. Also Shown Is an External Aligned 35-mm Camera. Distance From Sessile Drop to Front of Camera Lens is Approximately 35.5 cm (14 in.)

Figure 2-3. Profile Photograph of Liquid Drop of Silicon (1430 $\pm 10^{\circ}$C) on Slip-Cast Fused Silica Substrate. Lines on Silicon Drop Are Reflections of Gaps in Surrounding Graphite Heater Elements; Approx. Mag. 5X

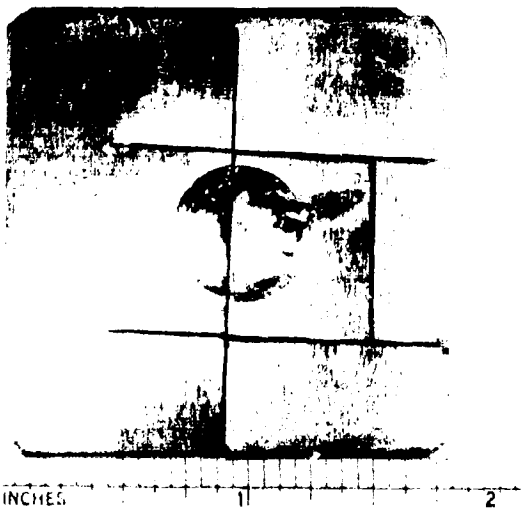

Figure 2-4. Example of Post-Test Sectioning Layup of Substrate/Silicon Drop

SECTION III

REFRACTORY MATERIALS

The essential relationship between the processing of materials and their resulting properties has grown in importance in recent years. Refractory materials can now be produced in varieties and by processes which were not practical a few years ago. Significant testing and evaluation of these refractory materials for use in specific applications, such as ribbon dies and containers for molten silicon, has not yet been accomplished, especially to relate unique processing variables with resultant silicon compatibility properties. The sessile drop experiments conducted in this study are a first step toward determining the compatibility of currently available refractory materials with molten silicon.

Table 3-1 shows the test refractory materials grouped according to fabrication techniques:

Table 3-1. Test Refractory Materials

Material	Fabrication Technique			
	Chemical Vapor Deposited	Hot Pressed	Reaction Sintered	Other
Silicon carbide (SiC)	X	X		X
Glassy carbon (C)	X			X
Graphite (C)	X			
Silicon nitride (Si_3N_4)		X	X	
Si-Al-O-N (B', 8H, 15R and polyphase)		X		
Boron nitride (BN)	X	X		
Black glass ($C \cdot SiO_2$)		X		
Silica (SiO_2)				X

Table 3-1. Test Refractory Materials
(Continuation 1)

Material	Fabrication Technique			
	Chemical Vapor Deposited	Hot Pressed	Reaction Sintered	Other
Mullite ($3Al_2O_3 \cdot 2SiO_2$)			X	
Sapphire (Al_2O_3)				X
Silicon oxynitride (SiOXYN)			X	
Hafnium oxide (HfO_2)	X			
Hafnium carbide (HfC)	X			
Yittrium oxide (Y_2O_3)		X		
Cerium sulphide (CeS)		X		
Lanthanum hexaboride (LaB_6)		X		

SECTION IV

MATERIAL CHARACTERIZATION AND TEST RESULTS

A. SILICON CARBIDE (SiC)

Lab No.	Supplier	Process	Density gm/cc	Contact Angle
SD-1	Norton	Hot-pressed (Norac 31)	3.28	40 ± 3°
SD-2	Norton	Hot-pressed (Norac 31)	3.28	38 ± 3°
SD-3 and 4	UKAEA	Siliconized (Refel)	3.10	No angle[a]
SD-5 and 6	Carbo-rundum	Siliconized (KT)	3.10	No angle[a]
SD-7	Ultramet	Vapor-deposited	-	40 ± 2°
SD-34	Norton	Recrystallized (Crystar HD430)	3.06	No angle[a]

[a]Silicon absorbed into specimens.

General Properties

Structure:	cubic + hexagonal beta SiC (cubic) transforms to alpha SiC (hexagonal) above 1650°C
Density	3.20 g/cm^3
Specific heat	210.5 J/kg-K @ 21°C (0.163 Btu/lb-F @ 70°F) 390 J/kg-K @ 1096°C (0.302 Btu/lb-F @ 2000°F)
Thermal conductivity	53.4 W/m-K @ 21°C (100 Btu/hr-ft F @ 70°F)
Linear thermal expansion	0.16 @ 316°C (600°F) 0.55 @ 1096°C (2000°F)

1. Hot-Pressed

Hot-pressed SiC (Norac 31, SD-1, and SD-2) was manufactured by Norton Company, Worcester, Mass., by a fabrication technique wherein the ceramic material was simultaneously subjected to temperatures in excess of 1600°C and pressures exceeding 13.79 x 10^6 N/m^2 (2000 psi). No oxide additives were used to promote densification. The substrate material consisted of voids and three distinguishable phases which appeared to be SiC and small amounts of free carbon and silicon.

a. Sessile Drop Tests. High-bulk density SiC (SD-1 and SD-2) exhibited good wetting (~40°, Figure 4-1), consistent with previously published data (Reference 4-1).

b. Compatibility. Examination of materiallographic sections of SD-1 and SD-2 revealed: (1) an interface that appeared clean and essentially two-phase, silicon/SiC (Figure 4-3), (2) fine particles of SiC, 2.5 to 12.5 microns (approximately 0.0001 to 0.0005 inch) in size, distributed near and along the free surface of the silicon drop (Figures 4-2 and 4-3), and (3) some evidence of grain boundary impurity phases in the silicon matrix (Figure 4-2).

In the family of SiC products tested and evaluated, hot pressed material seemed the most promising. There appeared to be fewer and smaller SiC particles than had been observed in silicon melted on other SiC products. However, the quantity of SiC in silicon solar cells that can be tolerated without decreasing efficiency excessively has not been established.

2. Siliconized

Refel SiC (SD-3 and SD-4) was manufactured by United Kingdom Atomic Energy Authority (U.K.A.E.A.) at Springfield, England, from graphite powder and fine alpha SiC (Reference 4-2) which was mixed with an appropriate plasticizer and formed into shapes by means of die-pressing, extrusion or isostatic pressing. Through adjustments of graphite and SiC contents, the amount of free silicon present in the final microstructure can be controlled. However, fabrication techniques limit the remaining free silicon content to a minimum of 8%. The fabrication process consists of siliconizing, which occurs in a partially evacuated chamber, with a green-machined part placed in a pool of molten silicon. Evaporated silicon monoxide reacts with the outer surfaces of the parts at temperatures from 1600 to 1700°C. The inner surfaces of the part act as a wick through which the silicon flows by capillary action, reacting exothermically with the free graphite to form beta SiC. This beta phase bonds the fine alpha grains together, leaving an excess of silicon in a continuous matrix through the structure. The Refel SiC used in this wetting experiment consisted of a relatively fine-grained structure with roughly 30% free silicon and 5% void content (Figure 4-4).

The KT SiC (SD-5 and SD-6) was manufactured by the Carborundum Company, Niagra Falls, New York, and was formed by a method similar to Refel. Mixtures of graphite and SiC (Reference 4-3) plasticized with carbon-bearing binders are formed into a variety of shapes by extrusion or pressing. This material, after curing, is heated to between 2000

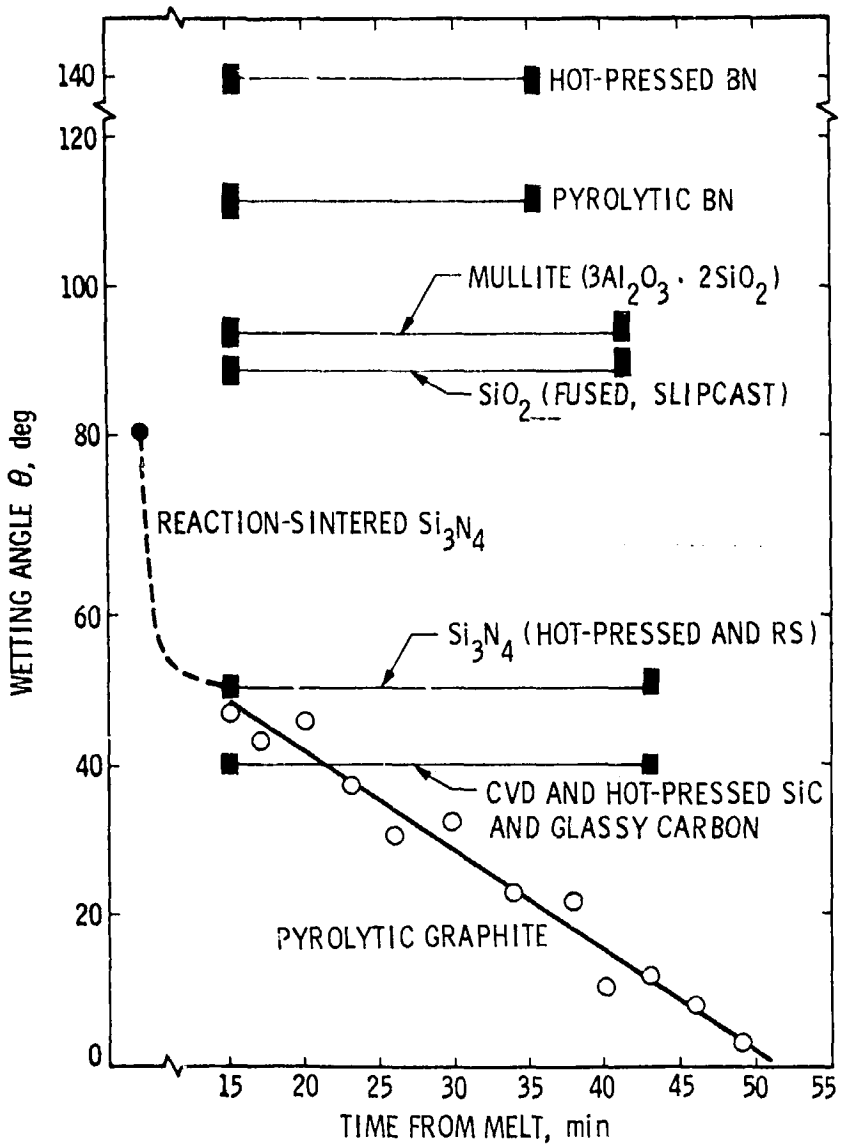

Figure 4-1. Wetting Angle vs Time From Melt for Molten Silicon (1430 ±10°C) on Various Refractory Materials

Figure 4-2. SiC Particles at Surface of Silicon Drop (Left) and Impurity Phases in Silicon Matrix (Right) for Hot-Pressed SiC, SD-1

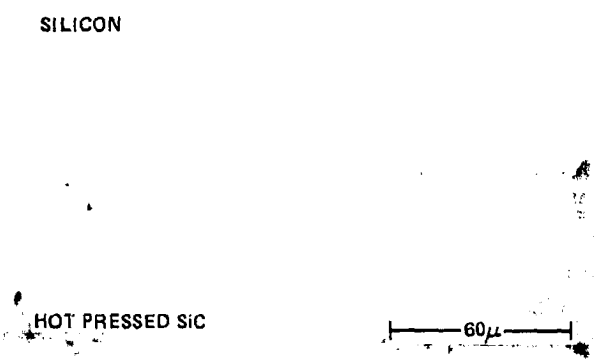

Figure 4-3. Silicon/SiC Interface, SD-1, Hot-Pressed SiC, Showing Lack of Interface Reactions

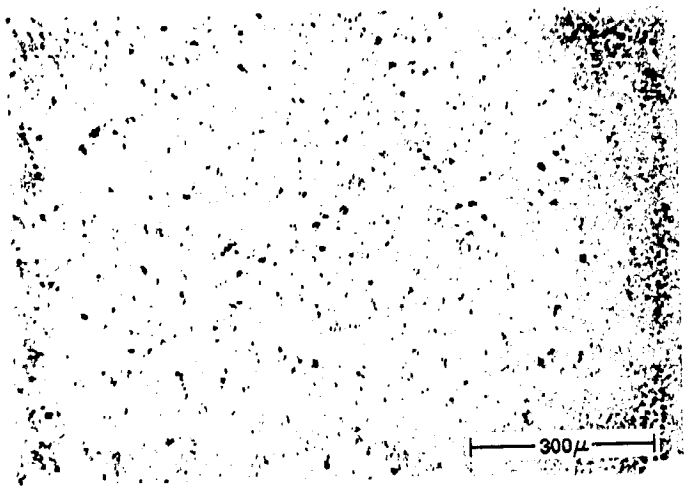

Figure 4-4. Refel SiC Structure, SD-3, as Polished

and 2250°C in an atmosphere in which vapors rising from a molten silicon pool react with the carbonaceous material and form SiC. Free silicon is dispersed throughout the microstructure and appears as a white phase in polished sections. The material used for this experiment consisted of approximately 20% free silicon and less than 5% voids (Figure 4-5).

Crystar HD 430 SiC, SD-34, was manufactured by Norton Industrial Ceramics Division, Worcester, Mass., from high-purity (99%) SiC grain and silicon. It is a recrystallized body having a small amount of inherent porosity (6 to 13%) which is filled with free silicon.

a. Sessile Drop Tests. Silicon sessile drops permeated each of these substrates (SD-3, 4, SD-5, 6, and SD-34), with excess silicon solidifying out on the bottom side. Figure 4-6 is a typical example of this phenomenon.

b. Compatibility. The types of fabrication procedures used in producing Refel, KT and Crystar HD 430 SiC intrinsically led to a structure containing a significant amount of free silicon (>5%) and porosity. This inherent presence of interconnected porosity throughout the structure, even when filled with free silicon, allowed for capillary flow of the molten silicon through the substrate.

3. Vapor-Deposited

Vapor-deposited SiC, SD-7 (Figure 4-7), was manufactured by Ultramet, Pacoima, Calif., by reducing methyltrichlorosilane at approximately 1400°C in the presence of a graphite substrate. According to the manufacturer,

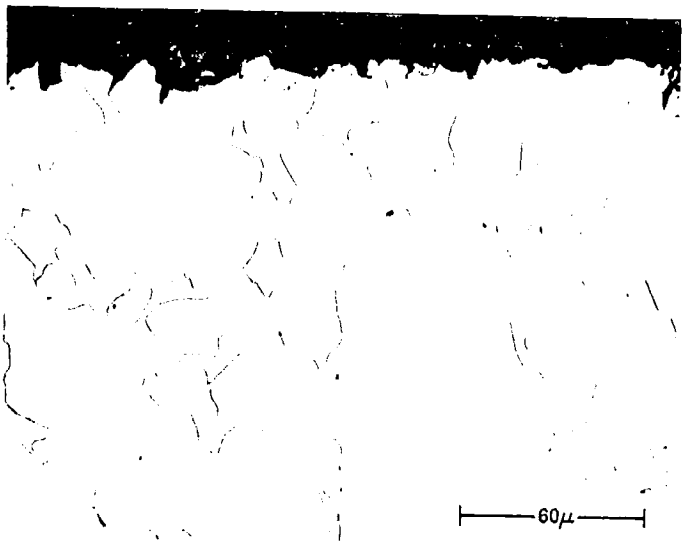

Figure 4-5. KT SiC Microstructure, SD-5 and SD-6, as Polished, Showing Free Silicon (White) and SiC (Grey)

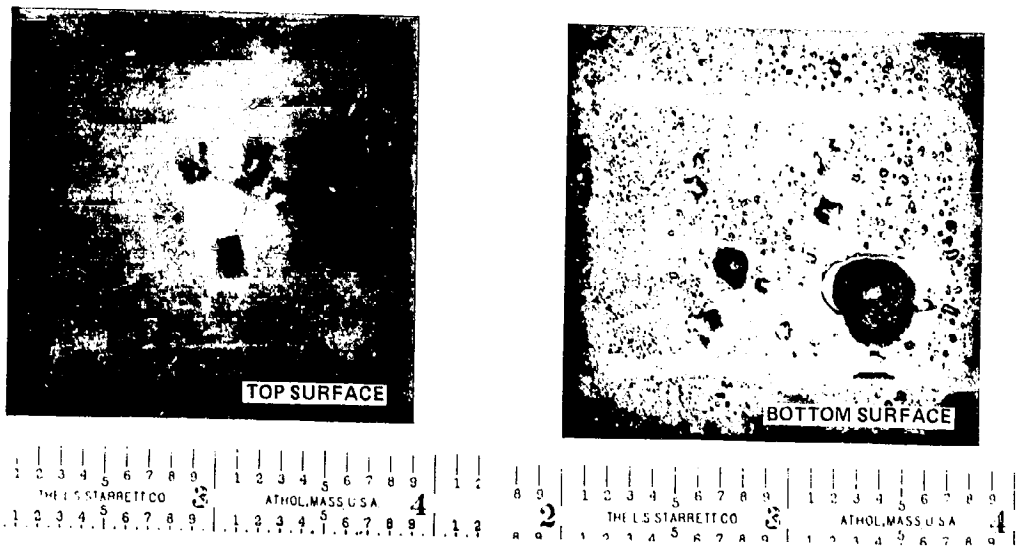

Figure 4-6. Photomacrographs of Refel SiC Substrate SD-3, Showing Silicon Penetration of Surface (Left) and Subsequent Solidification on the Bottom Surface (Right)

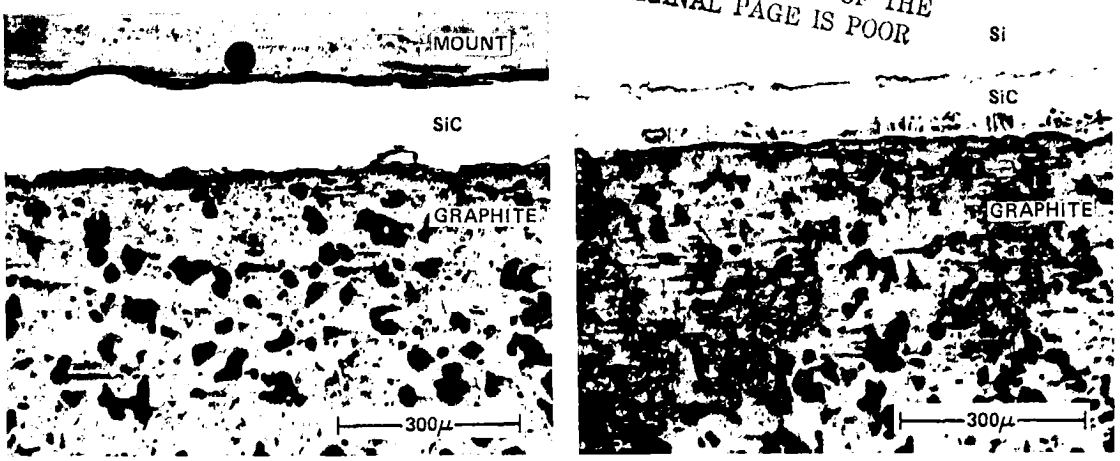

Figure 4-7. Sectional Micrographs of Vapor-Deposited iC Layer on a Graphite Substrate, SD-7, Before (Left) and After (Right) Sessile Drop Test

the deposited SiC is theoretically dense and stoichiometric if the deposition process is handled correctly.

a. Sessile Drop Test. Silicon wet this substrate at a mechanically stable contact angle of 40 ± 2° (Figure 4-1), which makes it a candidate for use in capillary ribbon shaping dies.

b. Compatibility. Materiallographic examination of the sectioned sessile drop/substrate showed a general attack of the SiC layer by the silicon (Figure 4-8). The silicon appeared to preferentially attack what might be crystallographic interfaces and formed throughout the entire deposit layer thickness as a fine network of free silicon (Figure 4-9). The nonuniform infiltration of silicon into the SiC appeared to leach out particles of this layer, which were found just off the interface surface and near the free surface of the silicon drop, ranging in size from 2.5 to 25 microns (0.0001 to 0.001 inch).

4. Discussion

Whalen and Anderson reported an equilibrium molten silicon contact angle of 40 ± 5° for both self-bonded SiC and hot-pressed SiC. These results were consistent with the work conducted at JPL. However, for the lower density (≤3.10 gm/cc) SiC products, no mechanically stable contact angle was observed. Molten silicon was drawn into these substrates and flowed through a free silicon interconnecting network in the SiC body. Subsequently, this material is of no use as ribbon-producing dies.

Recent investigators have suggested that the predominant mode of breakdown of pressed SiC powder in molten silicon is particulate

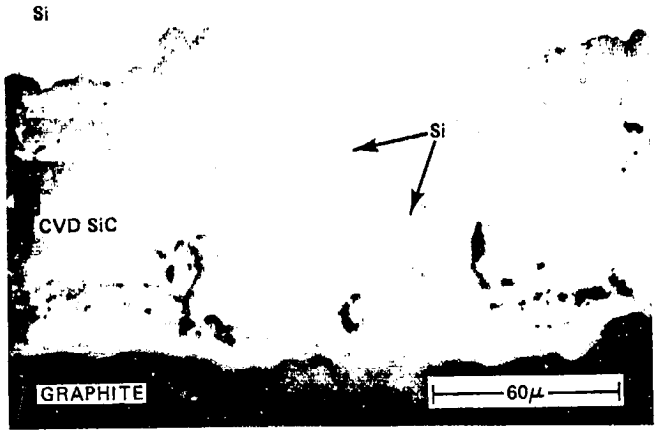

Figure 4-8. Close-up View of Attacked SiC Layer, SD-7, as-Polished, Showing Permeation of Silicon (White Phase) Into SiC (Grey Phase)

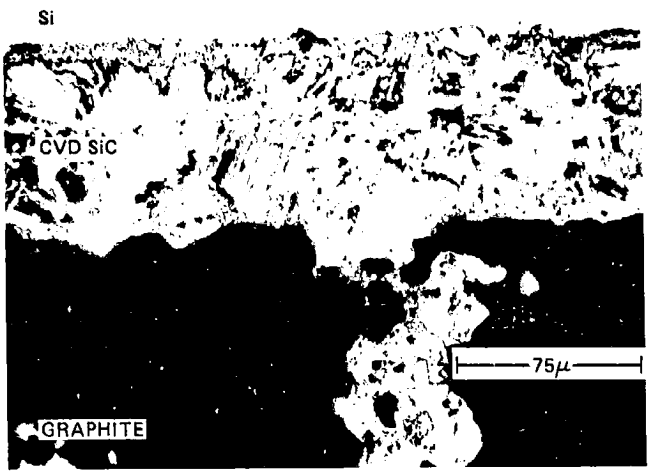

Figure 4-9. Close-up View of Attacked SiC Layer, SD-7, Electrolytic Etch, Showing Penetration Morphology of Silicon

erosion (intergranular corrosion) but admit that the ability of the material itself to resist dissolution was not clear (Reference 4-4).

All carbon and SiC substrates tested which exhibited mechanically stable contact angles imparted various amounts and sizes of β-SiC particles into the silicon. The size and presence of these particles is best explained by a particulate erosion mechanism. The apparent grain boundaries in SiC appeared to be subject to the severest attack by a molten silicon environment. The rate of attack on the Si/C bonding in SiC is felt to be much lower in comparison.

While these SiC particles are felt to be electrically inactive in and of themselves, they do cause silicon ribbon growth anomalies. SiC inclusion particles that are carried to the liquid/solid interfaces of a growing ribbon become trapped in the silicon structure. The trapped particles lead to the formation of dislocation clustering and various kinds of grain boundaries (Figure 4-10). These boundaries can be twins, low-angle and/or high-angle grain boundaries. The dislocations and boundaries formed in silicon ribbons are known to be electrically active in various degrees, causing a decrease in the final cell efficiency.

Recently, IBM has monitored the performance of a single SiC-coated graphite die. The graphite grade was Ultracarbon UT-86, and the SiC coating was applied by chemical vapor deposition. It was used to grow 17 ribbons (13 meters total), of which seven were completely free of SiC surface particles.

Commercial grade SiC typically contains small amounts of Fe, Al, W, and Ca. Semiquantitative analysis of silicon melted on HP SiC revealed the presence of all these elements. Impurity levels ranged from 170 ppm to 1300 ppm (Table 4-1). Impurity levels of this magnitude are known to be detrimental to solar cell efficiency. Since contamination from these elements is extrinsic in nature, the attainment of a higher purity HP SiC is a possible and necessary step to obtaining and maintaining purer molten silicon if these products are to be used.

One possible means of producing relatively pure SiC is by chemical vapor deposition. Semiquantitative analysis of silicon melted on CVD SiC revealed the presence of detrimental levels of Al and Mg (Table 4-1). The concentrations of these elements, however, were much lower than the level of impurities found in silicon on HP SiC. It remains to be seen whether greater quality control in the deposition process will ultimately result in significant reductions in silicon impurity contamination.

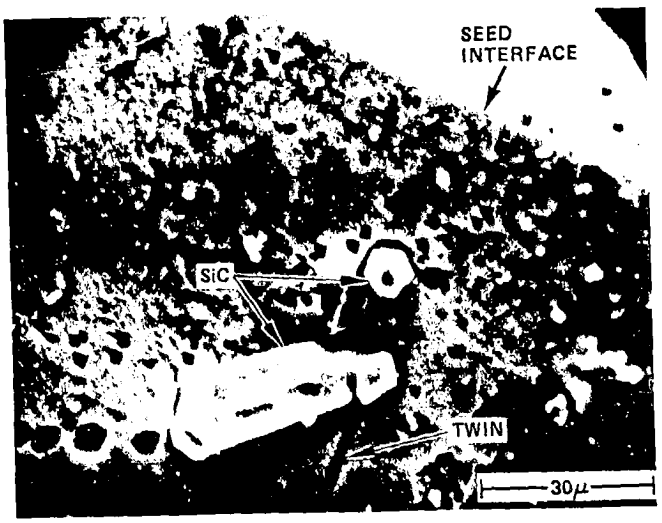

Figure 4-10. Scanning Electron Microscope Photomicrograph of SiC Particles in EFG Silicon Ribbon. Note Point and Line Defect Structure That Was Generated

B. GLASSY CARBON

Lab No.	Supplier	Process	Density, gm/cc	Contact Angle
SD-26	Tokia Electrode Corp.	Thermal decomposition and post heat	1.53	41 ± 3°
SD-27	Tokia Electrode Corp.	Thermal decomposition and post heat	1.53	40 ± 2°
SD-39	Tylan Corp.	Proprietary (Vitregraf)	---	44 ± 2°
SD-71	Fluorocarbon Co.	Cyclization and ring fusion polymers by compression, then thermal degradation (Vitrecarb)	1.47	41 ± 2°

Table 4-1. Semiquantitative Determination of Impurity Levels in Silicon Melted on Various Refractory Materials

Substrate Material	Impurity Level (ppm) in Silicon						
	Fe	Al	W	Mg	Mn	Ca	B
Glassy Carbon		80				30	
Hot-pressed silicon carbide (SiC)	230	930	1300			170	
CVD SiC		70		50		60	
Hot-pressed silicon nitride (Si_3N_4)	70	40		20			
Reaction-sintered silicon nitride (Si_3N_4)	250-660	90-120			30-730	70-390	
Hot-pressed sialon (β and 15R phase)	100-430	1500-9300	670			70-620	
Pyrolytic boron nitride (BN)							3200
Hot-pressed BN	590						1700
Hot-pressed black glass ($C \cdot SiO_2$ + B)							760
Mullite ($3Al_2O_3 \cdot 2 \cdot SiO_2$)	590 and Ti 120	6600		40		70	180

Glassy carbon material (SD-26 and SD-27), designated GC-20, was manufactured by Tokia Electrode Corp., Japan, by thermal decomposition of methyl alcohol and furfuryl alcohol ($2 - C_4H_3O - CH_2OH$), with a final heat treatment at 2000°C. This very amorphous structure had a thickness of approximately 3.2 mm (1/8 in.). Glassy carbon material (SD-39, Vitregraf) was deposited on a graphite substrate in a proprietary method used by the Tylan Corporation, Torrance, Calif. (Figure 4-11). The thickness of the coating was measured to be 500 - 750 microns (approximately 20 - 30 mils) and was found to be discontinuous and double layered in several locations (Figure 4-12). Glassy carbon material (SD-71, Vitrecarb) was produced by the Fluorocarbon Company, Anaheim, Calif., from cyclization and ring fusion polymers of the phenolaldehyde novolac and resole types, which give a high degree of crosslinking. This process results in the turbostratic lattice rather than the graphite structure.

1. Sessile Drop Tests

Wetting properties for all glassy carbon substrates were found to be very similar to those of silicon carbide material (θ of 40-44°, Figure 4-1). The degree of wetting was not observed to increase with time as has been reported for the wetting of carbon by silicon in a vacuum (Reference 4-1).

2. Compatibility

The interface reaction for all glassy carbon substrate consisted of a β-SiC precipitation, a layer growth and dissolutionment and/or cracking. In this study, the SiC layer appeared to be adhered to the carbon substrate, with SiC particles breaking off of the layer and floating into the silicon matrix (Figures 4-13 and 4-14). A significant SiC reaction layer, 20 microns (0.8 mil) thick, was observed to form at a molten SiC interface after only one minute of contact time (Figure 4-15).

C. GRAPHITE (PYROLYTIC)

Lab No.	Supplier	Process	Density, gm/cc	Contact Angle
SD-52	Union Carbide	Chemical vapor deposition	3.2	47 to 0° in 40 min

Pyrolytic graphite, SD-52, block grade HPG, was fabricated by the Carbon Product Division of Union Carbide, Cleveland, Ohio.

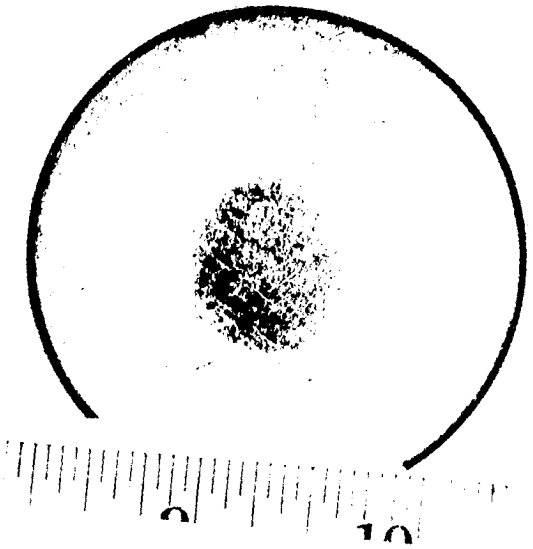

Figure 4-11. Photomacrograph of Glassy Carbon (Vitregraf) Coating on Graphite Substrate, SD-39

Figure 4-12. Photomicrographs Showing Nature of "As Received" Vitregraf Coating (White Layer) Deposited on Graphite, SD-39

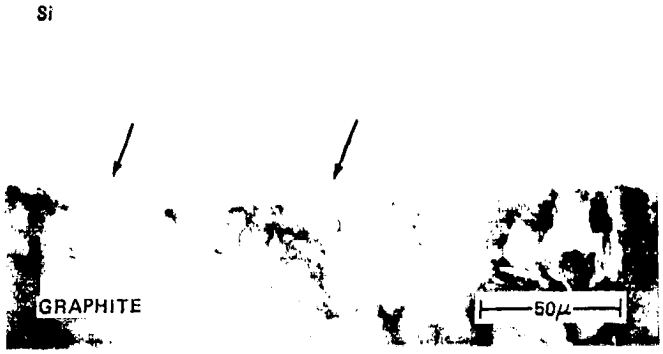

Figure 4-13. Sectional Micrograph, SD-39, of Post-Test Silicon/Discontinuous Glassy Carbon (Arrows) Interface Showing the Extent of SiC Formation

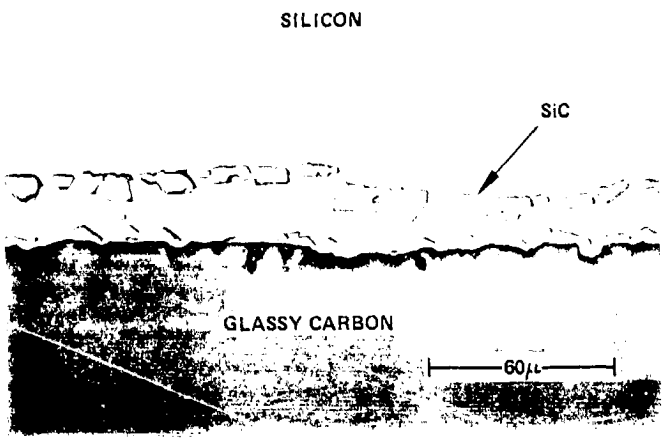

Figure 4-14. As-Polished Silicon/Glassy Carbon Interface Showing βSiC Layer and Particles

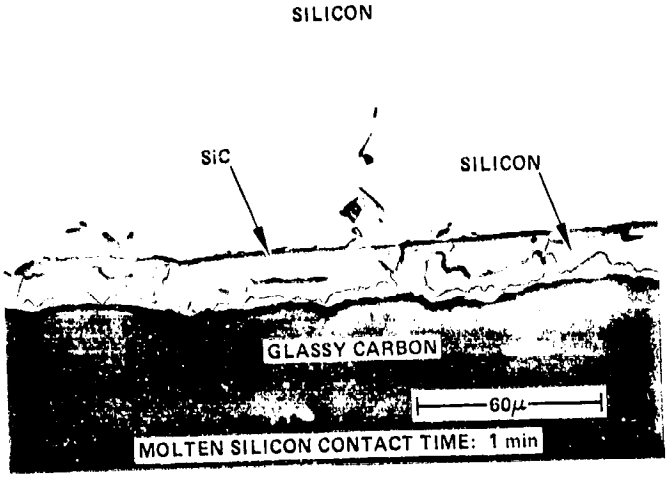

Figure 4-15. As-Polished Silicon/Glassy Carbon Interface After One Minute Contact With Molten Silicon

1. Sessile Drop Test

Molten silicon was observed to wet the graphite surface at approximately 47° after the initial 15-min contact period. Photographic results indicated the rate at which the silicon was absorbed into the substrate (2×10^{-4} gm/sec). The contact angle decreased as silicon was absorbed (Figure 4-1). It is important to note that the decrease in the contact angle from 47 to 0° in 40 min was not due to spreading. Essentially, all free silicon was being absorbed and converted to SiC. No free silicon was left on the test surface (Figure 4-16). Weak planar bonds of the pyrolytic graphite were attacked by the molten silicon, resulting in an exfoliation or delamination phenomenon (Figure 4-17). Growth of the SiC zone resulted in stresses which disrupted the deposited graphite layers.

2. Discussion (Si and C)

When molten Si contacts C, β-SiC is formed at the interface (Reference 4-5). Whalen and Anderson (Reference 4-1) state that there is abundant evidence of reaction and in some cases infiltration of the carbon by liquid silicon. Chang and Siekhaus (Reference 4-6) observed very fast diffusion rates of silicon and carbon into each other with the formation of SiC. They also proposed a diffusion mechanism whereby silicon atoms first form a carbide layer with the surface carbon atoms, followed by repeated cracking of the carbon lattice and diffusion of silicon

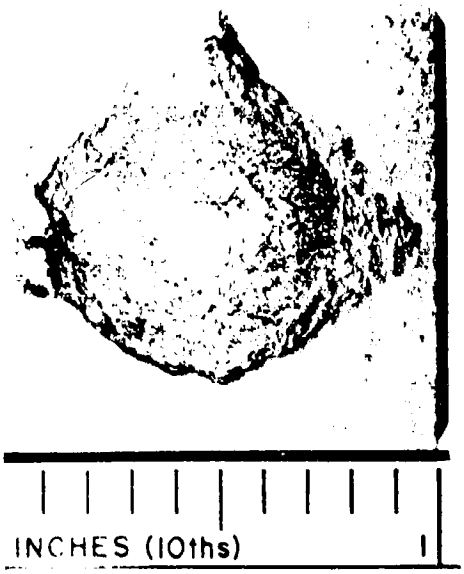

Figure 4-16. Post-Sessile Drop Test Surface, SD-52

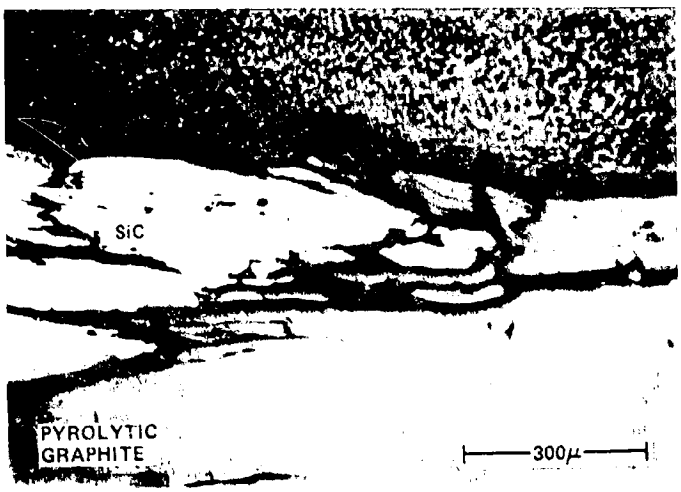

Figure 4-17. Section Taken Through Delaminated Area, Which Also Shows SiC Formation, as-Polished, SD-52

through the carbide layers. Growth of the SiC layer causes distortion of the structure, which is relieved by cracking. The interface reactions for Si and C observed in this study were qualitatively explained by this mechanism. In general, it appeared that the formation and subsequent cracking of SiC at the molten silicon/glassy carbon interface occurred more rapidly than the surface dissolution or breakdown of hot-pressed SiC in contact with molten silicon. IBM (Reference 4-7), however, has stated that the much greater SiC particle pickup from graphite (dies) than from SiC-coated graphite dies is not thought to be related to a difference in solubility. The difference was accounted for by the nature of the nucleation sites for crystallization of excess SiC from the carbon-saturated liquid silicon at the SiC die top. If the SiC die material promotes better adherence of SiC grown from solution than does graphite, then less free particulate SiC would be available in the meniscus region for incorporation in the growing ribbon. This concept has neither been verified nor disproved as yet.

Carbon which is incorporated substitutionally into silicon leads to lattice constriction. A possible result of this lattice constriction is stress-relief twinning. Twinning occurs profusely in CAST ribbons grown with carbon dies; no way to eliminate it is presently known (Reference 4-8).

To date, high-density graphite (poco grade) has been used for most silicon ribbon growth. It is not, however, completely nonreactive (Figure 4-18). Good crystallographic quality has been achieved on small, carefully grown ribbon segments (References 4-9 and 4-10), but the structure of large ribbons grown fast is full of all sorts of planar, line and point defects.

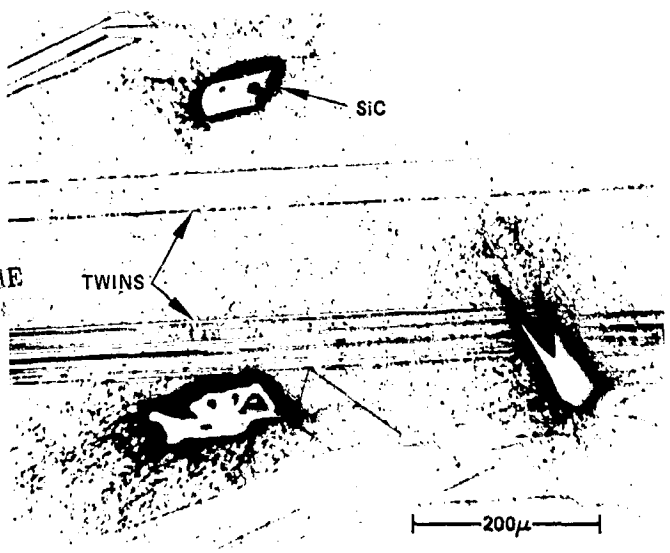

Figure 4-18. Surface of Silicon Ribbon Grown by EFG Method Using Poco Graphite Die. Note Point and Line Defects

D. SILICON NITRIDE (Si_3N_4)

Lab No.	Supplier	Process	Density, gm/cc	Contact Angle
SD-9[a]	Norton	Hot-pressed (HS-130)	3.19	46 ± 3°
SD-10	AVCO	Hot-pressed	3.18	50 ± 3°
SD-11	AVCO	Hot-pressed	3.18	52 ± 3°
SD-49[b]	KBI[c]	Hot-pressed	3.23	49 ± 2°
SD-50	KBI	Hot-pressed	3.23	50 ± 3°
SD-12	Norton	Reaction-bonded	2.50	34 ± 2°
SD-13[b]	KBI	Reaction-sintered	2.96	~110 → 68°
SD-14[b]	KBI	Reaction-sintered	2.96	~110 → 91 ± 2°
SD-15	KBI	Reaction-sintered	2.96	51 ± 2°
SD-64	Sylvania	Sintered	3.00	82 ± 3°

[a] 6μ surface finish.

[b] As fabricated surface was tested.

[c] Kawecki-Berylco Ind.

GENERAL PROPERTIES

Structure	Hexagonal
Melting point	1870°C sublimes
Density	3.2 gm/cc
Specific heat	245 J/kg-K @ 21°C (0.19 Btu/lb-F @ 70°F) 387 J/kg-K @ 1096°C (0.30 Btu/lb-F @ 2000°F)
Thermal conductivity	0.9 watts/m-K (1.7 Btu/ft-hr-F)
Linear thermal expansion%	0.03 @ 316°C (600°F) 0.28 @ 1096°C (2000°F)

Table 4-2. Typical Chemistry Data Si_3N_4 Products (wt %)

Element	Norton HS-130 (Reference 4-13)	Norton "350"	KBI
Si		98	60.4
N			37.0
Fe	0.5	0.4	0.8
Al	0.1 - 0.2	0.2	0.6
Ca	0.003 - 0.008	0.05	0.5
Na	0.004 - 0.01		---
K	0.004 - 0.008		---
Mg	0.3 - 0.4		---
O_2		0.5	

1. Hot Pressed

Si_3N_4 powder is commonly mixed with an additive and hot-pressed between 1600 - 1850°C at applied pressures less than 34.5×10^6 N/m^2 (5000 psi) (References 4-11, 12, 13) in nitrogen or inert gas atmospheres. The resultant product is a maximum-density, high-strength, beta-phase Si_3N_4 (Table 4-2).

Several investigators (References 4-15 through 4-18) have studied the sintering effects of MgO in the hot-pressing of Si_3N_4, and all reported obtaining an MgO - SiO_2 liquid grain boundary phase. M. Mitomo (Reference 4-19) further investigated the sintering of Si_3N_4 with 5% MgO and surveyed the sintering effects of other additives (5% wt). The various additives and density values obtained after fabrication are shown in Table 4-3. It is important to note that little is known about the particular effect of molten silicon on such densification additives as noted in this table. However, dissolution of Mg from hot-pressed Si_3N_4 has been observed in this program and is discussed later.

It is apparent that the wetting of Si_3N_4 by silicon is affected significantly by both temperature and pressure. Whalen and Anderson (Reference 4-1) measured a contact angle for Si on Si_3N_4 of 43° @ 1427°C (2600°F) and 10° at 1482°C (2700°F). Swartz (Reference 1-7) noted that substantial pressure effects occurred for all Si_3N_4 materials tested, but not for other materials, i.e., fused silica, graphite or vitreous carbon.

Table 4-3. Various Sintering Additives to Silicon Nitrides

Additive (5% wt)	Density	
	g/cc	% Theoretical density obtained
Y_2O_3	2.58	80.9
Al_2O_3	2.62	82.1
Y_2O_3 - Al_2O_3	2.66	83.4
La_2O_3	2.40	75.2
Ga_2O_3 - Al_2O_3	2.35	73.7
AlN - Al_2O_3	2.35	73.7

The equilibrium N_2 partial pressure over the Si/Si_3N_4 material system at the melting point of silicon is not a well-established value. However, work of several years ago (References 4-15 and 4-20) has tended to establish a value of approximately 130 - 270 N/m^2 (1-2 torr). Most experiments to date with Si_3N_4/molten silicon material systems have revealed high erosion and dissolution rates or an interfacial reaction zone for the Si_3N_4 substrate (Reference 4-4). However, only cursory attempts were made in characterizing the refractory material. In general, the impurity content of Si_3N_4 in hot-pressed or reaction-sintered forms is usually much higher than is acceptable in semiconductor technology. On the basis of this fact, it appears that dense and relatively pure Si_3N_4 coatings prepared by chemical vapor deposition (CVD) should be more compatible with silicon crystal growth. Preliminary results with CVD Si_3N_4 in contact with molten Si for an extended period of time (24 hours) indicate much less electrical degradation occurred than in similar tests with reaction-sintered and hot-pressed Si_3N_4 substrates (Reference 1-18). Continued development and evaluation of CVD Si_3N_4 in contact with molten silicon is in progress at RCA.

a. Sessile Drop Tests. Hot-pressed HS130 Si_3N_4 from Norton (SD-9), AVCO (SD-10 and SD-11) and Kawecki-Berylco Ind. (SD-49 and SD-50) exhibited little differences in wetting characteristics and bulk chemical reactions. In the first initial minutes after melt, high contact angles were observed for all these samples. The silicon drops rapidly spread to a mechanical equilibrium condition from which no kinetic

spreading was recorded. Photographs shown in Figure 4-19 illustrate the silicon sample melting and spreading on hot-pressed Si_3N_4, SD-49. The average contact angle for all hot-pressed products was 50^o. Initial high contact angles may be a function of a surface silica present or formed at the interface and may be related to the MgO-SiO_2 glassy phase which is present in the structure (References 4-14 through 4-18). Relatively successful attempts have been made to reduce the high oxygen content (SiO_2) present in starting Si_3N_4 powder by thermal treatments (Reference 4-21).

Surface or "micro" wetting was observed for silicon melted on as-fabricated surfaces but not for silicon on polished surfaces (Figure 4-20). In general, the silicon was tightly adhered to all substrates and the silicon matrix was full of cooling cracks.

b. Compatibility. Very little if any interfacial dissolution or particulate erosion was observed in the hot-pressed Si_3N_4 samples (Figure 4-21). The observed mechanical equilibrium contact angles probably indicate that the molten silicon had reached an equilibrium level in nitrogen content. This nitrogen content will tend to control the erosion rate and will influence the contact angle. It is expected that silicon containing less nitrogen than the equilibrium level will show a higher erosion rate and a higher contact angle. For the above samples the contact angle reached steady state in approximately 3 to 5 minutes.

Other observations for silicon melted on hot-pressed Si_3N_4 include:

(1) Unacceptable impurity levels of iron, aluminum and magnesium (Table 4-3).

(2) Formation of impurity phases consisting of a very few interface particles that appeared to be Si_3N_4 (Figure 4-22) and both grain boundary and matrix type precipitates (Figure 4-23).

(3) Morphology and location of the Si_3N_4-like precipitates (Figure 4-22), indicated that a nucleation and growth force existed at the test temperature (1430^oC); near the interface, nitrogen must be present in high enough concentration so that, with time, a diffusion process through the molten silicon can occur.

(4) Some second-phase precipitates did not occur in the matrix lattice, but along the grain boundaries (Figure 4-24). These precipitates did not occur continuously with time in a given region, but discontinuously when the grain boundary passed through this region on cooling (Reference 4-22). Energy dispersive analysis of X-ray (EDAX) readings performed on the grain boundary phase revealed the presence of a high Al, low silicon and very low copper content.

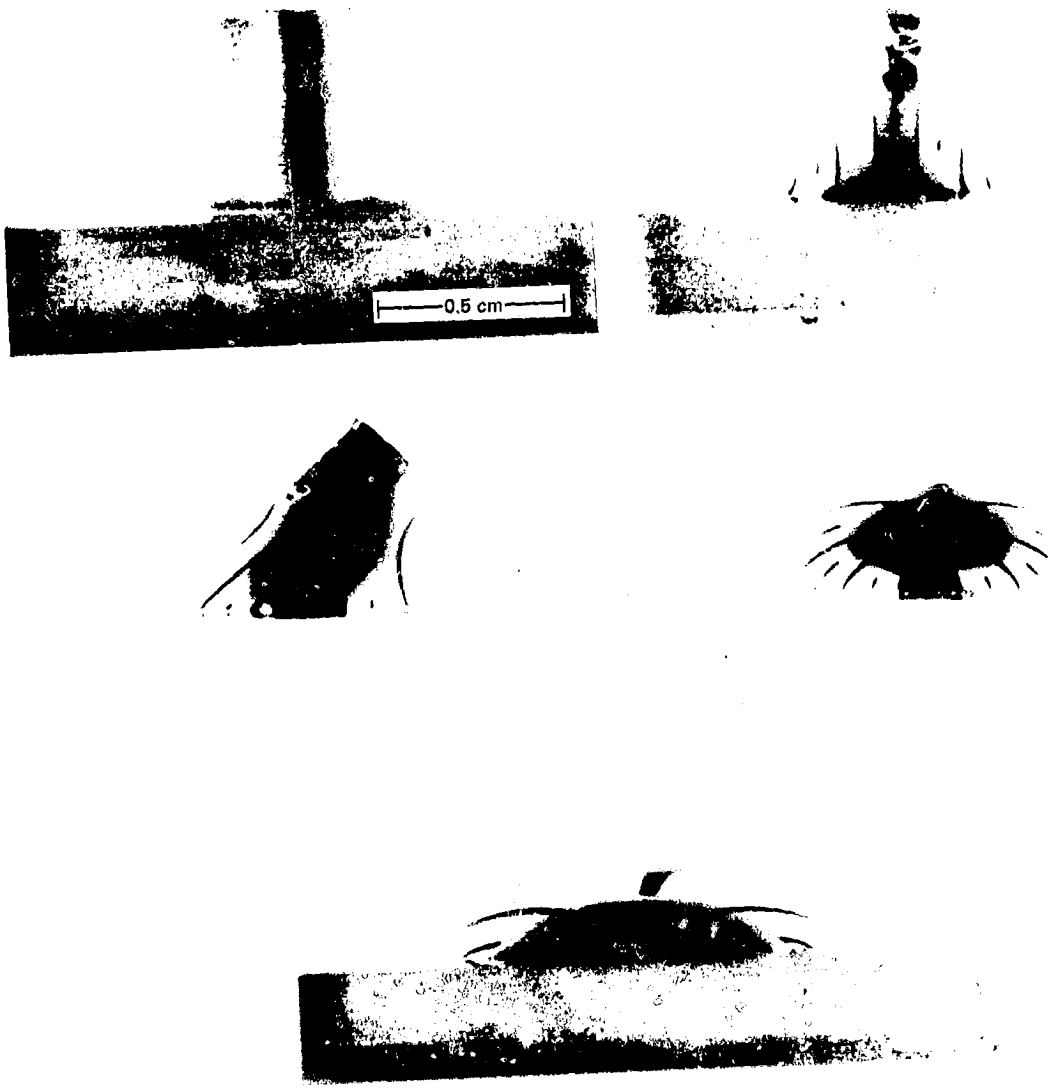

Figure 4-19. Silicon (on Si_3N_4, SD-49) Melting and Spreading to Mechanically Stable Contact Angle. Total Elapsed Time Approx 3 min; Surrounding Lines Are Reflections From Heater Element

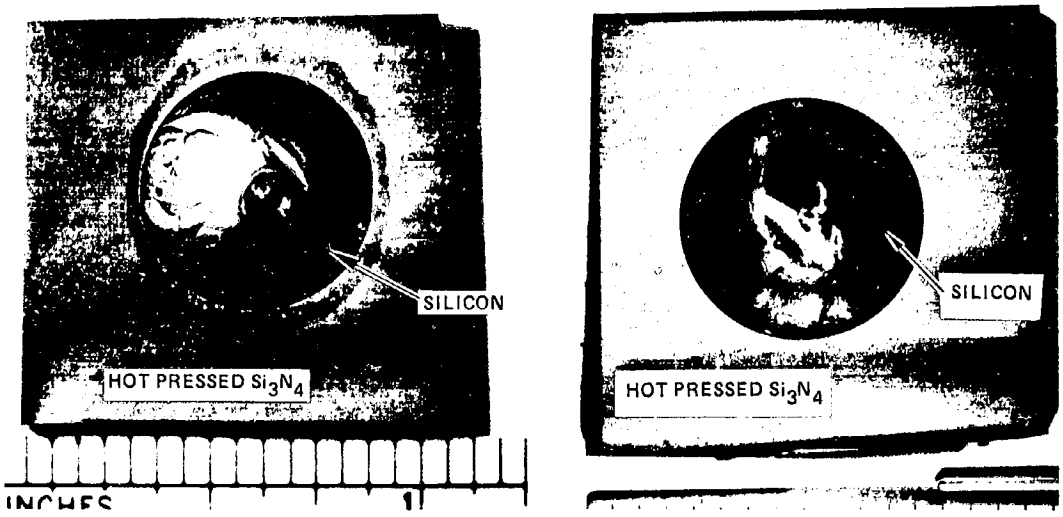

Figure 4-20. Silicon Sessile Drop on as-Fabricated Test Surface, SD-49 (Left), and on a 15μ Surface Finish SD-50, (Right). Note Microwetting Around Sessile Drop on the Left

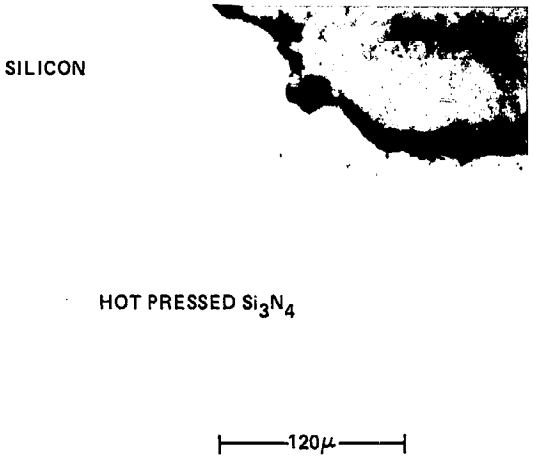

Figure 4-21. Photomicrograph of Silicon/Si_3N_4 Interface, SD-50, as-Polished

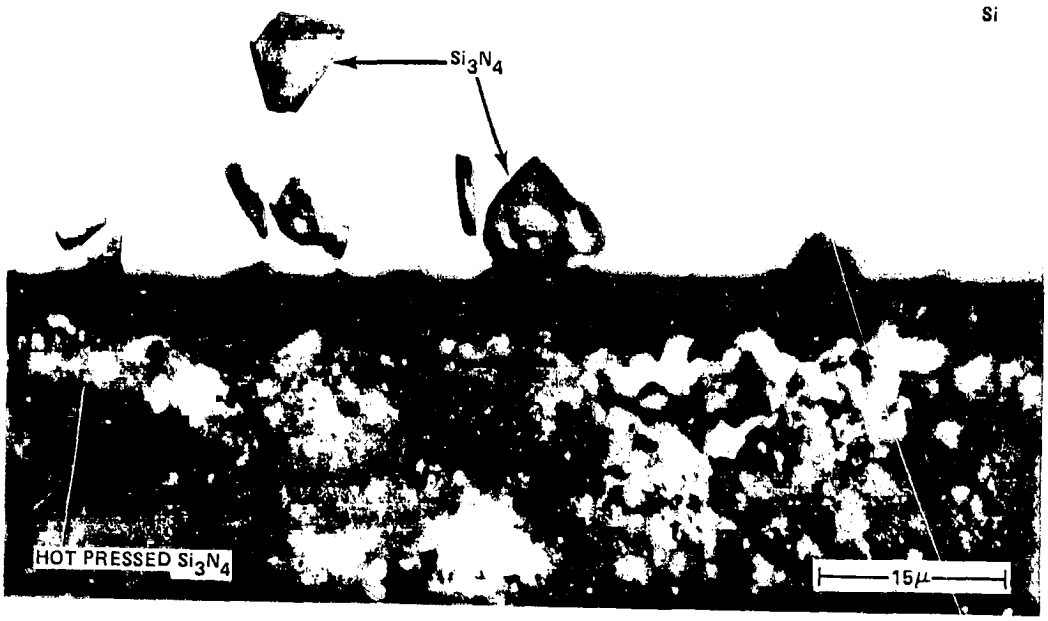

Figure 4-22. Si_3N_4 Appearing Particles at Si/Si_3N_4 Interface and Slight Silicon Permeation Into Substrate, SD-9, Hot-Pressed Si_3N_4.

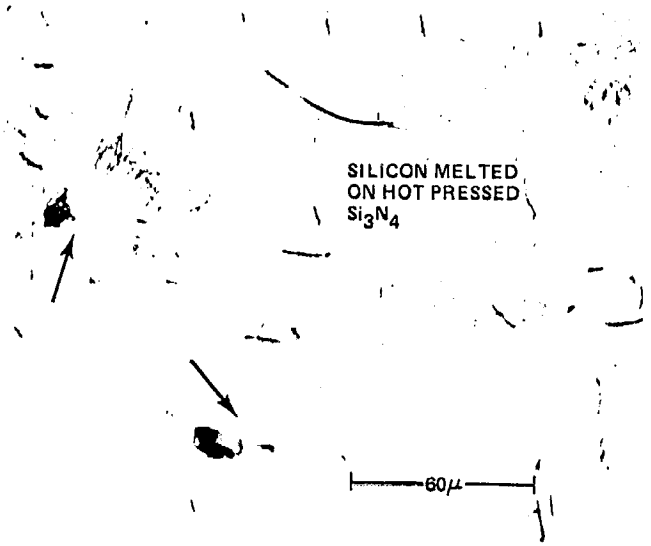

Figure 4-23. Photomicrograph of Silicon Microstructure, SD-64, Sirtl Etch. Note Dislocations and Impurity Phases (arrows)

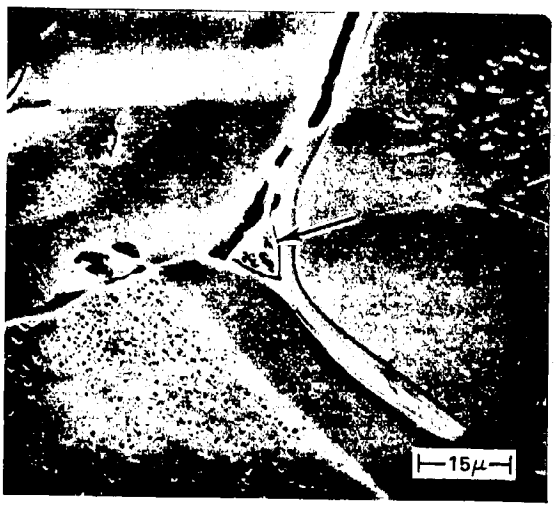

Figure 4-24. Scanning Electron Microscope Photomicrograph of Grain Boundary Impurity Phase, SD-64. EDAX Readings in area indicated by the arrow show: High Al, Low Si, and Very Low Cu

2. Reaction-Sintering/Bonding

In reaction-sintering/bonding, the required shape is made from compacted silicon powder nitrided in nitrogen in the range of 1400°C. This gives a product of mixed α and β silicon nitride with about 25% porosity. After a product is compacted, the original dimension remains essentially unchanged during nitriding, which allows for complex finish shapes. Reaction-sintered Si_3N_4 (SD-13, SD-14, and SD-15) was made by Kawecky-Berylco Industries.

a. Sessile Drop Tests. Samples SD-13 and SD-14 were tested using the as-fabricated surface. These samples showed (1) very high initial wetting angles during the first minutes of melt (≈110° initially), and (2) a spreading contact angle, which for SD-14 appeared to stabilize at 91 ± 2° and for SD-13 decreased to 68° in approximately 35 min of melt time. Reaction-sintered sample SD-15, 15μ test surface finish, exhibited essentially the same wetting kinetics and final contact angle as hot-pressed Si_3N_4 (51°).

Other observations for silicon melted on RS Si_3N_4 included:

(1) Silicon was tenaciously bonded to the Si_3N_4, which caused the solidifying silicon to crack. This is because of differing thermal expansion/contraction characteristics (Figure 4-25).

(2) Silicon wicked along the test surface for unpolished substrates, indicating a possible surface "micro" wetting phenomenon (Figure 4-26), but did not for polished substrate.

b. Compatibility. The high initial contact angle observed on both hot-pressed and reaction-sintered Si_3N_4 is believed to be caused by a thin layer of silica which is present at the interface. The source may be SiO_2 on initial Si_3N_4 powder, producing an influence on initial wetting behavior.

Sample SD-14 retained a high contact angle (91°) throughout the total 35-min melt time. The silicon/Si_3N_4 interface of this sample was observed in the scanning electron microscope. SEM photomicrographs revealed the presence of a thin interface layer (Figure 4-27). Energy-dispersive analysis of X-rays (EDAX) which were performed on this layer and surrounding areas revealed three separate and distinct silicon counts. The highest count was on the Si matrix; the lowest count was on the Si_3N_4 matrix. The thin interface layer is believed to be a silicon oxide. Actual phase determination, however, was not accomplished.

Silicon melted on reaction-sintered Si_3N_4 substrates revealed (1) in general, the lack of any interfacial reaction zone, (2) very high detrimental impurity levels of iron, aluminum, manganese and calcium (Table 4-3), (3) a greater quantity of precipitates in the silicon than for silicon on hot-pressed Si_3N_4 products, and (4) a larger size and quantity of Si_3N_4-appearing particles at the interface than with hot-pressed Si_3N_4.

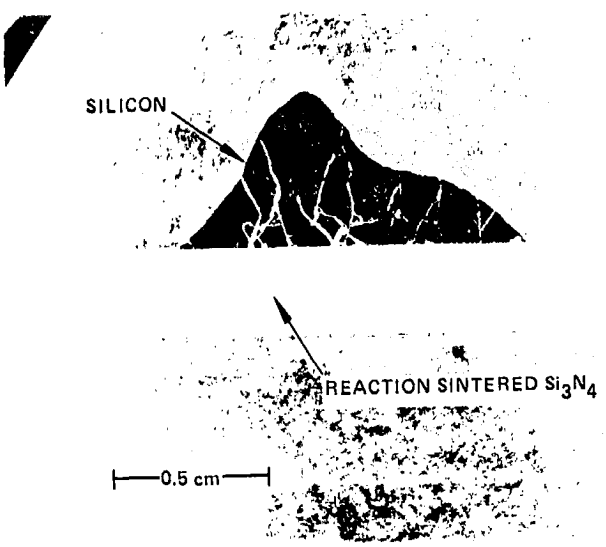

Figure 4-25. Photomacrograph of Sectioned Sessile Drop, SD-15, Showing Cracks in Silicon. Irregular Sessile Drop Shape is Due to Expansion Characteristic of Solidifying Silicon

3. Discussion (Si on Si_3N_4)

Single-phase, dense, hot-pressed silicon nitride is impossible to obtain by present production methods. However, single-phase material may not be necessary. For example, chemically pure, two-phase α and β Si_3N_4 may prove a feasible substrate. The problem with present-day hot-pressed Si_3N_4 is its impurity content. The presence of impurity elements in Si_3N_4, i.e., iron, aluminum, calcium and magnesium in the Si_3N_4, will result in detrimental contamination of the silicon, which subsequently results in an electrically deficient solar cell. To attack and solve this problem will require greater quality control in maintaining starting powder purity. One way of almost entirely eliminating the extrinsic contamination problem with Si_3N_4 is the use of a Si_3N_4 CVD film. Table 4-4 shows the relative impurity levels for various Si_3N_4 products.

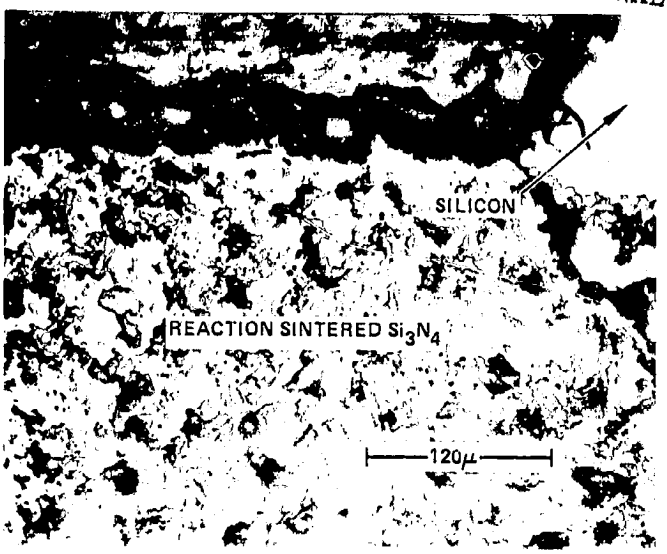

Figure 4-26. Photomicrograph of Interface, SD-14, Near Edge of Sessile Drop. Note the Presence of Free Silicon Beyond the Edge of the Silicon Drop (Microwetting)

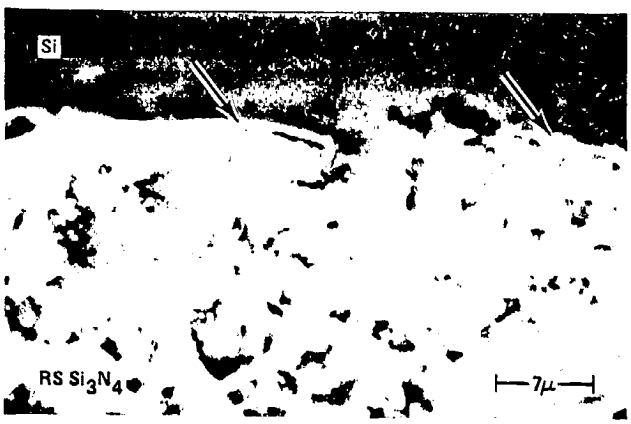

Figure 4-27. Scanning Electron Microscope Photomicrograph of Silicon/RS Si_3N_4 Interface SD-14, Showing Thin Layer of Intermediate Si Content (Arrow)

Table 4-4. The Emission Spectrographic Analyses of Various Silicon Nitrides (ppm) (Reference 4-23)

Element	Hot-Pressed (Atomergic)[a]	Hot-Pressed (Cerac)[b]	Reaction-Bonded (Cerac)	CVD Film
Cu	6-60	60-600	60-600 –	0.1-1
Ti	30-300	300-3000	300-3000	-
V	-	20-200	20-200	-
Ba	1-10	100-1000	10-100	-
B	15-150	60-600	6-60	10-100
Si	S[c]	S	S	S
Mg	0.3%-3%	0.3%-3%	30-300	1-10
Mn	1-10	100-1000	100-1000	0.3-3
Cr	-	100-1000	60-600	-
Fe	30-300	60-600	500-5000	0.3-3
Al	0.6%-6%	1%-10%	1%-10%	3-30
Be	-	3-30	0.6-6	-
Mo	-	3-30	30-300	-
Ca	30-300	600-6000	300-3000	-
Ni	3-30	60-600	100-1000	-

[a]Atomergic Chemetals Company, Carle Place, N.Y.

[b]Cerac, Inc., Milwaukee, Wisc.

[c]Strong.

E. SILICON OXYNITRIDE (Si_2ON_2)

Lab No.	Supplier	Process	Density, gm/cc	Contact Angle
SD-35	Norton	Sintered (SiOXYN)	2.46	115 ± 3^{o}
SD-37[a]	Norton	Sintered (SiOXYN)	2.46	117 ± 2^{o}

[a]As-fabricated surface tested.

Commercial grade multi-phase silicon oxynitride, SD 35a and 35b, was synthesized by Norton Industrial Ceramics Division by reacting mixtures of silicon and silica with nitrogen at elevated temperatures. SiOXYN shapes are self-bonded and are formed in the desired shape before firing. Fully reacted SiOXYN powder alone, when compacted and sintered, does not exhibit good strength properties; however, the addition of other binders will help, but is likely to limit the product's performance capabilities. Typical contents of SiOXYN are 75 to 90% Si_2ON_2, 1 to 7% cristobalite, 0.7% iron, 0.4% calcium, and the balance silicon nitride.

1. Sessile Drop Test

   (1) Both samples exhibited equilibrium wetting at approximately 116^{o}.

   (2) There were no apparent differences in wetting characteristics between the as-fabricated and polished surface.

   (3) Molten silicon wicked along the SiOXYN surface all around the sessile drop ("micro" wetting) (Figure 4-28).

2. Compatibility

   (1) An interface reaction zone approximately .08 mm (3 mils) thick was formed (Figure 4-28).

   (2) Silicon penetrated the substance in the center portion of the interface area

   (3) Surface "microwetting" was observed (area B, Figure 4-28).

   (4) An oxide type film was observed on portions of the molten silicon drop surface.

Figure 4-28. Silicon Oxynitride, Photomacrograph (Left) of Sectioned Sample Showing, A - Unreacted Test Surface, B - Reacted Surface (Silicon Wicked in) and C - Silicon Drop. Photomicrograph (Right) of Interfacial Reaction Zone

3. Discussion

To date, single phase Si_2ON_2 has not been known to be fabricated by hot pressing or reaction bonding. There is evidence of pyrolytically produced Si_xO_yN films (Refs. 1-18, 4-11, 4-24). Complete documentation of the resulting structure was not readily available. Preliminary tests with CVD layers of silicon oxynitride in contact with molten Si have been encouraging (Ref. 1-18). It is expected that the physical properties of an amorphous silicon oxynitride film in contact with molten Si will be strongly dependent on the oxygen concentration.

F. SILICON-ALUMINUM-OXYGEN-NITROGEN (SIALONS)

Lab No.	Supplier	Phase (all material was hot pressed)	Density, gm/cc	Contact Angle
SD-28	JPL	X_2, two phase[a]	3.33	$(65\text{-}80\text{-}62^\circ) \pm 3^\circ$
SD-29	JPL	β'	3.09	$(55\text{-}48^\circ) \pm 3^\circ$
SD-30	JPL	β'	3.09	$54 \pm 3^\circ$
SD-58	JPL	β', SiO_2 + AlN	3.23	$44 \pm 2^\circ$
SD-57	JPL	15R, AlN + Si_3N_4 + Al_2O_3	3.37	$91\text{-}52^\circ$

F. SILICON-ALUMINUM-OXYGEN-NITROGEN (SIALONS) (Continued)

Lab No.	Supplier	Phase (all material was hot pressed)	Density, gm/cc	Contact Angle
SD-59	JPL	15H, high Si_3N_4 -1% MgO	2.54	112-59°
SD-62	JPL	15R, w/1% B_2O_3	3.06	Not tested
SD-63	JPL	15R, AlN + SiO_2	3.10	Not tested
SD-60	JPL	8H, polyphase	3.37	90-57°
SD-61	JPL	8H, polyphase 1% MgO	3.37	62-52°
SD-65	JPL	Polyphase B[a]	3.30	84-53°
SD-66	JPL	Polyphase A[a]	3.34	80-51°

[a]See Figure 4-29

All hot-pressed sialon samples used in sessile drop tests were fabricated at JPL. (Samples were provided by Wayne Phillips). No binder additives were used except for SD-59, SD-61, and SD-62, so that, at temperature, all densification occurred by reaction-bonding. No liquid phase sintering can be expected at the fabrication temperatures used. Further fabrication information not included in the above table is given in Table 5.

Jack (Reference 4-25) has studied sialons and related nitrogen ceramics and has reported much useful information. The results of hot-pressing appropriate mixtures of Si_3N_4, AlN, Al_2O_3, SiO_2 and Si_2N_2 at high temperatures (usually 1750°C, but ranged from 1550 - 2000°C) in a graphite die are shown in Figure 4-29. At best, this diagram can be considered idealized behavior and does not necessarily represent thermodynamic equilibrium.

The phase "X" was reported by Oyama and Kamigaito (Reference 4-26) to have the composition $3Al_2O_3 \cdot Si_3N_4$. However, work by Jack indicates that the X-phase sialon composition, $SiAlO_2N$ (Reference 4-27), is more rich in Al_2O_3 (Reference 4-25), but that further work is needed in this area. There is the suggestion that describing the X-phase as a "nitrogen-mullite" is not misleading. Attempts have been made at the United Technologies Research Center to prepare $Si_{6-x}Al_xO_xN_{8-x}$ solid solution ceramics by reacting X-phase liquid and a complementary sialon composition and subsequently homogenizing them to a single phase (Reference 4-28).

Table 4-5. Sialon Material Processing Variables

Lab No.	Phase	Process Variables
SD-28	X_2 composition	1825°C, 6.9 x 10^6 N/m^2 (1000 psi) for 1 hr without sintering aids or SiO_2 added
SD-29,	β'	1825°C, 6.9 x 10^6 N/m^2 (1000 psi) for 1 hr Mixture of Si_3N_4 - AlN - Al_2O_3
SD-58	β'	1810°C, 13.8 x 10^6 N/m^2 (2000 psi) for 1 hr Mixture of SiO_2 - AlN (85% phase Cerac AlN)
SD-57	15R polyphase	1830°C, 13.8 x 10^6 N/m^2 (2000 psi) for 1 hr Mixture of AlN - Si_3N_4 - Al_2O_3
SD-59	15R polyphase	1750°C, 13.8 x 10^6 N/m^2 (2000 psi) for 1 hr Mixture at high Si_3N_4 end of 15R range, 1% MgO for sintering aid
SD-60	8H polyphase	1825°C, 13.8 x 10^6 N/m^2 (2000 psi) for 1 hr 1.3 cm (1/2-in.) thick original sample
SD-61	8H polyphase	1750°C, 13.8 x 10^6 N/m^2 (2000 psi) for 1 hr 1% MgO for sintering
SD-65	Polyphase B[a]	1725°C, 13.8 x 10^6 N/m^2 (2000 psi) for 1 hr

[a]See Figure 4-29

Reaction of silicon nitride and alumina usually gives β' and the silica-rich X-phase, but the amount of X-phase decreases as the hot-pressing temperature is increased above 1800°C. To date, β' phase has been the only sialon that has been examined in any detail and because until recently specimens usually contained other vitreous or crystalline phases (e.g., X or 15R), it is not certain whether the intrinsic properties of β' have yet been evaluated.

1. Sessile Drop Tests

For X_2 composition, SD-28, an initial contact angle of 65° was observed; then the drop drew back to about 80° and gradually proceeded to spread out again. The contact angle appeared to stabilize at 62 ± 3°. The silicon drop did not remain attached to the substrate during solidification. The X_2 composition was a two-phase product, most likely 8H and 15R (Figure 4-29).

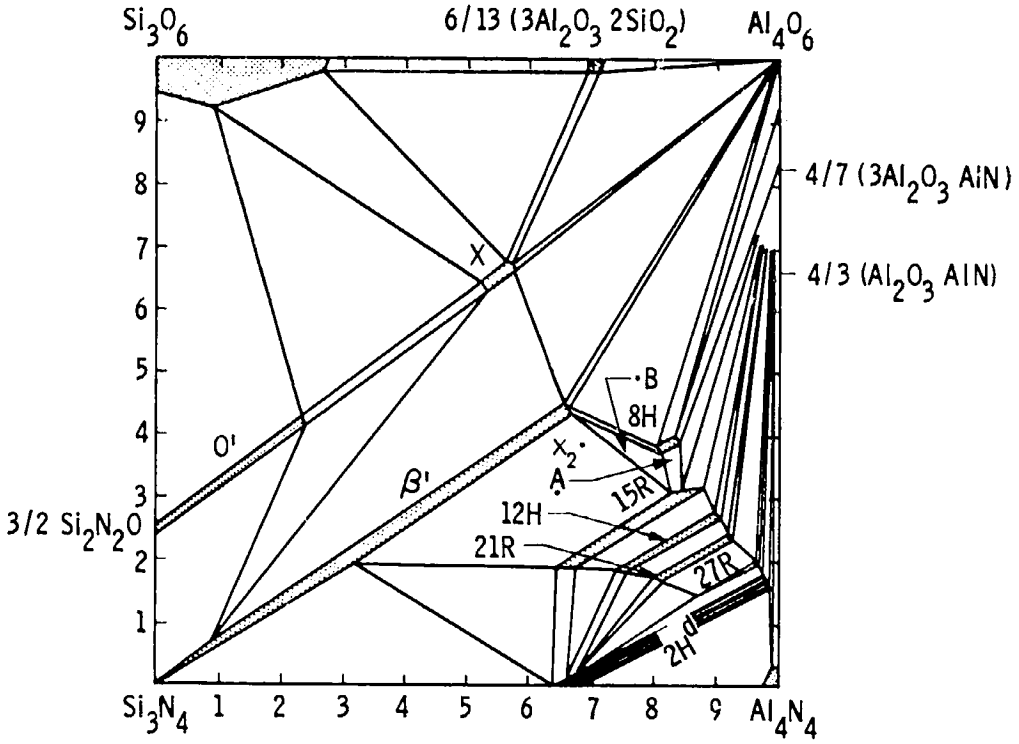

Figure 4-29. The Si_3N_4 - AlN - Al_2O_3 - SiO_2 System Based on Research at Newcastle

All sialon material tested (except X_2 composition and one β' phase) exhibited high contact angles when the silicon initially melted.

Kinetic contact angles were observed for all sialon material tested with the possible exception of SD-30, β' phase material. SD-30 exhibited the typical high contact angle initially after melt, but then appeared to immediately settle at 54 ± 3°. Charts showing contact angle vs time from melt for the other sialon samples tested are given in Figures 4-30 and 4-31.

Obviously, the kinetics of sialon materials, especially polyphase, wet by molten silicon, are a complex and presently little understood phenomenon. In a polyphase material the dissolution of one phase preferentially over the others would cause a decrease in the interfacial free energy. This decrease would correspond to a decrease in interfacial tension by an amount equal to the free energy of the effective chemical reaction per area at the interface (Reference 1-12). Thus, in the sessile drop experiment, spreading of the liquid silicon is observed.

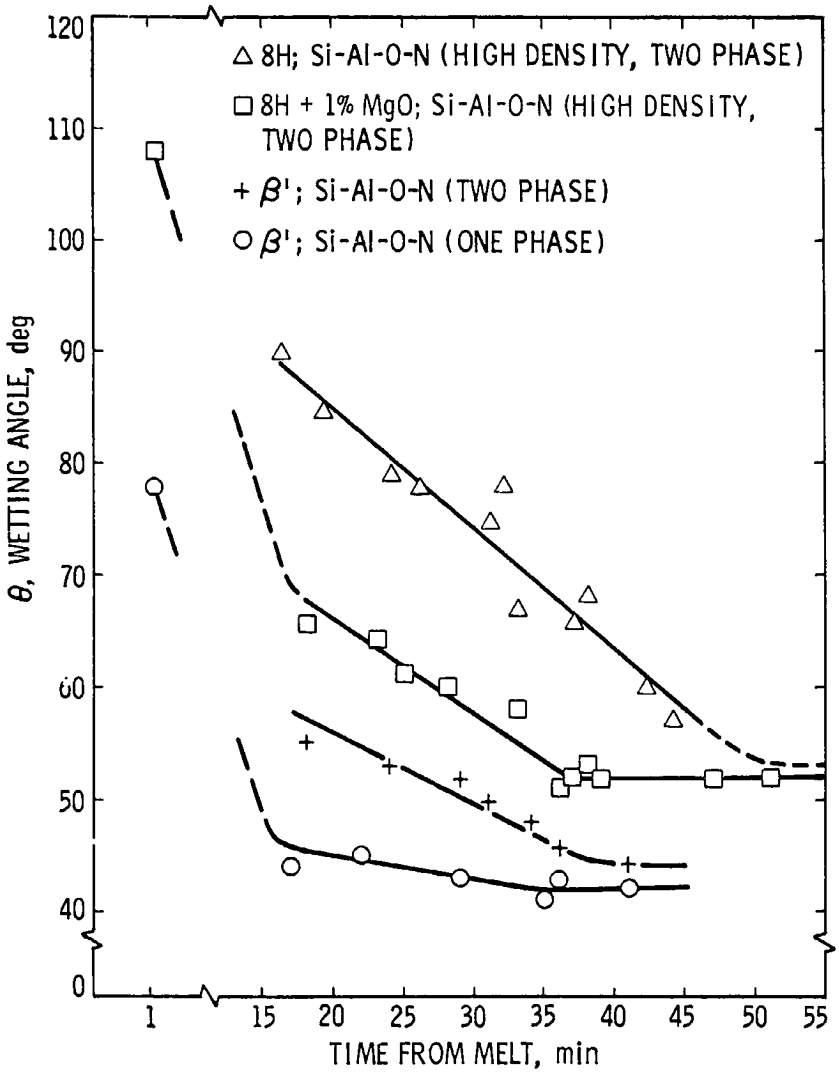

Figure 4-30. Wetting Angle vs Time from Melt for Molten Silicon (1430°C) on Si-Al-O-N Refractory Material

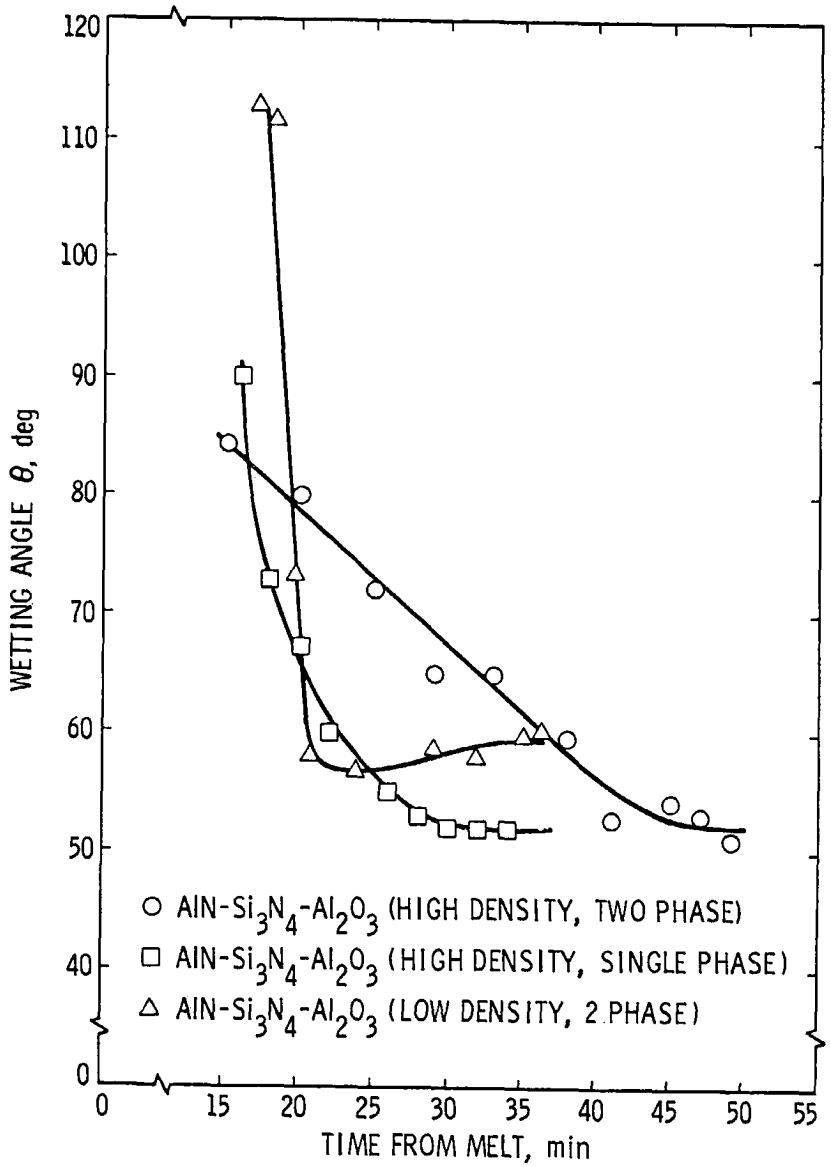

Figure 4-31. Wetting Angle vs Time from Melt for Molten Silicon (1430°C) on Si-Al-O-N Refractory Material

2. Compatibility

For X_2 composition, SD-28, the presence of an additional phase (light gray), besides the two original substrates phases (medium gray and dark brown), was found near the interface zone as observed in reflected light. Also, narrow, long shaped impurity phases consisting of a white matrix with gray aggregite particles have been observed in the silicon drop.

All silicon melted on β' phase sialon material SD-29, SD-30 and SD-58 showed (1) generally, a relatively clean interface region (Figure 4-32), but with some high magnification evidence of mild interface reactions and cracking which indicated a lack of bonding at the Si/β' phase interface (Figures 4-33 and 4-34), (2) impurity grain boundary formation in the silicon matrix (Figure 4-35), and (3) severe doping levels of aluminum, iron, tungsten and calcium in silicon melted on SD-58 (Table 4-3). Energy dispersive analyses of X-ray (EDAX) results for grain boundary impurities are shown in Figure 4-36.

Substrate microstructures, SD-57 and SD-59, reported as 15R phase, were not similar. SD-57, which was hot pressed at a higher temperature, was essentially single phase, while SD-59, which contained a higher Si_3N_4 content, was obviously multiphase (Figure 4-37). Up to 25 microns (0.001 in.) of SD-57's interface underwent some extent of dissolution (Figure 4-37) but showed no evidence of any new interface compounds. Slight dissolution and silicon penetration occurred at the outer edges of the molten silicon contact zone for substrate SD-59 (Figure 4-37), with evidence of Si_3N_4 - appearing particles in the silicon at the interface. Silicon melted on both substrates showed (1) impurity phase precipitation in the Si matrix (Figure 4-38), and (2) severe doping levels of aluminum, iron, and calcium (Table 4-3).

Samples SD-60, SD-61 and SD-66 all exhibited similar (1) polyphase microstructures (Figure 4-39), (2) slight interface dissolution (Figure 4-40), (3) internal precipitation of impurity phases (Figure 4-40), and (4) lack of adhesion between the bulk silicon drop and substrate. The solidifying silicon drops literally "popped off" the substrates as they cooled down and left patches of silicon still adhered to the substrate (Figure 4-41). No satisfactory mechanism has been developed to completely explain this phenomenon. Although no semiquantitative analyses were performed on silicon melted on these last substrates it is expected that severe impurity doping similar to the other sialon material would be found.

3. Discussion (Si on Sialons)

The term "sialon" was originally given to new compounds derived from silicon nitrides and oxynitrides by simultaneous replacement of nitrogen and silicon by oxygen and aluminum. The discovery was made concurrently and independently at Newcastle-upon-Tyne and in Japan. Investigators soon realized that other metal atoms could be incorporated, and the term has become a generic one applied to materials where the structure units are (Si, Al) $(O, N)_4$ or (Si,M) $(O,N)_4$ tetrahedra (Reference 4-25).

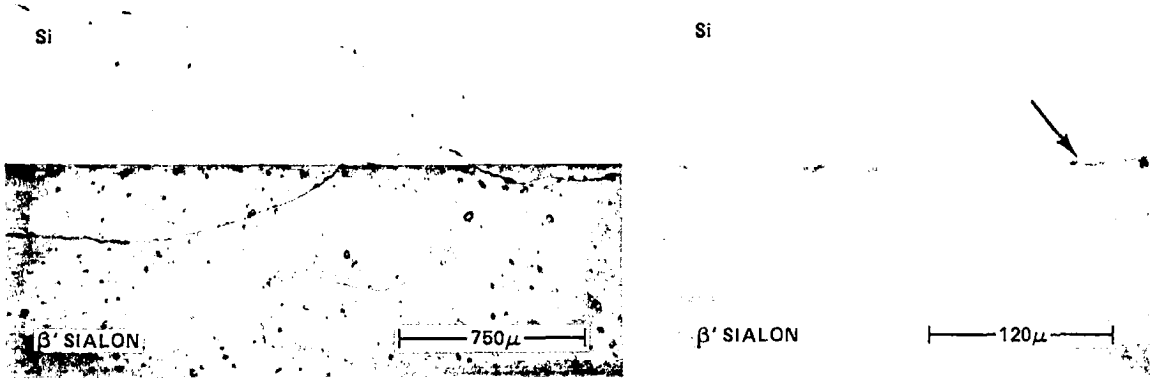

Figure 4-32. SD-30, β' Phase Silicon/Sialon Interface Showing Some Evidence of Grain Boundary Precipitates and a Relatively Clean Interface (Arrow)

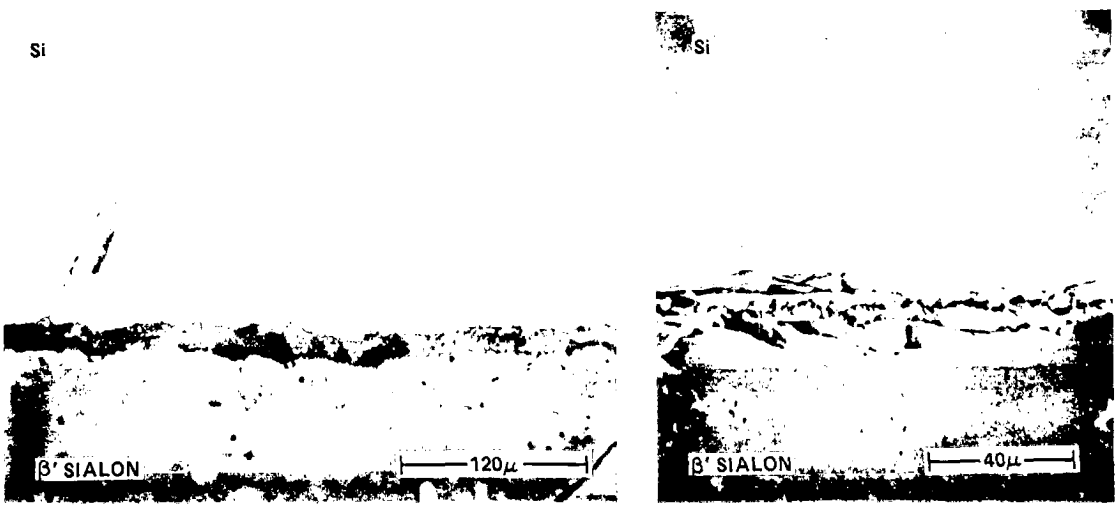

Figure 4-33. β' Phase Silicon/Sialon Interface, SD-30, Reflected Light (Left) and a Scanning Electron Microscope Image (Right)

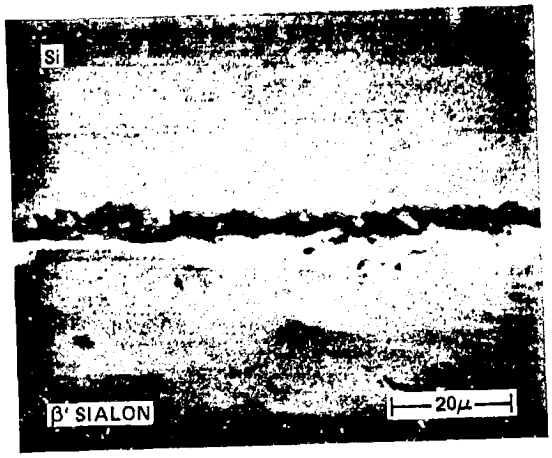

Figure 4-34. Scanning Electron Microscope Photomicrograph of β' Phase Silicon/Sialon Interface, SD-30

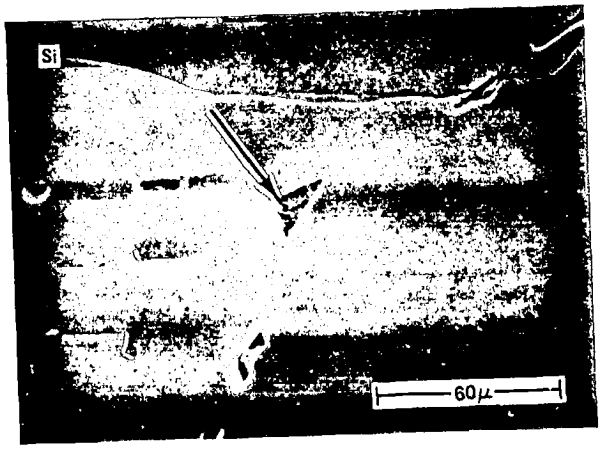

Figure 4-35. Scanning Electron Microscope Photomicrograph of Grain Boundary Impurity Phase in Silicon Melted on β' Phase Sialon, SD-30. Arrow Indicates Area of EDAX Analysis

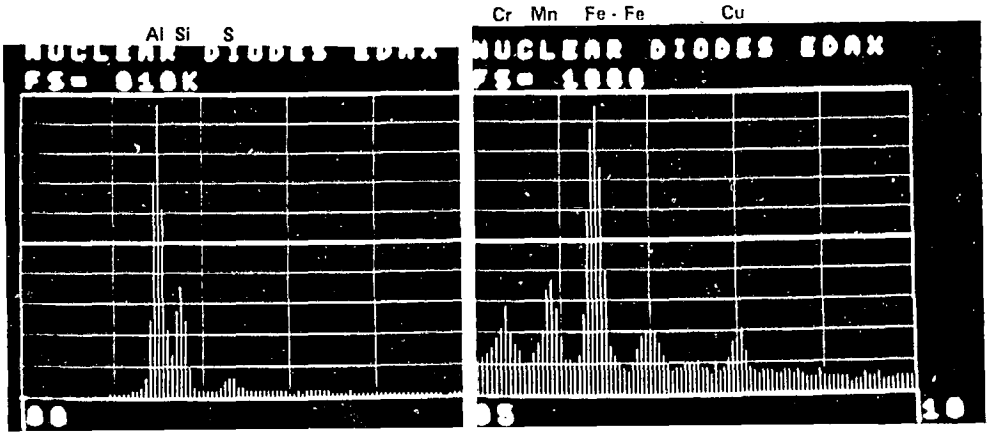

Figure 4-36. Energy-Dispersive Analysis of X-rays (EDAX) Showing That the Impurity Phase Shown in Figure 4-35 Consisted of (in Order of Peak Intensity) Al, Si, Fe, S, Mn, Cr and Cu

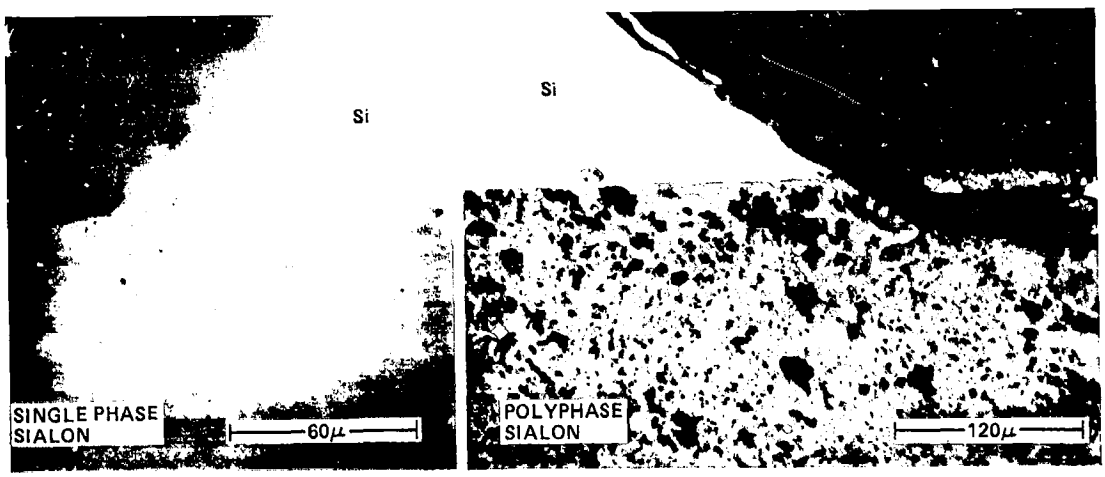

Figure 4-37. Silicon/15R Single-Phase Sialon Interface, SD-57, Shown at Left and Silicon/15R Polyphase Sialon Interface, SD-59 (Shown at Right)

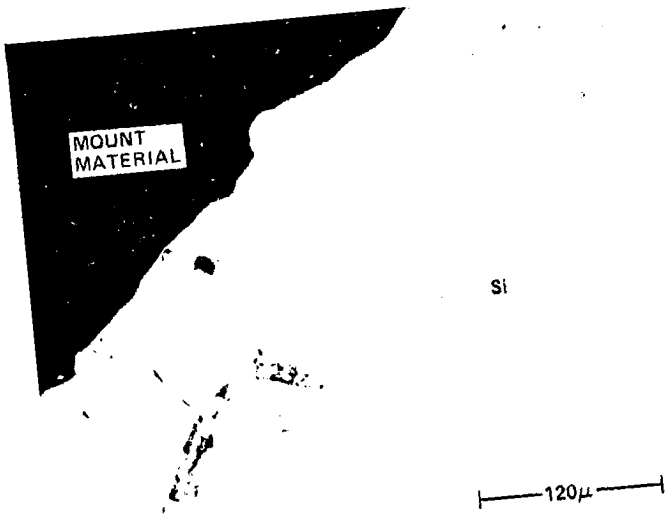

Figure 4-38. Impurity Phases in Silicon Melted on Sialon Material, SD-59, as-Polished

Figure 4-39. Typical Polyphase Sialon Material, SD-60, as-Polished

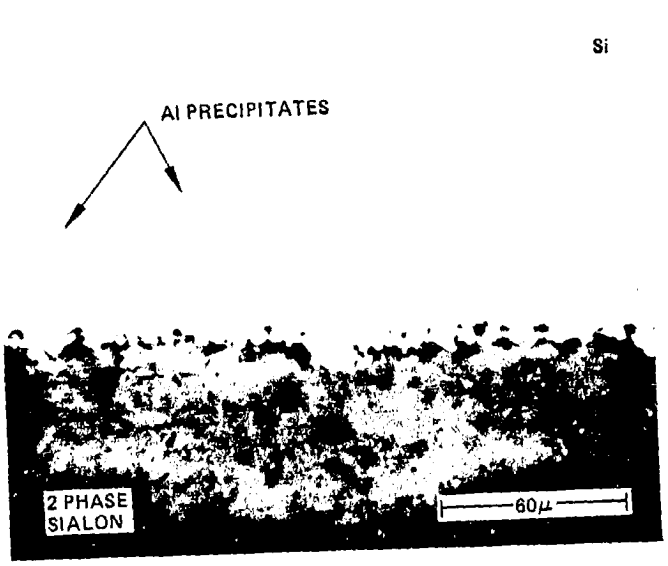

Figure 4-40. Silicon/Sialon Interface, SD-61, Showing Aluminum-Type Impurity Phase in the Silicon, as-Polished

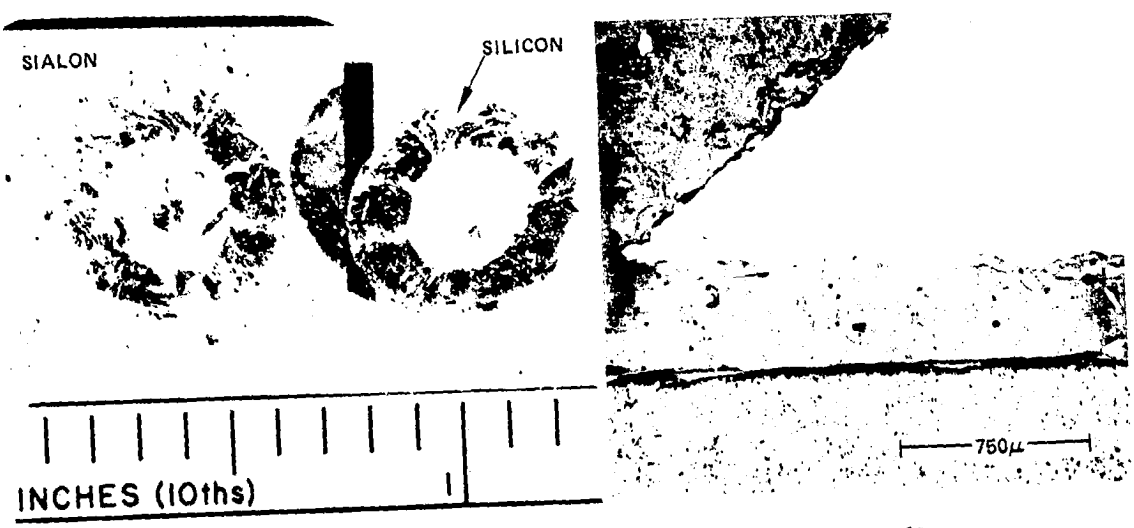

Figure 4-41. Photomacrograph of Sialon Substrate, SD-65, Showing the Separated Silicon Sessile Drop (Left) and a Sectional Micrograph of the Silicon/Substrate Interface (Right), as-Polished

The relationship between molten silicon compatibility and the microstructure of nitrogen ceramics is not known in any detail but it is suggested that a very low aluminum, low oxygen, high silicon and nitrogen content could prove advantageous. The incorporation of small amounts of Al and O in the structures of β-Si_3N_4 and silicon oxynitride should result in lowering of the N_2 vapor pressure with a SiO partial pressure expected to be below that for fused silica. Aluminum contamination remains a major concern along with the need for a low breakdown rate in Si-O and S-N bonds.

One potential advantage of sialon material over silicon nitride is in fabrication. With sialons, economic ceramic techniques of slip-casting, pressing and extrusion can be done to fabricate shapes which can then be fired at around 1600°C in inert atmospheres to near theoretical densities. Pressureless sintering of β - Sialon has been carried out successfully without the use of additives (Reference 4-26)

G. SAPPHIRE (Al_2O_3)

Lab No.	Supplier	Process	Density, gm/cc	Contact Angle
SD-69[a]	RCA	EFG[c]	3.97 (typ)	88 ± 3°
SD-70[b]	RCA	EFG	3.97 (typ)	86 ± 1°

[a] 15μ finish.

[b] 0.05μ finish.

[c] Edge-defined film-fed growth of a ribbon shape.

Sapphire, in nature, occurs as a crystalline gem stone in the corundum family, basically single crystal forms of aluminum oxide. Its crystallographic structure is rhombohedral single crystal with orientation in the R plane (1102) in the A plane (1010) and in the C plane (0001).

Sapphire samples, SD-69 and SD-70, were obtained from a section of approximately 5-cm-wide ribbon grown at RCA, Princeton, New Jersey. The surface was smooth but slightly rippled, as grown from the melt. SD-69 was mechanically polished to a 15μ surface finish, SD-70 was polished to a 0.05μ finish.

1. Sessile Drop Test

Sapphire sample SD-69 was initially observed to wet at 90° and stabilized at about 88°. SD-70 was initially wet at 97°, then

spread and appeared to reach an equilibrium contact angle of 86°. Figure 4-42 illustrates the change and stabilization of these contact angles plotted against exposure time to molten silicon. The different spreading kinetics may be attributed to the test surface texture.

SD-69 was cooled from the test temperature very slowly, while SD-70 was cooled as usual (shutoff furnace). For both samples, the sapphire substrate shattered upon cooling (Figure 4-43). Even though the silicon sessile drop cracked off SD-70, a thin layer of silicon was observed to be adhered to the entire contact area. Evidently strong bonding occurs, possibly forming a mullite interface, Al_2O_3/SiO_2.

2. Compatibility

It is expected, but not documented, that silicon melted on sapphire has been severly contaminated with aluminum and oxygen.

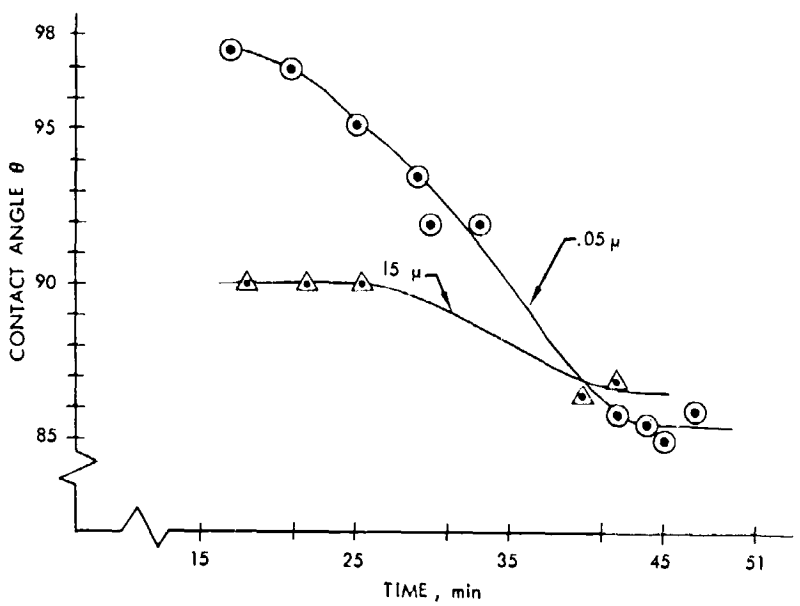

Figure 4-42. Contact Angle θ vs Contact Time for Molten Silicon on Sapphire

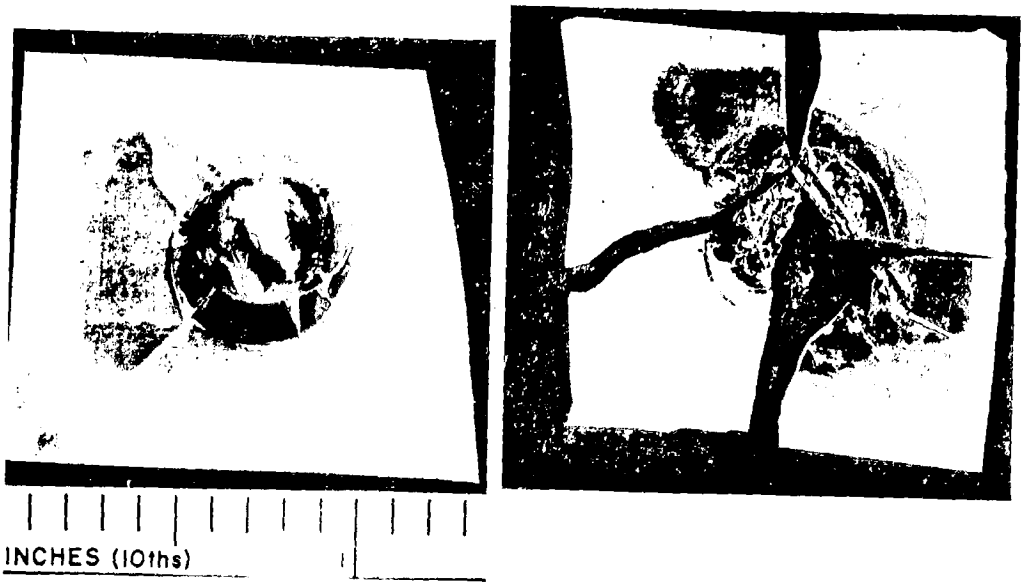

Figure 4-43. Photomacrograph of Silicon on Sapphire, SD-69, (Left) and SD-70 (Right)

H. MULLITE ($3Al_2O_3 \cdot 2SiO_2$)

Lab No.	Supplier, grade	Process	Density, gm/cc	Contact Angle
SD-36[a]	Honeywell, MV-20[c]	Rolled and fired	2.52	90 ±5°
SD-40[b]	Coors, S1S	Pressed and fired	2.74	93 ±3°
SD-41	Coors, S1S	Pressed and fired	2.74	98 ±3°

[a]Oxide coating formed on molten silicon drop.
[b]As-fabricated surface tested.
[c]McDanel body, Honeywell processed.

Table 4-6. Emission Spectroscopy Chemical Analyses of Various Mullites (Performed at Honeywell), wt %

McDanel (MV-20)	McDanel (MV-30)	American Lava
Fe 0.89	0.55	0.75
Ti 0.78	0.54	0.021
Mg 0.20	0.13	0.48
Ma 0.28	<0.1	<0.1
Ca 0.11	<0.03	<0.03
Mn 0.041	0.01	<0.01
V 0.031	0.03	<0.01
Cu ≲0.01	≲0.01	<0.01

Table 4-7. Typical Chemical Analysis of McDanel MV-20 and MV-30 Mullite, wt %

Compound	MV-20	MV-30
Al_2O_3	55 4	60.0
SiO_2	42.0	38.0
K_2O	0.7	0.5
Na_2O	0.5	0.08
CaO	0.5	0.01
Fe_2O_3	0.8	0.5
TiO_2	0.5	0.5
MgO	0.04	0.2

Mullite ($3Al_2O_3 \cdot 2SiO_2$), manufactured by McDanel, was rolled and fired at approximately 1630°C by Honeywell and Mullite was also fabricated by Coors in a somewhat similar procedure. Coors samples were round discs approximately 2.54 cm (1 in) in diameter by .48 cm (3/16 in) thick, while Honeywell's samples were unevenly flat, approximately .16 cm (1/16 in) thick, rectangular shapes.

Honeywell Corporate Material Sciences Center (Reference 4-29) has been involved with the technical and economic feasibility of producing solar-cell-quality sheet silicon by applying a thin coating of silicon on an inexpensive ceramic substrate. Mullite, protectively coated or not, has been and is still being considered the main candidate substrate material. Optimization of the Al_2O_3/SiO_2 composition, however, has not yet been accomplished.

The Honeywell Chemistry Laboratory used emission spectroscopy to identify impurities in three candidate ceramic bodies (Tables 4-5 and 4-6):

(1) McDanel MV-20 rolled, dried and fired mullite.

(2) McDanel MV-30 slip-cast mullite.

(3) American Lava hot-pressed mullite.

McDanel MV-20 was the only material tested in the JPL study.

Honeywell has concluded that the dip coating process will probably require a mullite substrate with a composition containing an excess of SiO_2 in order to better match the thermal coefficient of silicon.

Even though the contact time between the mullite substrate and molten silicon is very short, dissolution of the mullite still occurs rapidly in the first few minutes. It appears that the aluminum impurity level of the melt increases rapidly during the first 2 or 3 minutes of contact time with the substrate, and then increases exponentially at a lesser rate, becoming very nearly saturated after an hour of contact time (Reference 4-30).

Indications that the dissolved aluminum and other impurities transferred to the molten silicon are electrically active can be observed in plots of electrical resistivity vs accumulated time of exposure to mullite (Figure 4-44). A layer of carbon on the mullite surface has been used to effectively reduce this contamination problem. However, β-SiC has been observed to form (Figure 4-45).

1. Sessile Drop Tests

Observations from sessile drop tests were (1) mullite exhibited what can be considered a borderline to nonwetting property (equilibrium contact angles $\theta \sim 95^\circ$); (2) an oxide-type coating formed on the molten silicon, SD-36, and may have influenced its wetting behavior; (3) interface bubbling occurred, which is a possible indication of SiO evolution; and (4) a rougher as-fabricated surface, SD-40, exhibited a contact angle 6° less than a polished surface.

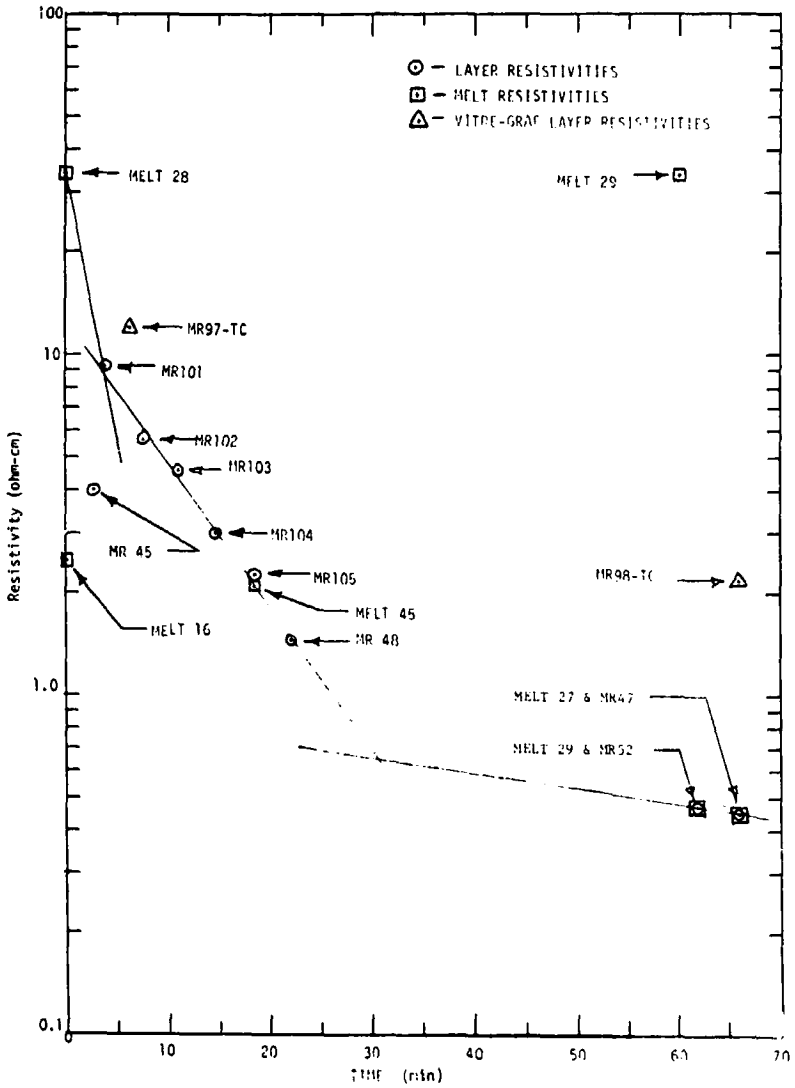

Figure 4-44. Layer and Melt Resistivities vs Accumulated Time That the Respective Melts Were Exposed to Mullite (Reference 4-29)

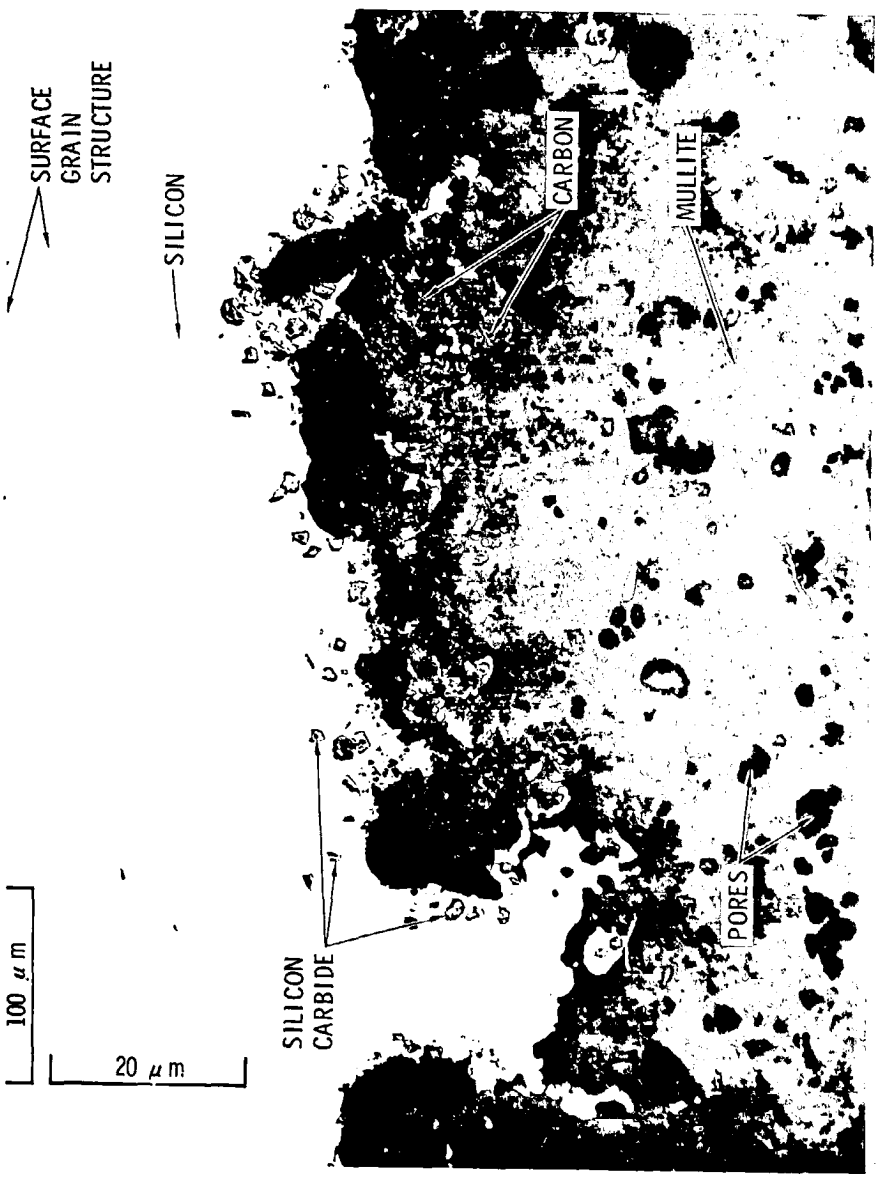

Figure 4-45. Silicon on Carbon-Coated Mullite Substrate Showing Formation of SiC Particles

2. Compatibility

Both bulk grain boundary and near interface impurity phases were present in the silicon melted on mullite from Honeywell, SD-36 (Figure 4-46). The grain boundary impurity elements consisted of a two-phase precipitation (Figure 4-47). Energy dispersive analyses of X-ray (EDAX) measurements were made on these precipitates and results indicate the white phase (A) to be a high silicon/low aluminum alloy and the white/black pepper phase (B) to be a high aluminum/low silicon alloy. Aluminum and silicon form a eutectic which contains 11.7 wt% Si and melts at 577°C. All along the mullite/silicon interface, within approximately 10 microns (0.004 in) of the mullite surface, silicon oxide precipitates were observed (Figure 4-48). These precipitates were believed to be SiO_2 because EDAX count readings on these particles were nearly identical to readings taken on the SiO_2 phase in the mullite substrate (Figure 4-49). Actual determination of chemical contents of these impurity phases would require oxygen-detecting methods such as the ion microprobe.

Silicon melted on mullite from Coors, SD-40 and SD-41, exhibited (1) silicon penetration 635 microns (0.025 in.) into the mullite pores, which occurred only in the center portion of the molten silicon contact area (Figure 4-50), (2) no interfacial phase formations, (3) similarity to SD-36, in that Al-Si eutectic phases were present in the silicon matrix, and (4) high elemental impurity doping levels as revealed by semiquantitative analysis (Table 4-1). These impurities included, but were not limited to, aluminum, iron and titanium. Titanium has a very drastic effect on electrical efficiency (Figure 1-5).

I. SILICA (SiO_2)

Lab No.	Supplier	Process	Density, gm/cc	Contact Angle
SD-54	General Electric	Fused	2.18	92 $\pm 3^{\circ}$
SD-56	Thermo-Sil	Slip-cast	2.18	91 $\pm 2^{\circ}$

All forms of silica, when heated to sufficiently high temperatures, fuse and form amorphous silica glass or fused silica. Fused silica, SD-54, was obtained from General Electric in the form of a 30.5 cm (12-in.) diameter crucible dish 0.64 cm (1/4-in.) thick. Slip-cast silica, SD-56, 1.9 cm (3/4-in.) thick, was obtained from Thermo-Sil. Table 4-7 shows data on typical impurity levels in GE-204 fused silica.

Fused silica has been the major material used in containing molten silicon. There are, however, several problems encountered with its use. Molten silicon reacts with SiO_2 in the following manner:

$$Si\ (l) + SiO_2\ (s) \rightleftharpoons 2SiO(g)$$

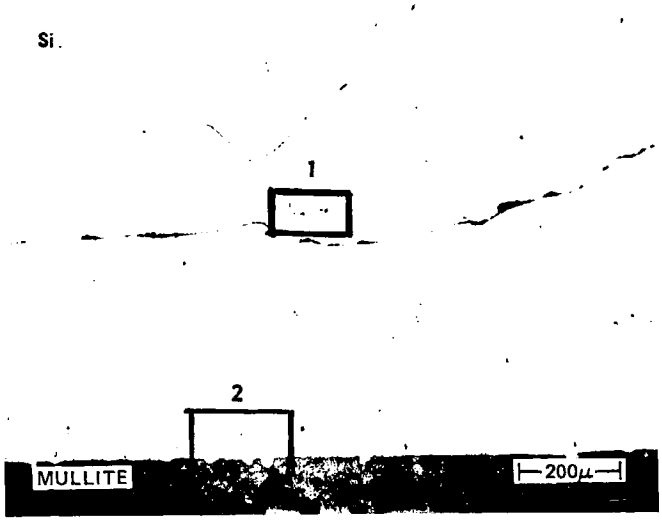

Figure 4-46. Sectional Micrograph of Silicon (Top)/Mullite (Bottom) Interface

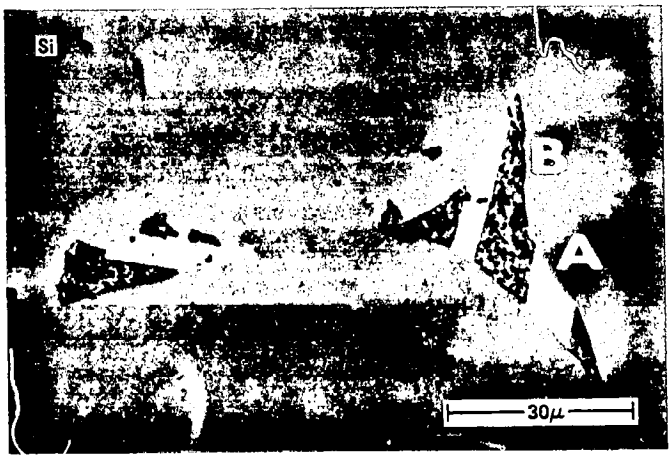

Figure 4-47. Enlarged View of Area 1, Figure 4-46, Showing Nature and Morphology of Impurity Phases: A - High Silicon, Low Aluminum; B - High Aluminum, Low Silicon

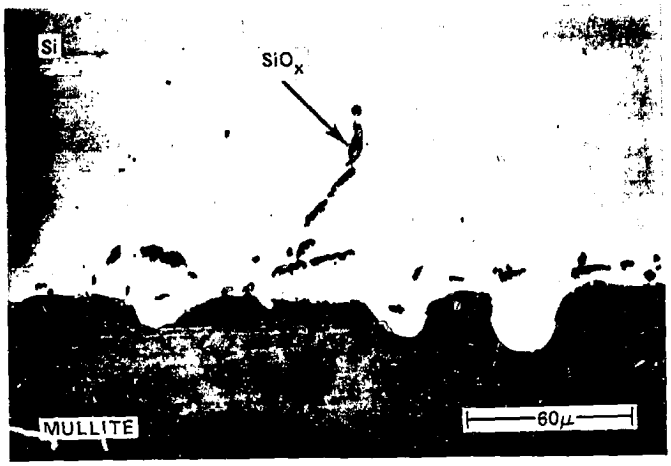

Figure 4-48. Enlarged View of Area 2, Figure 4-46, Showing Nature of Precipitates Near Interface; Suspected Phase Is SiO_2

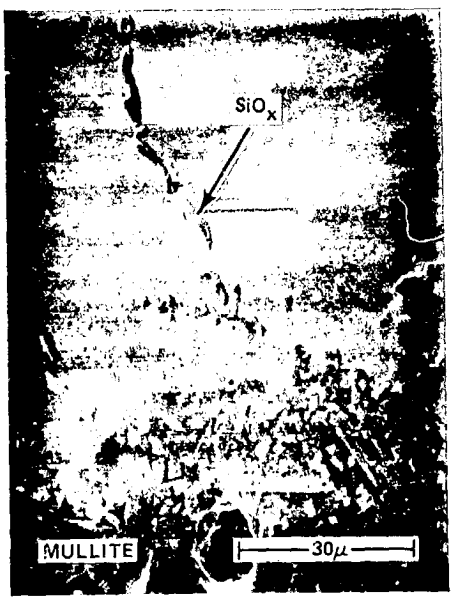

Figure 4-49. Scanning Electron Microscope Photomicrograph Showing Silicon/Mullite Interface and Precipitates in Silicon Matrix.

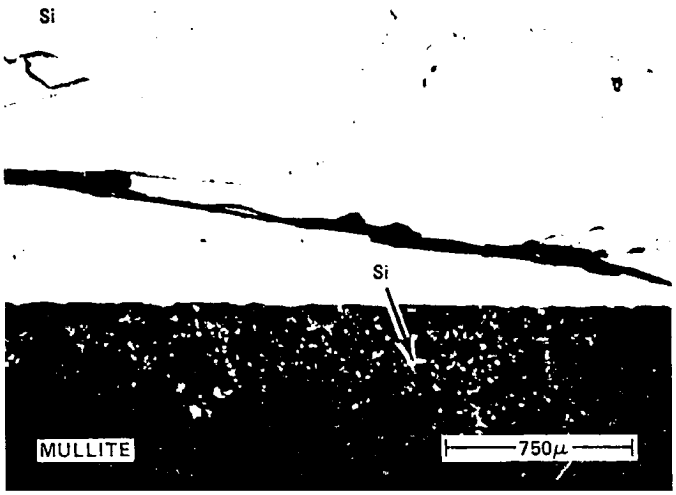

Figure 4-50. Sectional Micrograph of Silicon/Mullite Interface, SD-40, Showing Silicon Penetration Into Mullite Porosity, as-Polished

After a period of time, SiO vapors build up on surfaces above the pool of molten silicon. These layer deposits will flake off, drop into the molten silicon and act as nucleation sites, causing single-crystal Czochlarski boules or ribbons to become polycrystalline in structure. In addition, since the fused silica is being dissolved, any impurities in it are also being added to the melt along with oxygen. Silicon saturated in oxygen will typically contain 10^{18} atoms/cm^3, which can influence the semiconductor properties of silicon considerably (Reference 4-31). Though there is a contamination problem, generally acceptable solar cells (~15% efficiency) have been and are being fabricated from sliced Czochlarski ingots drawn from fused silica crucibles.

Mobil-Tyco (Reference 4-32) encountered an aluminum contamination problem in EFG grown ribbon when a 15.24 cm (6-in.)-long fused silica crucible was used. The crucible length has since been decreased to 10.16 cm (4-in.) to bring the ratio of the crucible surface-to-melt volume closer to that existing in induction furnace growth systems in which the aluminum adsorption was rarely observed.

Fused silica crucibles used in ribbon and ingot fabrication continue to be a major cost item. Molten silicon left in the bottom of the crucible bonds to the fused silica, and because of differing thermal expansion coefficients, both silicon and container usually fracture during cooling. This occurs below 650^{o}C (Reference 4-33). Also, softening and devitrification

Table 4-8. Typical Chemical Analysis of General Electric Type 204 Fused Silica Tubing (supplied by GE)

Element	Parts per Million		Element	PPM	
	Average	Range		Average	Range
Al	27	22-35	Titanium	2	1-2
Fe	4	1-6	Zirconium	2	0.7-4
Ca	3	1-4	Boron	1	---
Mg	1	1-2	Chromium	1	1-3
K	3	8-6	Copper	1	-
Na	3	2-4	Manganese	2	2-3
Li	0.5	0-1	Total	50.5	32.5-70.0

occur as thermal cycling proceeds, making the crucible structurally weak. IBM (Reference 4-7) has demonstrated satisfactory performance in the reuse of fused silica crucibles through four meltdown cycles. However, most crucibles used in industry today are scrapped after one run.

Crystal Systems (Reference 4-34) has used fused silica in its heat exchanger method (HEM) for producing cast silicon ingots but encountered severe cracking of the ingots during cooldown. This problem can be overcome if the crucible is weak and thereby cracks itself during the cooldown cycle before cracking the ingot. Recently, use of a graded density silica crucible wall has produced crack-free silicon ingots.

1. Sessile Drop Tests

Both samples of silica (fused and slip-cast) exhibited similar wetting characteristics (contact angle 91°), interface bubbling in the silicon during the test (due to SiO and O_2 evolution), and tenacious interface bonding.

Silicon melted on slip-cast SiO_2 contained very few cracks, but silicon solidified on fused SiO_2 exhibited gross cracking. Also, substrate SD-56 (slip-cast) was free of interface cooling cracks whereas SD-54 (fused) was not (Figure 4-51). The fused silica substrate contained a 25 micron (approx. 0.001-in.) layer network of cracks at the interface, with some of these extending through the entire thickness of the substrate.

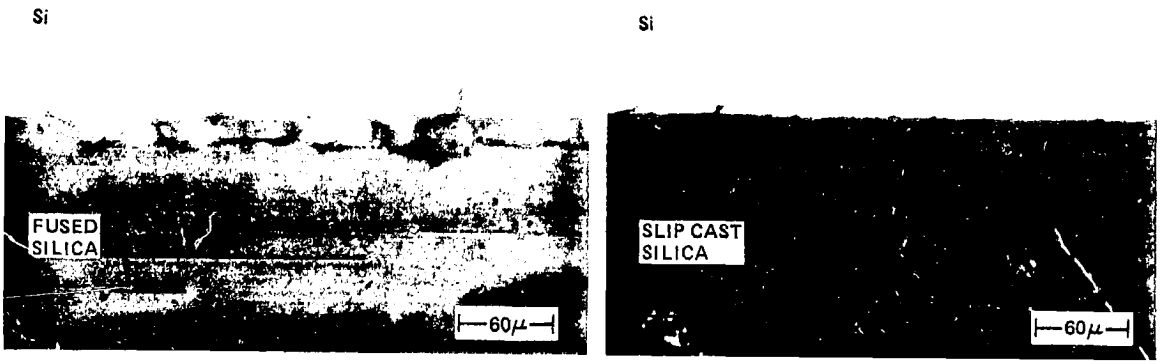

Figure 4-51. Silicon/Silica Interface for Fused Silica, SD-54 (Left), and Slip-Cast Silica, SD-56 (Right). Note Cracking of Fused Silica Interface, as-Polished

2. Compatibility

There was no silicon permeation into the fused silica but some into the slip-cast substrate. There were no observable phase impurities in silicon melted on fused silica, but for silicon on slip-cast silica there was evidence of light gray, oxide-appearing precipitate along the outer portion of the silicon drop.

Typically, silicon melted on fused silica exhibits very low levels of impurity contamination (Table 4-3).

J. BLACK GLASS ($C \cdot SiO_2$)

Lab No.	Supplier	Process	Density, gm/cc	Contact Angle
SD-45	Alfred Univ. Research Foundation	Hot-pressed	1.58	95 $\pm 5^{o}$a
SD-46	Alfred Univ. Research Foundation	Hot-pressed + BN	2.17	56 $\rightarrow$ 46 $\pm 3^{o}$
SD-48	Alfred Univ. Research Foundation	Hot-pressed	2.33	82 $\pm 5^{o}$

[a]Measured from sectioned sessile drop profile.

All black glass samples were prepared at the Alfred University Research Foundation in New York. SD-45 was an air-cooled sample fabricated by hot-pressing Cabosil and Carbowax in a graphite die to 68% of theoretical density. SD-46 was a hot-pressed mixture of silicic acid, carbowax and a small amount of boron nitride. SD-48 was furnace-cooled after hot-pressing silicic acid and carbowax to its theoretical density. All samples were 1/4-in. thick and 2 in. in diameter.

"Black glass" is a general term used to describe an amorphous silica glass having carbon distributed through its structure. The exact way in which this carbon is placed in the silica glass has been described by C. F. Smith in his Ph.D. thesis at Alfred University entitled "The Vibrational Spectra of High Purity and Chemically Substituted Vitreous Silicas", dated May 1973. Patent No. 3378431, "Method of Making C-Containing Glass and Products Thereof", was granted in 1968 to C. F. Smith and W. O. Crandall.

The difference between ordinary or clear amorphous (fused) silica and black glass is not just in the color, but also in its properties. Black glass has been found to have superior resistance to devitrification above 1000°C, where ordinary fused silica has an increasing tendency to crystallize and destroy itself. All other features of black glass, like high thermal shock resistance, etc., are quite similar to ordinary fused silica.

1. Sessile Drop Test

Photographic records of contact angles on SD-45 were not possible because the outer circumferential portion of the substrate began and continued to uniformly warp upward when the temperature exceeded about 1300°C. The contact angle was measured on the post-test mount section. When the sample was removed from the furnace it was observed that the properties of the black glass had significantly changed. Density was much lower, physical dimensions had enlarged and the material was friable. Wetting angle measurements on SD-48 were also difficult to obtain due to high temperature (>1300°C) glazing of the test surface and some warpage of the outer circumference.

No substrate warpage occurred with SD-46, which made in situ contact angle documentation possible. The contact angle on SD-46 appeared to stabilize at 46° after approximately 20 min of contact time. However, as noted with both other tests, SD-45 and SD-48, an oxide-type film appeared on the silicon during the test.

The silicon sessile drop "popped off" on samples SD-46 and SD-48 (Figure 4-52) but remained intact on SD-45.

2. Compatibility

All samples showed evidence of carbide-type precipitates having formed in the molten silicon. These silicon carbide-appearing particles were generally found near the free surface of the silicon drop. The carbide quantity was considerably lower than for silicon melted on

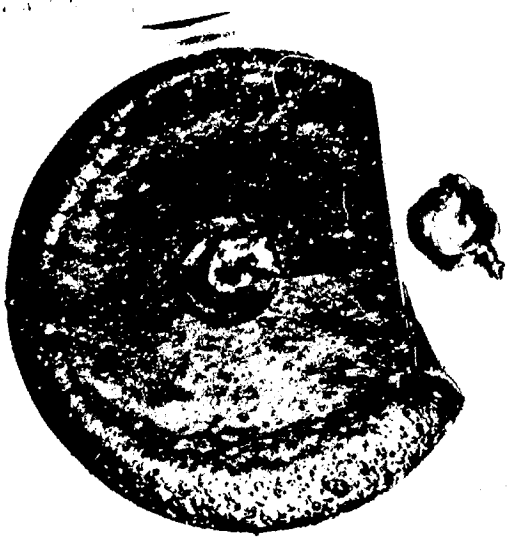

Figure 4-52. Photomacrograph of Black Glass SD-48, Showing Substrate Surface Glazing and Separated Silicon Sessile Drop (at Right)

carbon and SiC products. This fact tends to indicate a greater chemical stability for molten silicon/black glass material systems. Silicon did permeate SD-45 (Figure 4-53) but not SD-46 or SD-48. These last two substrates showed a general lack of interfacial reactions. Semi-quantitative chemical analysis of silicon melted on SD-48 revealed a contamination level of boron greater than 500 ppm (Table 4-1). This level was much lower than for silicon melted on SD-46 revealed a however, it is still detrimental. No other elements were found in any excess, but carbon and oxygen levels were not determined.

3. Discussion

Reasons for the wide variation in observed contact angles are not known. Preliminary analysis indicated that both chemical and mechanical stability of the black glass in the temperature range of interest are dependent on the fabrication technique. Therefore, material developed and tested in this program may not truly characterize its inherent properties. Black glass wetting and potential noncontamination properties indicate a material that should not be eliminated from further testing and evaluation as improvements are made.

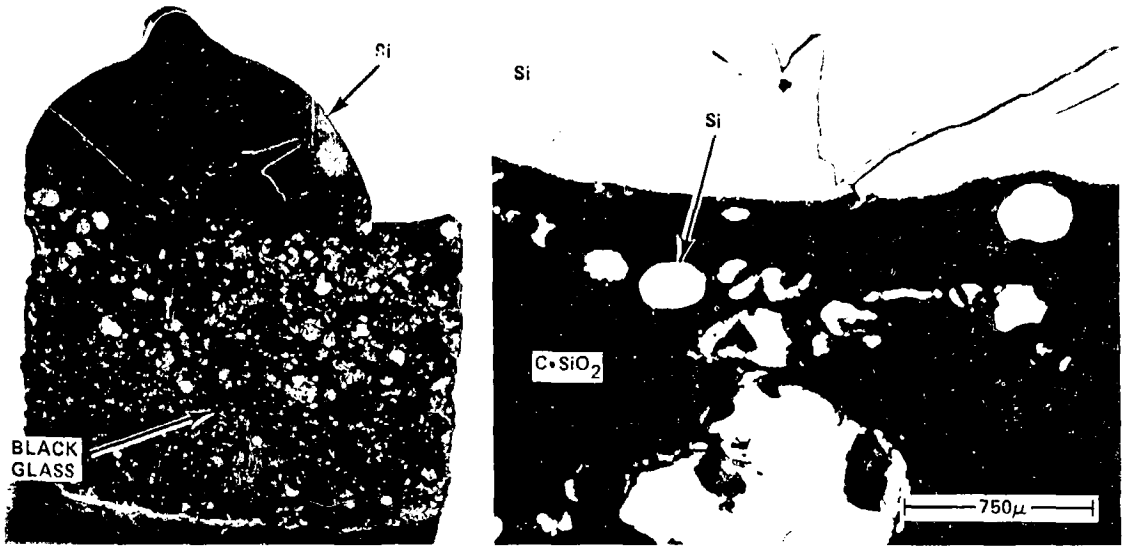

Figure 4-53. Silicon on Black Glass, SD-45; Photomacrograph (Left) is Approximately 5X. Photograph (40X) on Right is a Close-up View of the Silicon/C • SiO_2 Interface Showing Silicon Penetration

K. BORON NITRIDE (BN)

Lab No.	Supplier (grade)	Process	Density, gm/cc	Contact Angle
SD-16[a]	Union Carbide	Pyrolytic	2.19	112± 3°
SD-17[a]	Union Carbide (HBR)	Hot-pressed	2.03	146± 4°
SD-19[a]	Union Carbide (HBR)	Hot-pressed	2.03	145± 3°
SD-20[b]	Duramic Products[c]	Hot-pressed	2.12	136± 4°

[a]As received, surface-tested.

[b]6μ surface finish-tested.

[c]A subsidiary of Kawecki-Berylco Ind.

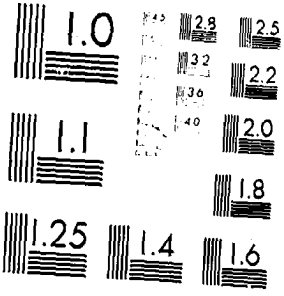

Pyrolytic boron nitride, Boralloy, SD-16, was fabricated by Union Carbide. It is a pure, opaque-white, gas-deposited composite which is a highly oriented anisotropic crystalline material. Some typical property data (supplied by Union Carbide) is given below:

Total Thermal Expansion		
"a" direction at 260°C (500°F)	12.7 microns/micron	(0.0005 in./in.)
"a" direction at 1093°C (2000°F)	43.2 microns/micron	(0.0017 in./in.)
(Linear) "c" direction at 1093°C (2000°F)	1016 microns/micron	(0.040 in./in.)
Total Chemical Impurities <100 ppm		

Solid boron nitride samples, SD-17 and SD-19, UCAR grade HBR, were made by Union Carbide. Hot-pressed BN, SD-20, was supplied by Kawecki Berylco Ind. This type of sample is typically prepared by hot-pressing powdered BN at approximately 1982°C (3600°F) and 6.9 x 10^6 N/m^2 (1000 psi). As a result, the BN polymerizes to form a structure similar to the anthracene ring. Subsequent fabrication is usually accomplished by machining the hot-pressed cylinders to finished tolerances.

Typical chemistry data for hot-pressed BN (supplied by Duramic Products) is as follows:

Composition	Regular	Low Oxygen
%BN	96.0	99.0
%N_2	54.0	55.99
%B	42.70	43.40
%C	0.20	0.20
%O_2	3.09	0.40
% others	0.01	0.01

C-2

Some general property data for hot-pressed BN (supplied by Duramic Products) is given below:

Thermal Conductivity	Against Grain	With Grain
302°C (575°F)	5.3 (10)	12.8 (24) W/m-k (Btu/hr-Ft-°F)
982°C (1800°F)	4.3 (8)	9.6 (18) W/m-k (Btu/hr-Ft-°F)

Coefficient of Thermal Expansion	Against Grain	With Grain
75 - 700°F	142 (56)	7.6 m/m/k · 10-9 (3 in./in./°F · 10-7)
75 - 1650°F	114 (45)	12.7 m/m/k · 10-9 (5 in./in./°F · 10-7)
75 - 1850°F	102 (40)	10.2 m/m/k · 10-9 (4 in./in./°F · 10-7)

When BN is heated above 1200°C (2190°F), 80% of expansion remains as permanent set.

Special handling of boron nitride samples was incorporated into the lab, since experience had shown that contact with water and subsequent heating caused interlamellar flaking. This material is also attacked by carbon tetrachloride, alcohol and acetone.

1. Sessile Drop Tests

It appeared that the wetting characteristics of pyrolytic BN were inherently different from hot-pressed BN. On pyrolytic BN, SD-16, a contact angle 20% lower than for silicon on hot-pressed BN was observed. The presence of a highly oriented surface crystallographic plane is thought to be the reason for this difference.

Hot-pressed BN from Kawecki Berylco exhibited a slightly different contact angle (about 5% lower) than the Union Carbide product. This effect may be the result of different sample histories (note density variation) and/or the surface texture tested, i.e., 6μ finish for SD-20 vs as-fabricated surface for SD-17 and SD-19. Further sessile drop tests were needed to fully clarify the wetting properties of various hot-pressed BN products but were not conducted in view of the high B content observed in the Si.

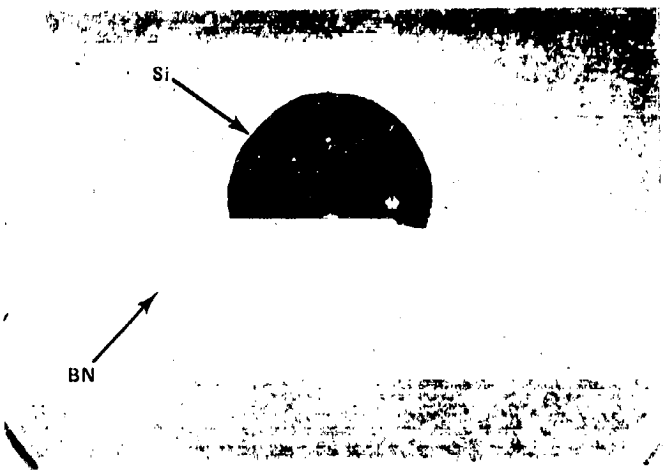

Figure 4-54. Photomacrograph of Silicon Sessile Drop and Hot-Pressed BN Substrate, SD-16. Mag. 4X

2. Compatibility

Some observations of BN in a molten Si environment were:

(1) Silicon did not adhere to BN during or after solidification and therefore did not exhibit cooling cracks (Figure 4-54).

(2) Very fine, linearly aligned, black precipitates were found in the silicon matrix (in the last areas to solidify). These precipitates appeared to be grain-boundary-oriented and were distinguishable only at high magnification (>300X).

(3) Very high levels of boron doping were determined for silicon on both pyrolytic and hot-pressed BN, and a high level of iron contamination was found in silicon melted on a hot-pressed BN (Table 4-1). The determined level of boron doping ($\sim 10^{20}$ atm/cc) corresponds to a bulk silicon resistivity in the range 0.001 - 0.002 ohm-cm.

L. HAFNIA (HfC_2) and HAFNIUM CARBIDE (HfC)

Lab No.	Supplier	Process (material)	Density, gm/cc	Contact Angle
SD-32[a]	Ultramet	Vapor-deposited (HfO_2)	9.68[b]	78 $\pm 3^{o}$ – 0^{o}c
SD-33[a]	Ultramet	Vapor-deposited (HfC)	12.20[b]	$<5^{o}$

[a]As-deposited, surface-tested.
[b]Theoretical density.
cSilicon absorbed into graphite substrate.

Hafnia, SD-32, and hafnium carbide, SD-33, were both chemical-vapor-deposited on 5.08 cm (2-in.)-diameter graphite substrates by Ultramet in Pacoima, Calif. HfO_2, SD-32, which has a melting point of 2610^{o}C, was deposited by reacting hafnium chloride ($HFCl_4$), oxygen (O_2), hydrogen (H_2), and saturated water vapor (H_2O) at 1400^{o}C in the presence of a graphite substrate. HfC, SD-33, which has a calculated melting point of 3890^{o}C (Reference 4-35), was deposited by reacting hafnium chloride ($HfCl_4$), methane (CH_4), and hydrogen (H_2) at 1400^{o}C in the presence of a graphite substrate.

1. Sessile Drop Test

Silicon melted on HfO_2, SD-32: (1) exhibited an initial contact angle of approximately 78^{o} and (2) was absorbed into the graphite substrate through cracks in the CVD layer (Figure 4-55). Mudcracking patterns were evidence in the HfO_2 layer in and around the molten Si contact area. Four major cracks extended into the graphite substrate such that graphite acted as a wick and completely absorbed the molten Si drop in 25 minutes total contact time.

HfC, SD-33, was wet immediately and completely by molten Si (Figure 4-56). No contact angle was measured, but it was obviously below 5^{o}.

2. Compatibility

CVD HfO_2 on graphite, SD-32, appeared to be mechanically unstable, due to cracking, in the presence of molten Si. Chemical reactions in the HfO_2/molten Si material system were not observed because the silicon was absorbed into the graphite substrate. Molten Si on HfO_2 would be expected to react with the Hf in the CVD layer, forming hafnium silicides (Reference 4-36).

Molten Si in contact with CVD HfC, SD-33, reacted extensively and formed several new hafnium silicide phases (Figure 4-57). Complete identification of these phases was not determined.

Figure 4-55. HfO_2, SD-32 Post-Test Surface Condition Showing Absence of Silicon, Mudcracking Pattern in CVD Layer and Substrate Cracks (Arrows)

M. YTTRIA (Y_2O_3)

Lab No.	Supplier	Process	Density, gm/cc	Contact Angle
SD-31	Coors	Hot-pressed	4.84	63 $\pm 2^{o}$

Yttria (Y_2O_3), which melts at 2410°C, was supplied by the Ceramic Division of Coors, in Golden, Colorado. It was fabricated by hot-pressing a mixture to 97% of theoretical density. Polished sections of the as-received sample revealed the presence of about 98% Y_2O_3 and 2% unknown phase.

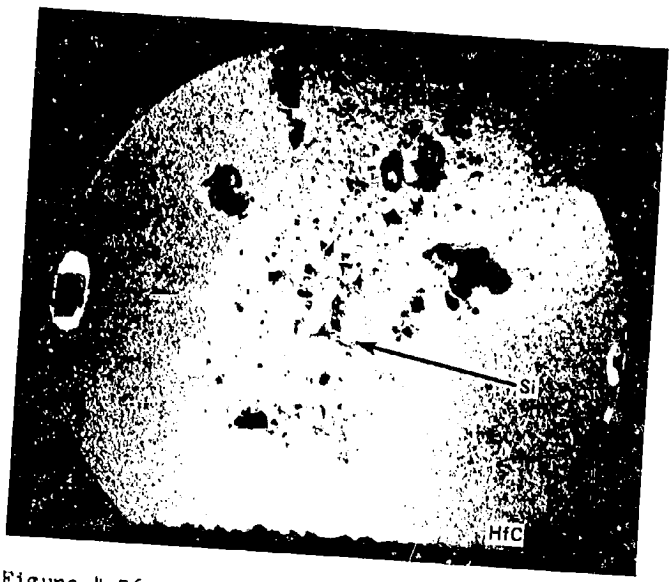

Figure 4-56. Photomacrograph of Silicon on HfC, SD-33, Mag. 2X

1. Sessile Drop Test

The contact angle, 63°, was very stable during the entire 50 min at temperature. Fine radial cracks emanating from the silicon drop were produced in the Y_2O_3 substrate when the silicon solidified (Figure 4-58). These through-thickness cracks extended to the edges of the substrate. The silicon drop remained bonded to the Y_2O_3 after solidification.

2. Compatibility

Chemical reactions in the Y_2O_3/molten Si system appeared to proceed in both directions:

(1) Silicon permeated the substrate to a maximum depth of approximately 300 microns (0.012 in.) (Figure 4-59). Free silicon and a yttrium silicate phase formed in a patchy network with a semicircular penetration boundary. The maximum penetration occurred in the center portion of the contact area.

(2) Gross second phase precipitation occurred in the silicon matrix (Figure 4-60).

The Y_2O_3/molten Si interface did not move, indicating that the reaction occurred with yttria being replaced by silicon and vice versa.

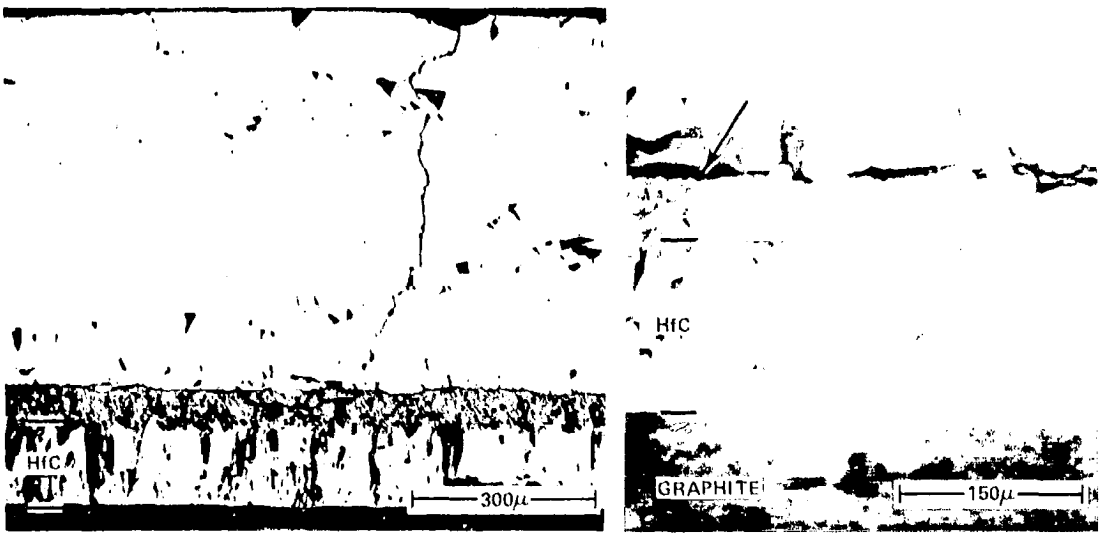

Figure 4-57. HfC/Silicon Interface Region Showing the Formation of Various Hafnium Silicides, as-Polished Condition. Arrow Indicates Original CVD HfC Surface

N. CERIUM SULPHIDE (CeS)

Lab No.	Supplier	Process	Density, gm/cc	Contact Angle
SD-73	Electronic Space Products	Hot-pressed	3.99	$\approx 50^{o} \rightarrow 0$ in 5 minutes

A hot-pressed disc 2.5 cm (1 in.) diameter, 0.64 cm (1/4 in.) thick, of cerium sulphide was supplied by Electronic Space Products, Inc., Los Angeles, Calif. CeS degrades at temperatures greater than 2100^{o}C (Ref. 4-34).

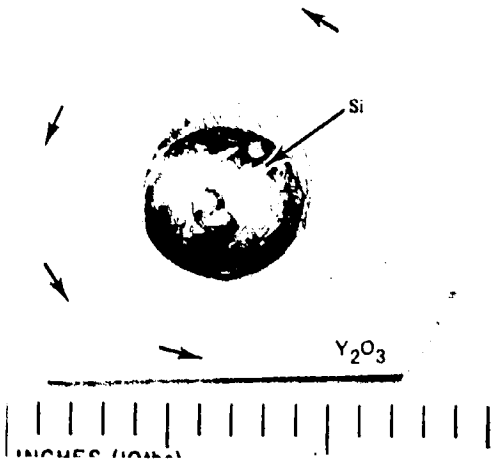

Figure 4-58. Top View of Silicon on Y_2O_3 SD-31, Showing Fine Cracks (Arrows) Emanating from Silicon Sessile Drop

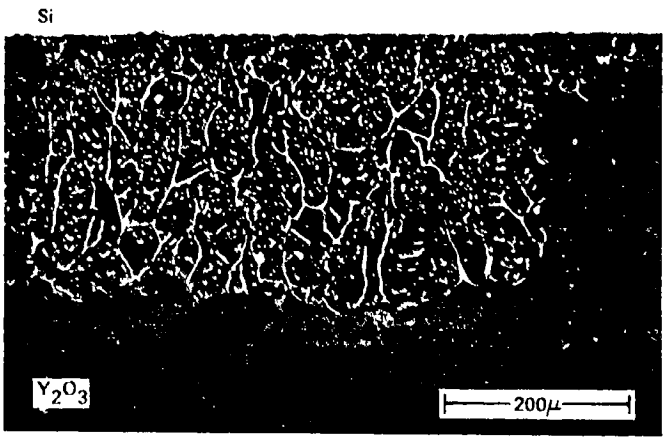

Figure 4-59. Sectional Macrograph of Silicon/Y_2O_3 Interface, SD-31, Showing Penetration of Silicon Into Y_2O_3 Substrate

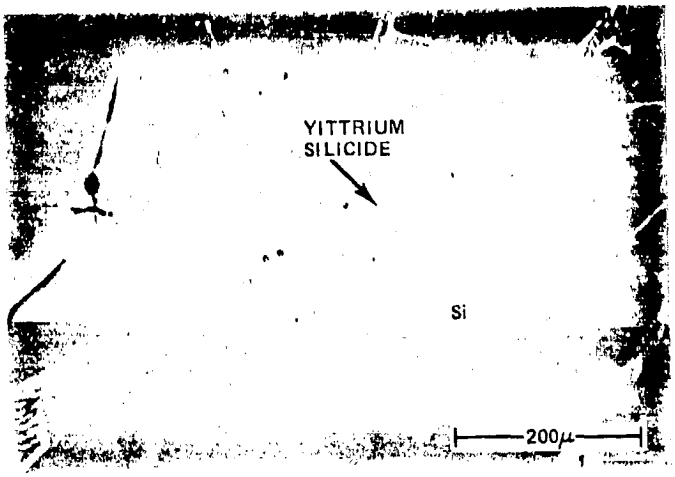

Figure 4-60. Silicon Matrix, SD-31, as-Polished. Mag 150X

1. Sessile Drop Test

   (1) Silicon initially wet the CeS substrate at 50°. The molten silicon was then absorbed into the substrate in approximately 5 minutes.

   (2) CeS chemically and physically degraded in the presence of molten Si at 1430°C. The post-sessile drop CeS sample had expanded dimensions and was cracked and friable (Figure 4-61).

2. Compatibility

   (1) Silicon absorbed into the CeS structure formed a multitude of new and complex phases (Figure 4-62).

   (2) The reaction proceeded only one way, silicon into CeS, so no data could be obtained on contamination levels in the silicon.

   (3) The material appears to have no potential for use in contact with molten Si.

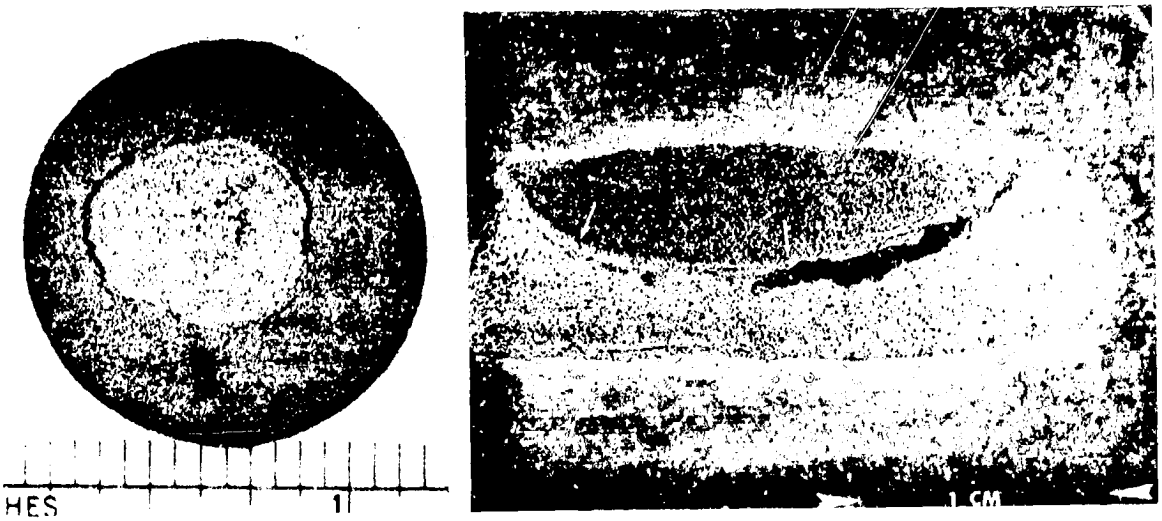

Figure 4-61. CeS, SD-73, Showing the Post Sessile Drop Test Surface (Left) and a Cross-Sectional View Showing the Extent of Silicon Absorbtance and the Dimensional Change in the CeS.

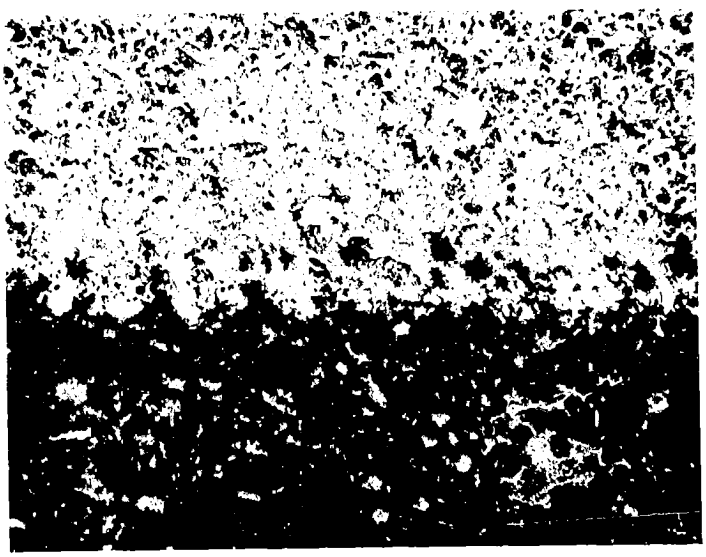

Figure 4-62. Sectional Micrograph of the Reacted Si + Ce + S (Top Area) and Unreacted Ce + S (Lower Area). Mag 40X

O. LANTHANUM HEXABORIDE (LaB_6)

Lab No.	Supplier	Process	Density, gm/cc	Contact Angle
SD-74	Electronic Space Products	Hot-pressed	4.56	52 $\pm 3^{\circ}$

A hot-pressed disc 2.5 cm (1 inch) diameter, 0.64 cm (1/4 in.) thick of lanthanum hexaboride was supplied by the Electronic Space Products, Inc. LaB_6 has a melting point of 2210°C.

1. Sessile Drop Test

   (1) Silicon wet LaB_6 and exhibited a mechanically stable contact angle of approximately 52°.

   (2) The silicon cracked off the LaB_6 substrate during solidification, leaving a thin layer of silicon bonded to the substrate (Figure 4-63).

2. Compatibility

   (1) Several fine cracks 2-5 mm long originating from the Si/LaB_6 interface were observed in the LaB_6 substrate. The cracks, which were at right angles to the surface, were not filled with silicon and are believed to have been caused by thermal stresses.

   (2) Interestingly, for a material wet by silicon to 52°, there was little or no silicon penetration or degradation of the LaB_6 interface. The silicon material at the interface, however, appears to have undergone some reaction. (Figure 4-63).

   (3) Detrimental doping of the silicon melted on LaB_6 is highly likely but undocumented to date.

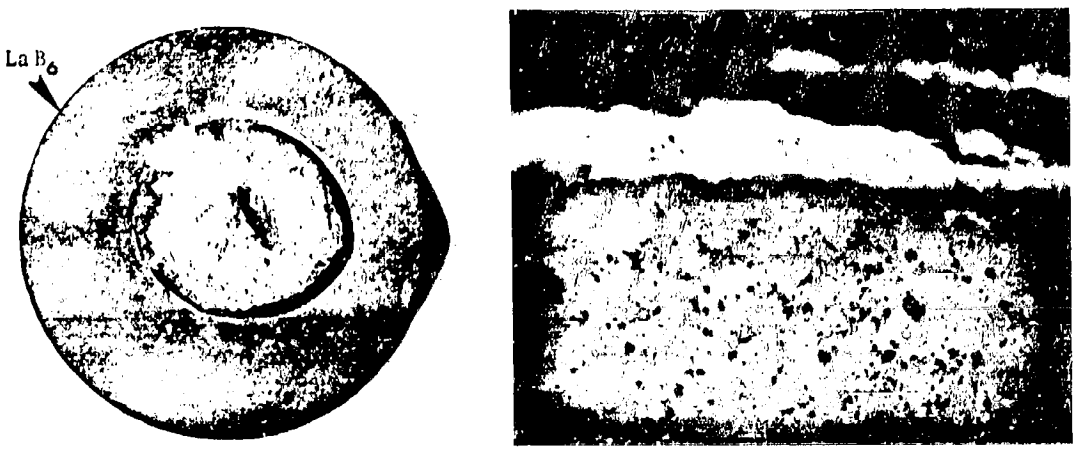

Figure 4-63. LaB_6, SD-74, Showing Silicon Material Adhering to the Substrate (Left) and the Remaining Si/LaB_6 Interface (right, magnification 200X) The Light Layer is the Silicon, Which Shows Evidence of Reaction Products

SECTION V

SUMMARY

Molten Si acted as a solvent in various degrees on all refractory materials used as a sessile drop substrate. Research and compatibility studies conducted reveal that, to date, no ideal material exists which will remain inert to a molten Si environment. However, several potentially useful materials have emerged. Sessile drop tests conducted categorized refractory materials as "wetting" ($\theta < 85^{\circ}$), "nonwetting" ($\theta > 95^{\circ}$) or "borderline" ($85^{\circ} \leq \theta \leq 95^{\circ}$). Refractory material used for silicon ribbon producing capillary dies must be wetting and nonreactive to molten Si. Refractory material used for crucibles or containers may be in any wetting category, yet, most importantly, must be nonreactive to the molten Si bath.

In relative order of importance, the four most desirable properties that a refractory material in contact with molten Si must possess are:

(1) Lack of detrimental chemical reactivity (both intrinsic and extrinsic).

(2) Wetting characteristics (only for capillary dies).

(3) Thermal/mechanical stability.

(4) Ease and low cost of fabrication.

Detrimental impurity contamination is arbitrarily defined as that impurity level which will cause electrical degradation below approximately 85% of a baseline (uncontaminated) efficiency. The baseline cell is a P-type silicon having an acceptor concentration in the 2.5×10^{15} to 7.0×10^{15} atoms/cc range (Reference 1-13). Intrinsic chemical contamination is defined as the detrimental dissolution, erosion, saturation or precipitation of any element or compound into the silicon which was initially part of the refractory material basic element structure, e.g., carbon from SiC and aluminum from the Al_2O_3, structure. Extrinsic chemical contamination is defined as the detrimental dissolution, erosion, saturation or precipitation of any element or compound into the silicon which initially was not a part of the refractory material basic structure. Examples of this include magnesium from hot-pressed Si_3N_4, iron from hot-pressed BN and calcium from sialon material.

On the basis of the four properties listed above, as analyzed from sessile drop tests, materiallographic studies, and/or chemical analyses, the tested refractory materials were graded. (The following list also reflects a refractory material potential for use in contact with molten Si.)

Refractory Material/Molten Si Compatibility Rating

Material (Process)	Chemical Compatibility	Wetting Characteristic	Test Rating	Potential
Si_3N_4 (CVD)[a]	Low I, low E	W	5	4
Si_3N_4 (HP)	Low I, med. E	W	4	4
β' sialon (HP)	Med. I, med. E	W	4	3
SiOXYN (RS)	Unk. I, interface phase reaction	NW	2	4
15R, 8H polyphase sialon	Med. I, high E	W	3	3
SiC (HP)	Med. I, med. E	W	3	3
SiC (CVD)	Med. ± (structure breakdown)	W	2	4
SiO_2 (fused)	Low I, low E	B	3	3
SiO_2 (slip-cast)	Low I, med. E	B	2	4
Glassy carbon	Med. I, low E	W	3	2
$3Al_2O_3 \cdot 2SiO_2$ (P+F)	Med. I, high E	B	2	3
$C \cdot SiO_2$ (HP)	Med. I (structure Unk E breakdown)	W	2	3
Al_2O_3 (EFG)	Unk I, low E	B	2	1
$C \cdot SiO_2$ + BN (HP)	Med. I, low E	W	2	1
LaB_6 (HP)	Unk I, low E	W	2	1
BN (HP)	High I, low E	NW	2	0
BN (CVD)	High I, low E	NW	2	0
HfO_2 (CVD)	Unk I, unk E	W	1	0
Intermetallic compound	High I, unk E	NW	1	Unk

Refractory Material/Molten Si Compatibility Rating

Material (Process)	Chemical Compatibility	Wetting Characteristic	Test Rating	Potential
SiC (siliconized)	Absorbs silicon	None	0	1
HfC (CVD)	High I, low E	W	0	0
Mo (rolled sheet)	High I, low E	W	0	0
CeS (HP)	Absorbs silicon	W	0	Unk

[a]Tested by RCA, Reference 1-18.

Process abbreviations

CVD - chemical vapor deposition

HP - hot-pressed

RS - reaction-sintered

P+F - pressed and fired

EFG - edged-defined film-fed growth

Chemical Compatibility Symbols

I - intrinsic contamination

E - extrinsic contamination

Wetting Characteristic Symbols

W - wetting

NW - nonwetting

B - borderline

Test Rating and Potential

5 - highest rating and potential for use in contact with molten silicon

0 - lowest rating and no potential for use in contact with molten silicon

A material may have a higher potential rating than test rating if it was felt that the specific refractory material tested did not represent the best quality material obtainable. A summary of silicon compatibility factors for die, container and substrate refractory materials is given below:

Silicon Carbide, Glassy Carbon and Graphite (Including Poco Grade)

1. Sufficiently wet by Si ($\sim 40^{\circ}$, see Figure 4-1), thus could be used as capillary dies.

2. Molten silicon inherently causes a precipitation or dissolution of β-SiC particles which are imparted into the Si matrix. On solidification these particles cause structure breakdown in silicon, which is electrically active.

3. SiC particle count appears to be lower for Si on SiC than Si on C (glassy or graphitic).

4. Silicon melted on low-density SiC containing appreciable amounts of free silicon is absorbed into the substrate.

Silicon Nitride and Silicon Oxynitride

1. Si_3N_4 exhibits sufficient wetting ($\sim 51^{\circ}$, see Figure 4-1) to be used as a capillary die.

2. Very little interfacial reaction or dissolution was observed on hot-pressed Si_3N_4 products.

3. Presently, impurity elements typically found in Si_3N_4 starting powders appear to be the inherent contamination problem for molten silicon. Silicon on RS Si_3N_4 exhibited higher contamination levels than silicon on HP Si_3N_4.

4. Pure single-phase silicon oxynitride has yet to be tested in contact with molten silicon. Commercial-grade polyphase SiOXYN exhibited nonwetting properties ($\theta \approx 115^{\circ}$) and therefore can be considered for containers or inverted ribbon growth dies.

Sialons

1. Various contact angle spreading rates were found for silicon on 15R polyphase, 8H polyphase, X_2 composition (two phase) and B' phase (single and poly) sialon material as evidenced by the complex spreading kinetics (Figures 4-30 and 4-31).

2. Single-phase material exhibited a lower kinetic spreading rate than polyphase material.

3. High initial wetting angles are attributed to a silicon oxide layer usually present on starting powder surfaces or in polyphase material.

4. Materials tested in this program can be considered wetting when used in contact with molten Si and are therefore candidates for use as capillary dies.

5. Analyses tend to indicate that silicon is intrinsically doped with Al from the Si-Al-O-N structure.

6. Extrinsic detrimental doping levels of iron, calcium and tungsten have been observed. These are impurities found in starting powders.

Mullite

1. "Borderline" wetting properties ($\theta \approx 94^{\circ}$) (see Figure 4-1).

2. Apparent intrinsic doping of silicon with aluminum.

3. Best match to the thermal coefficient of silicon.

Sapphire

1. Borderline wetting properties ($\theta \approx 86^{\circ}$).

2. Solidification of bulk Si on sapphire causes it to shatter.

3. Doping of Si with Al is expected.

Black Glass ($C \cdot SiO_2$)

1. Valid wetting properties for a $C \cdot SiO_2$-phase material were not obtained. Tested material was not chemically or mechanically stable at the test temperature.

2. Some substrates were observed to warp and glaze above $1300^{\circ}C$.

3. SiC precipitation was observed in the Si matrix. The rate and quantity of the SiC precipitation appeared to be less than for Si on C or SiC.

4. Small amounts of BN (≈5%) caused detrimental doping of Si with B.

Fused and Slip-Cast Silica

1. Both forms of silica exhibited similar borderline wetting properties ($\theta \approx 91^{\circ}$) (see Figure 4-1).

2. On solidification of Si sessile drops, more cracking was observed in fused SiO_2 compared to slip-cast SiO_2.

3. Silicon on fused SiO_2 contained the least impurities of all materials tested.

4. Silicon on slip-cast material contained visible impurity phases (optically); none were observed for Si on fused SiO_2.

Boron Nitride

1. Nonwetting properties $\theta \approx 112$ and 140° for CVD BN and HP BN, respectively (see Figure 4-1).

2. Intrinsic detrimental doping of Si with boron.

HfC, HfO_2, Pyrolytic Graphite, Molybdenum, Cerium Sulphide, and Siliconized Silicon Carbide

These materials react extensively with molten Si and have no potential for use in contact with molten Si.

Observations

1. Essentially no relationship existed between degrees of wetting and the amount of bulk or interfacial chemical reactions recorded.

2. Impurity elements present in single or polyphase refractory material are potentially a source for silicon contamination.

3. Single-phase material appears more desirable than polyphase.

REFERENCES

1-1. "Review, Silicon Solar Cells for Terrestrial Applications," J. Mater. Sci., Vol. 12, pp. 602-615, 1977.

1-2. Vogel, L., Gardner, G., and Cave, E. F., U.S. Patent 3, Vol. 124, p. 489, 1964.

1-3. Work presently being conducted by University of South Carolina and Westinghouse Electric Corporation.

1-4. "Large Area Silicon Sheet by EFG," First Quarterly Report 1977, Mobil Tyco Solar Energy Corporation, ERDA/JPL Subcontract No. 954355.

1-5. Marumo, C., and Pask, J. A., "Reactions and Wetting Behaviour in the Aluminum-fused Silica System," J. Mater. Sci., Vol. 12, pp. 223-233, 1977.

1-6. Ahmad, U. M., and Murr, L. E., "Surface Free Energy of Nickel and Stainless Steel at Temperatures Above the Melting Point," J. Mater. Sci., Vol. 11, pp. 224-230, 1976.

1-7. Swartz, J. C., "Atmosphere Effects on Wetting of Si_3N_4 by Liquid Si," J. Am. Ceram. Soc., Discussion and Notes, Vol. 59 No. 5-6, May-June 1976.

1-8. Hoge, C. E., Brennan, J. J., and Pask, J. A., "Interfacial Reactions and Wetting Behavior of Glass-Iron Systems," J. Am. Ceram. Soc., Vol. 56, No. 2, Feb. 1973; also Battelle, Columbus Laboratories, Die and Container Material Development of the Large Area Silicon Sheet Task of the Low-cost Silicon Solar Array Project. Proposed Research Program, Apr. 1, 1977.

1-9. Champion, J. A., Keene, B. J., and Allen, S., "Wetting of Refractory Materials by Molten Metallides," J. Mater. Sci., Vol. 8, pp. 423-426, 1973.

1-10. Quincke, G., "Concerning the Capillary Constants of Molten Chemical Compounds," Ann. Phys. Chemie, 138, 141, 1869.

1-11. Kingery, W. D., "The Role of Surface Energies and Wetting in Metal-Ceramic Sealing," Ceram. Bull., Vol. 35, pp. 108-112.

1-12. Aksay, I. A., and Pask, J. A., "Phase Distribution in Solid-Liquid-Vapor Systems," in "Surfaces and Interfaces of Glass and Ceramics," Materials Science Research, Vol. 7, pp. 299-331.

1-13. Keck, P. H., and Van Horn, W., "The Surface Tension of Liquid Silicon and Germanium Phys. Rev. Vol. 91, pp. 512-513, 1953.

1-14. Hopkins, R. H., et al., Silicon Materials Task of the Low Cost Solar Array Project (Phase II), Westinghouse R&D Center, Quarterly Report No. 6, ERDA/JPL 954331-77/3, Jan. 1977-Mar. 1977; also McCormick, J. R., Dow Corning Corp.

1-15. Schmid, F. M., Analysis of Effects of Impurities Intentionally Incorporated into Silicon, Second Quarterly Report, 2 May 1977 - 29 July 1977, ERDA/JPL Contract No. 954694.

1-16. Bates, H. E., and Leipold, M. H., personal communication.

1-17. Cullen, G., et al., Die and Container Material Development of the Large-Area Silicon Sheet Task of the Low-Cost Silicon Solar Array Project, Pricing Proposed, PP 77-032, Technical Proposal, Part 1, Radio Corporation of America, March 28, 1977.

1-18. Duffy, M. T., et al., Development and Evaluation of Die Material for Use in Producing Silicon Ribbons by the Inverted Ribbon Growth Process, First Quarterly Report December 1977, ERDA/JPL Contract No. 954901, Radio Corporation of America.

1-19. Patel, J. R., and Batterman, B. W., J. Appl. Phys. Vol. 34, p. 2716, 1963; Disk Faraday Soc. Vol. 38, p. 201, 1964; Bull. Soc. Fr. Mineral Cristalloga, Vol. 95, p. 700, 1972.

1-20. Kimerling, L. C., Leamy, H. J., and Patel, J. R., "The Electrical Properties of Stacking Faults and Precipitates in Heat Treated Dislocation Free Czochralski Silicon," Appl. Phys. Lett., Vol. 30, No. 5, 1 Mar. 1977.

1-21. Trumbore, F. A., "Solid Solubilities of Impurity Elements in Germanium and Silicon," Bell Syst. Tech. J., Vol. 39 pp. 205-233, 1960.

2-1. Hannay, N. B., Semi Conductors, Reinhold Publishing Corp., New York, 1959.

4-1. Whalen, T. J., and Anderson, A. T., "Wetting of SiC, Si_3N_4 and Carbon by Si and Binary Si Alloys," J. Am. Ceram. Soc., Vol. 58, No. 9-10, Sept. - Oct. 1975.

4-2. Manufacture of Dense Bodies of Silicon Carbide (Refel), C. W. Forrest to United Kingdom Atomic Energy Authority, U.S. Patent No. 3,495,939, Feb. 17, 1970.

4-3. Method of Making Refractory Bodies, J. C. Anderson to the Carborundum Company, U.S. Patent No. 2,938,807, Aug. 13, 1957.

4-4. Chaney, R. E., and Varker, C. J., "The Erosion of Materials in Molten Silicon," J. Electrochem. Soc., June 1976.

4-5. Beckmann, G. E. J., "Growth of Silicon Carbide from Molten Silicon," J. Electrochem. Soc. Vol. 110, No. 1, 84-86, 1963.

4-6. Chang, C., and Siekhaus, W. J., "Auger Analysis of Silicon Thin Films Deposited on Carbon at High Temperatures," J. Appl. Phys., Vol. 46, No. 8, Aug. 1975.

4-7. Schwuttke, G. H., Ciszek, T. F., and Kran, A., Silicon Ribbon Growth by a Capillary Action Shaping Technique, IBM Quarterly Technical Progress Report No. 7, ERDA/JPL 954144-77/1, Apr. 1, 1977.

4-8. Schwuttke, G. H., et al., Silicon Ribbon Growth by Capillary Action Shaping Technique, Quarterly Progress Report No. 8, ERDA/JPL 954444-77/1, July 1, 1977.

4-9. Bottoms, W. R., Gutterman, D., and Roitman, P., J. Vac. Sci. Technol., Vol. 12, No. 1, p. 134, Jan./Feb., 1975.

4-10. Gevers, R., Art, A., and Amelinckx, S., Phys. Status Solidi, Vol. 31, p. 363, 1963.

4-11. Dieley, G. G., Herbert, J. M., and Moore, N. C., "Dense Silicon Nitride," Powder Met., Vol. 8, pp. 145-51, 1961.

4-12. Dieley, G. G., "Bonding Silicon Nitride to Strong Dense Ceramic Bodies," British Patent 970, 639, Sept. 23, 1964.

4-13. Coe, R. F., "Silicon Nitride Products," British Patent 1,092,637, Nov. 29, 1967.

4-14. Kossowsky, R., "Creep, Fatigue and Microstructures of Si_3N_4," Vol. 2, Ceramics for High Performance Applications, Army Materials Technology Conference Series, 1972.

4-15. Wild, S., Grieveson, P., Jack, K. H., and Latimer, M. J., "Special Ceramics," No. 5, p. 377, edited by P. Popper, Brit. Ceram. Researc. Assoc., 1972.

4-16. Drew, P., and Lewis, M. H., J. Mater. Sci. Vol. 9, p. 261, 1974.

4-17. Powell, B. D., and Drew, P., ibid, Vol. 9, p. 1867, 1974.

4-18. Nuttall, K., and Tompson, D. P., ibid, Vol. 9, p. 850, 1974.

4-19. Mitomo, M., "Pressure Sintering of Si_3N_4," J. Mater. Sci. Vol. 11, pp. 1103-1107, 1976.

4-20. Colquhoun, I., Wild, S., Grieveson, P., and Jack, K. H., "Thermodynamics of the Silicon Nitrogen-Oxygen Systems, Proc. Br. Ceram. Soc., No. 22, pp. 207-27, 1973.

4-21. Greskovich, C. D., Prochanzka, S., and Rosolowski, J. H., Basic Research on Technology Development for Sintered Ceramics, Technical Report AFML-TR-76-179, General Electric Company, Nov. 1976.

4-22. Shewman, P. G., Transformations in Metals, McGraw, Hill, Inc., New York, 1969.

4-23. Kim, K. M., et al., Silicon Sheet Growth by the Inverted Ribbon Growth Process, Technical Report ERDA/JPL 954465, Radio Corporation of America, June 1977.

4-24. Brown, D. M., et al., "Properties of $Si_xO_yN_z$ Films on Si," J. Electrochem. Soc.: Solid State Science, Vol. 115, No. 3, Mar. 1968.

4-25. Jack, K. H., "Review, Sialons and Related Nitrogen Ceramics," Journal of J. Mater. Sci.," 1976 1135-1158.

4-26. Oyama, Y., and Kamigaito, O., Yogyo-Kyokai-Shi, 80, p. 327, 1972.

4-27. Jack, K. H., Trans. J. Brit Ceram. Soc., Vol. 72, p. 376, 1973; also Bates, H. E., et al., Thick Film Silicon Growth Techniques, Final Report to JPL, Subcontract No. 953365, Apr. 1975.

4-28. Layden, G. K., Pressureless Sintering of SiAlON Gas Turbine Components, Final Report NADC-75207-30, United Technologies Research Center, East Hartford, Conn., Contract N62269-69-C-0108, Feb. 23, 1977.

4-29. Briggs, J., Pressureless Sintering of SiAlON Ceramics, Mat. Res. Bull. Vol. 12, 1047-1055, 1977, Battelle, Geneva Research Centre.

4-30. Zook, J. D., et al., Dip Coating Process, Quarterly Report No. 6, Honeywell Corporate Research Center, ERDA/JPL 954356-77/1, July 1977.

4-31. Kaiser, W., and Breslin, J., "Factors Determining the Oxygen Content of Liquid Silicon at Its Melting Point," J. Appl. Phys., Vol. 29 No. 9, Sept. 1958.

4-32. Wald, F. V., Large Area Silicon Sheet by EFG, Second Quarterly Report, ERDA/JPL 954355/77-2, Mobil Tyco Solar Energy Corp., June 15, 1977.

4-33. Runyan, W. R., Silicon Semiconductor Technology, McGraw-Hill, New York, 1965.

4-34. Schmid, F., and Khattak, C., Cast Silicon by the Heat Exchanger Method, Crystal Systems, Inc. ERDA/JPL Contract 954373, Eighth Quarterly Report, July 1 - Sept. 30, 1977.

4-35. CRC Handbook of Chemistry and Physics, 48th Edition, 1967-68.

4-36. Elliot, R. P., Constitution of Binary Alloys, First Supplement, McGraw-Hill, 1965.